Ph. D. Dissertation

Study on Photoregulated Biomolecular Motor-based Microrobot and its Application in Active Transport

生体分子モーターを基礎とするマイクロロボットの 光制御と能動輸送への応用に関する研究

Mousumi Akter

Material Chemistry Laboratory

Graduate School of Chemical Sciences and Engineering

Hokkaido University, Japan

September 2020

Study on Photoregulated Biomolecular Motor-based Microrobot and its Application in Active Transport

（生体分子モーターを基礎とするマイクロロボットの 光制御と能動輸送への応用に関する研究）

A dissertation for the degree of

Doctor of Science

Mousumi Akter

Material Chemistry Laboratory

Graduate School of Chemical Sciences and Engineering

Hokkaido University, Japan

September 2020

CONTENTS

Chapter 4: Active cargo transport by the swarm microrobot

CHAPTER 1

General Introduction

1.1 Purpose

Robotics has emerged as the most promising arena in the development of science and technology which involves the design, construction, operation and use of robots.[1–4] The limitation of the conventional robot, however, lies in their macro size and low efficiency which restricted their application in nanotechnology.[5] Moving robotics from the macroscopic to the microscopic level, create a new discipline as microrobotics which aim to produce micrometer-scaled artificial robots for the development of engineering systems.[6–9] However, because of the small size, it has been always a challenge to construct microrobots.[7,10] Besides, the realization of robots assembled from these components is one of the ultimate goals to construct microsized robots integrating molecular devices. Several attempts have been reported to build such robots in a synthetic environment using natural,[7,10–13] chemically powered,[14–17] or mechanically self-propelled objects[9,18–22] as actuators. However, microrobots using the chemically powered or mechanically self-propelled objects can limit the dynamic behavior of the robots due to the motion or low speed of micromotors.[12] In contrast, self-propelled biomolecular motor systems, i.e. microtubule (MT)-kinesin and actin-myosin have been particularly promising as actuators in the microrobots due to their small size, high specific energy and scalability.[23–25] However, a systematic control over the direct interaction of a large number of self-propelled objects could limit the ability of the microrobot in further applications.[26,27] To overcome this limitation, a supramolecular building block DNA, a natural programmer could be used as a molecular processor to store complex information[28,29] and programs for controlling the interaction among them. Recently a microrobot named molecular robot was constructed with the integration of kinesin driven filamentous MT as an actuator, DNA as an information processor and sensor.[13,30] But using the chemical signal of DNA limits to control the motion of microrobots in a spatiotemporal manner. Incorporation of a photosensor in a microrobot could create a new paradigm to control the biomolecular motor based microrobots spatiotemporally by photo signal. Moreover, photoirradiation could be the most simple and advantageous approach to regulate the

robots and utilize them for further application which has not been addressed yet. Therefore, in this dissertation, I focus to construct photoregulated microrobots employing single strand of azobenzene incorporated DNA (*p*DNA) in the cytoskeletal filamentous protein MTs which was driven by kinesin motors. At first, I attempted to control the persistency in motion and direction of the microrobot under photoirradiation without interrupting the interaction between MT and kinesin which was the most challenging task. This work will advance the ability to control persistency in the motion of kinesin driven MTs which in turn is expected to contribute to the study of collective behavior exhibited by self-propelled particles or active matters. Then photoregulated collective motion i.e. swarming of the microrobots was explored using two complementary *p*DNA through DNA hybridization and systematically investigation also carried out on the effect of related physicochemical parameters on the swarm robots. At last, after successful optimization of the conditions for the swarm robot, I established it as a well-controlled active cargo transporter and regulate the cargo pickup-transport-unload effectively in a programmable and spatiotemporal manner. This work would help to develop complex microdevices utilizing swarming of microrobots in a bottom-up manner giving rise to new emergent functions in the microrobotics as well as in robotics.

1.2 The emergence of molecular robotics

A robot can exhibit complex tasks with the programmed manner by sensing, processing and actuating.[1,3] (**Figure 1.1**) In other words, the robots are the mechanical systems that depend on their functions on computing, store internal representations of their goal and coordinate sensing and any actuation of components required in response. Almost all mechanical robots are macro-sized and developed in a top-down fashion.[31] Due to the large size and low robustness, they restrict their utility at the micro-level.[6]

In the last two decades, robotics widens its field and entered into the micro level to emerge a new discipline, microrobotics through the fusion of various fields e.g. supramolecular chemistry, nanotechnology, chemical engineering, biomolecular engineering etc.[5] (**Figure 1.2**) Microrobot can be defined as an integrated system formed through the combination of different

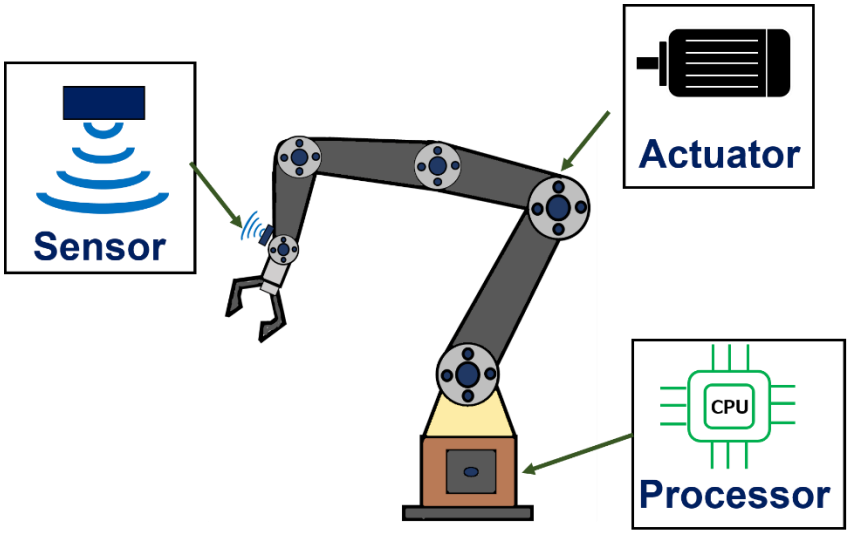

Figure 1.1 Schematic representation of the three basic components of a robot-sensor, actuator, and processor.

microdevices.[32] The realization of micrometer-sized robots assembled from these components is one of the ultimate goals to construct bioinspired microrobots on a molecular basis. The microrobots consisting of molecular actuators, sense to their environment by receiving molecular signals and making decisions with molecular processors are termed as molecular robots.[7,33] Their invention opens a new paradigm in the field of robotics as molecular robotics.

Unlike molecular machines at a supramolecular level, molecular robotics enables the more flexible design of self-assembled complex molecular systems by bringing nano-design

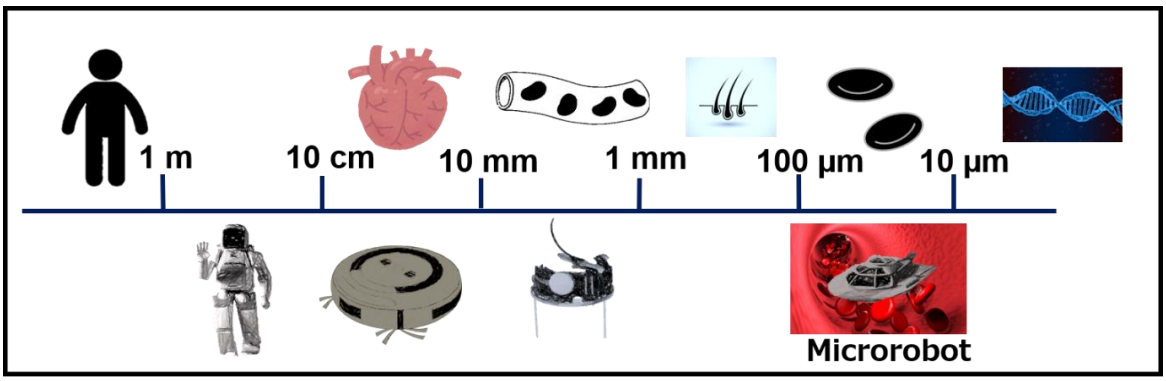

Figure 1.2 Comparison of the size of robots that range from the meter to micrometer scale. Here microrobots are of micrometer-scale.

technologies and programming technologies into the field of supramolecular machines.[29,34] Several attempts have been explored to build such robots in an artificial environment using actuators like natural, chemically or mechanically powered self-propelled objects.

In the mechanically powered microrobots, the mobility is remotely actuated, powered, and steered. Several investigations have been performed on magnetically driven,[22,35] acoustic powered[36,37] and optical powered[38] microrobots. Among them, magnetic field became the most viable source of actuation towards bioengineering applications of robots because of their advantages: no contamination in the biological substances, no direct contact, and precise positioning ability.[6] J. Li et al. constructed a magnetically driven microrobot with a burr-like porous spherical structure that was fabricated using 3D laser lithography to achieve in vivo transport and delivery of targeted cells.[20] The magnetic gradient field–driven mechanism was used so that the robot design was not constrained by the robot shape, providing flexibility in considering different robot structures for carrier cells. It was coated with Ni to achieve magnetic actuation and Ti to ensure biocompatibility. But in the magnetically driven molecular robots, the rate of change in gradient fields and the specific absorption rate could potentially cause tissue damage by heating. As a result, it is essential to take such safety concerns into account while optimizing the magnetic components of microrobots to remain within acceptable levels of magnetic field and gradient exposure set by regulatory guidelines.

In the self-propelled chemical microrobots, all components are typically synthetic, and the robot uses existing chemical energy from the microenvironment, e.g., a fuel, to power the mobility, sensing, and other functional capabilities.[39] The source of the input energy could be either organic, e.g., glucose, or inorganic, e.g., hydrogen peroxide, depending on the type of the catalyst used to process it. Most of the efforts along this line have so far focused on developing various types of micromotors, which can undertake the chemical conversion to release the energy stored in the chemical bonds, and then convert this free energy to do work in the form of directional motion. As inertia plays a negligible role in the propulsion of the low Reynolds regime, the chemical conversion needs to be continuous in order to sustain motion.

These mechanically or chemically powered molecular robots have so far lacked an integrated intercomponent communication and control, which requires more rigorous out-of-the-box thinking. Due to these limitations, scientists have focused on the natural self-propelled objects

as actuators for the development of molecular robots in highly robust and adaptive manners.[40] Their onboard machinery are continuously converting the available chemical energy in their surroundings into mechanical work and can regulate its power output by responding to forces, mechanical strain, and chemicals in their environment through highly sophisticated control pathways. In this way, a self-propelled biomolecular motor system, the smallest natural machine could be an appropriate approach for the actuation of the microrobots.

1.3 Self-propelled biomolecular motor system as an actuator

Biomolecular motors systems are the smallest natural machines which are known as the active workhorses of cells.[41] They are complexes of two or more proteins that convert chemical energy, usually in the form of the high-energy phosphate bond of adenosine triphosphate (ATP), into directed motion.[42] They consist of cytoskeletal filaments and biomolecular motors. (**Figure 1.3**) The cytoskeletal filaments, a component of the cytoskeleton in the eukaryotic cell, are micrometer-sized filamentous proteins polymerized from monomer proteins.[43] For example,

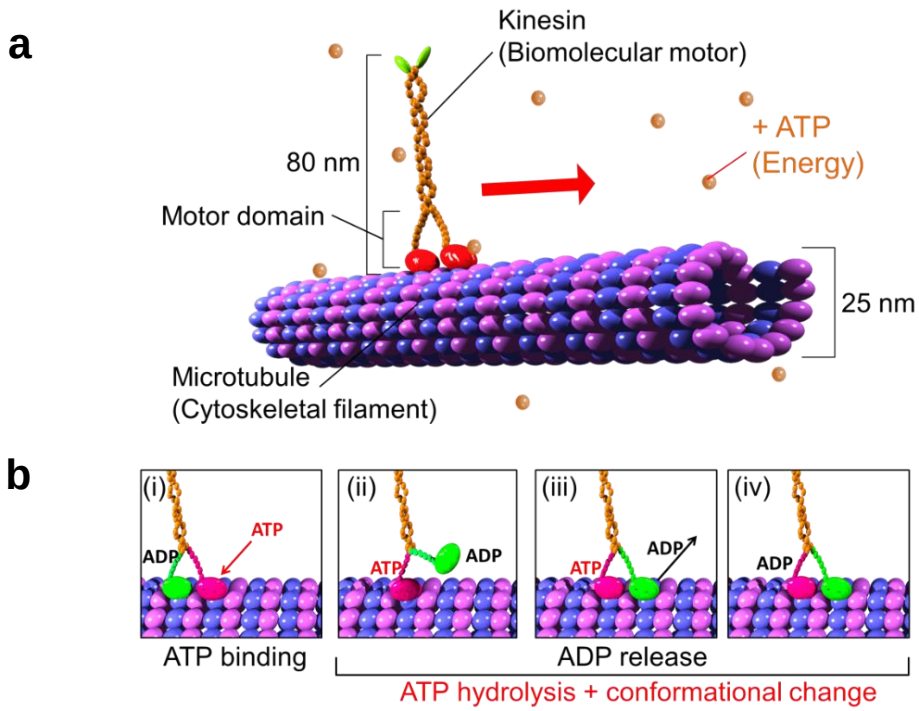

Figure 1.3 Schematic image of biomolecular motor system **(a)** structure of kinesin on MT track and **(b)** the movement of kinesin on the MT by ATP hydrolysis.

microtubule (MT) and F-actin are polymerized from tubulin and G-actin, consuming guanosine triphosphate (GTP) and ATP respectively.[44] In contrast, biomolecular motors such as kinesin/dynein and myosin are kinds of cytoskeletal filaments associated proteins and they move along MT and F-actin respectively.

The reason for the existence of biomolecular motors in cells is slow diffusion is for the efficient transport of molecules from its origin, typically near the nucleus, to where they are used, often at the periphery of the cell. For example, the passive diffusion of a small protein to the end of a 1-meter-long neuron would take approximately 1000 years, yet kinesin moves it in a week. This corresponds to a speed of 1-2 μm/s, which is typical for biomolecular motors.[45] In this study, I focused on the MT-kinesin system for its wide range of use.

MT, known as cytoskeletal 'track' are hollow cylinders polymerized of α, β-tubulin heterodimers.[46] During polymerization, tubulin dimers bind head-to-tail to form linear protofilament (PF) with an 8 nm repeat distance and a variable number (10-18, often 13) of PFs assemble into a cylindrical structure with an outer diameter of about 25 nm and a length of many micrometers[47] (**Figure 1.4**). Since the PFs bind to each other in the same orientation, the MT also develops structural polarity. The end exposing α-tubulin is slow-growing and called the minus end, and the fast-growing end exposing β-tubulin is named the plus end. The lateral inter-PF contacts are mostly electrostatic, but the intra-PF interactions (-αβ- αβ-) are hydrophobic.[48] The structural properties of MTs are critical to their cellular functions as well as their

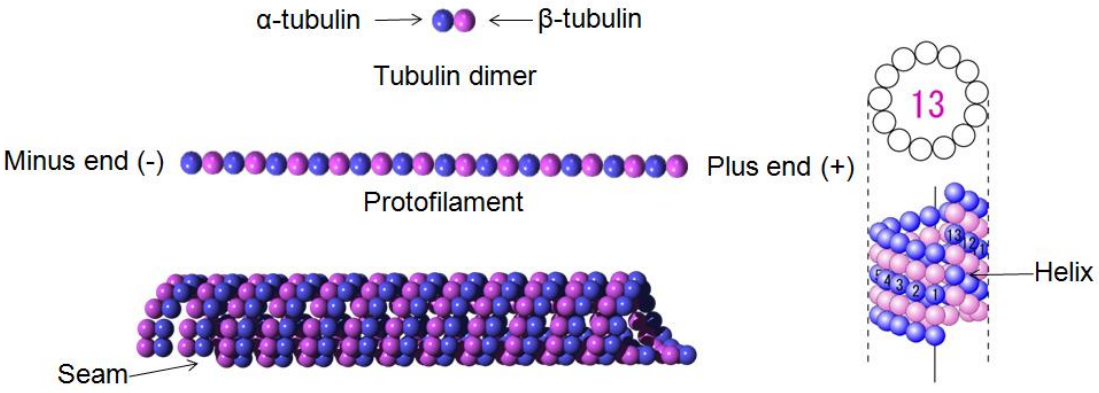

Figure 1.4 Schematic image of the helical structure of a MT formed by 13 laterally associated protofilaments of tubulin dimers.

nanotechnological applications.[49] MTs serve as scaffolds for a wide variety of MT-associated molecular motors or 'trucks' (i.e. kinesin and dynein families) in the cell.

These motors utilize chemical energy from ATP to generate mechanical motion. The motor protein, kinesin is a homodimer containing two heads-globular domains each of which has an ATP and a MT binding site.[50] It is a tetramer of two identical heavy chains and two associated light chains. The heavy chains fold into two globular heads at one end, a stalk with a hinge in the middle, and a tail domain at the other end. The heads step on the binding sites along with the MT PFs. These sites are spaced 8 nm apart.[51,52] Thus moving the entire molecule 8 nm in each step in a hand-over-hand mechanism. For every step, kinesin consumes one ATP molecule. Kinesin-1 motors are primarily involved in intracellular transport of vesicles and organelles, cell division, and the organization of cilia and flagella.[53] The kinesin-1 (conventional kinesin) is of particular utility in nanotechnology because its primary function is the exertion of force. Micromechanical recordings from single kinesin-1 molecules indicate that one motor can exert a force as great as 5 pN.[50] The efficiency of kinesin is in the order of 50%, considering the free energy available from ATP hydrolysis. Because of its high degree of processivity, even a single kinesin molecule is capable of propelling MTs along a surface. The small size and high efficiency of the biomolecular system make it fascinate to apply it as molecular devices for a wide range of purposes which become possible in a synthetic environment such as motility assay system.[54,55]

1.3.1 *In vitro* motility assay of the biomolecular motor system

The *in vitro* motility assay is the most promising setup for nanotechnological usage of the biomolecular motor system.[56,57] To investigate their property in *in vitro*, motor proteins and their associated cytoskeletal filaments have been fabricated on the same substrate by the latest technological advancements (**Figure 1.5**). Sheetz *et al* observed the movement of myosin coated fluorescent beads for the first time on F-actin fixed substrate.[58] Vale and his colleagues exposed the unidirectional gliding motion of MTs in the cell extract from squid axon on a substrate driven by biomolecular motors (kinesins and dyneins).[59] The method was termed as "*in vitro* motility assay" due to the direct observation of the gliding filaments which brought a revolutionary change in the investigation of the property of biomolecular motor systems. Later,

Spudich developed a similar *in vitro* motility assay where motility of F-actin on a glass surface coated with myosin was demonstrated.[60]

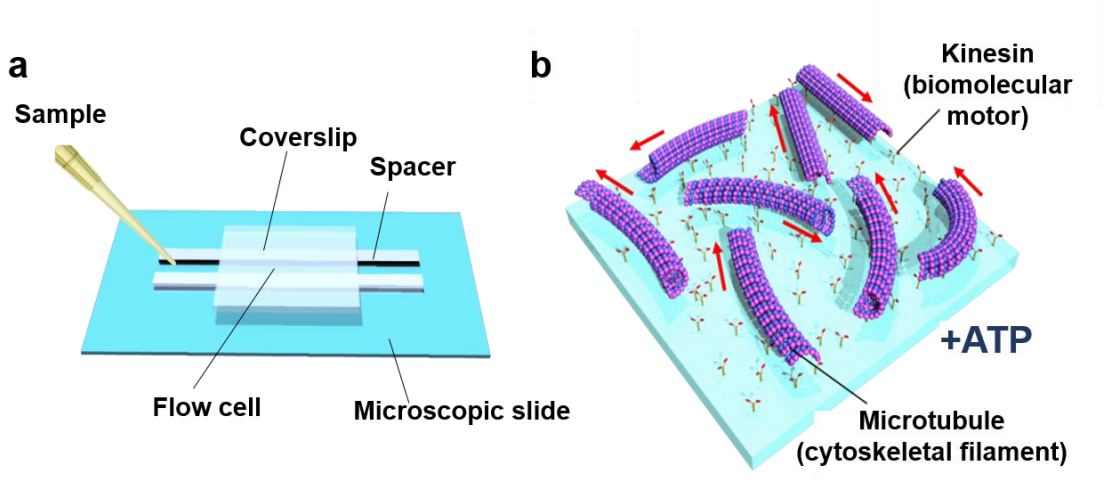

Figure 1.5 Schematic image of **(a)** a flow cell preparation using coverslip and microscopic slide **(b)** *in vitro* gliding assay of MTs on kinesin coated surface.

In MT gliding assays, surface-immobilized motor proteins drive MT propulsion which is widely used to study basic motor properties as well as the collective behavior of active self-organized systems. Additionally, these assays can be employed for nanotechnological applications such as analyte detection, biocomputation, and mechanical sensing. Biological motors (e.g. kinesins, dyneins) load/unload cargoes (e.g., vesicles, proteins) without external stimuli, and transport them along MTs by using the energy of ATP hydrolysis within eukaryotic cells (*in vivo*).[61] Because of these amazing biological capabilities of autonomous loading/unloading and transport of specified cargoes, there is considerable interest in incorporating kinesins and MTs into artificially created (*in vitro*) transporters and actuators in nanometer- or cell-scale systems and applications.[62,63] Such a system assisted to create highly miniaturized on-chip systems such as molecular sorters, molecular sensors, and molecular communication systems.[64] But in these applications, the biggest hurdle is to control the gliding motility of the biomolecular motor system.[76]

1.3.2 Controlling the gliding motility of biomolecular motor system

Gliding motility of the biomolecular motor system is very significant for their applications as they provide detailed data on the directionality, speed and force generation of molecular motors. With recent progress in nanotechnology, *in vitro* gliding assay has been attracting interest in serving the smallest autonomous moving objects. However, for use in nanotechnological applications, the movement of gliding filaments must be controllable in systematically and spatiotemporally.

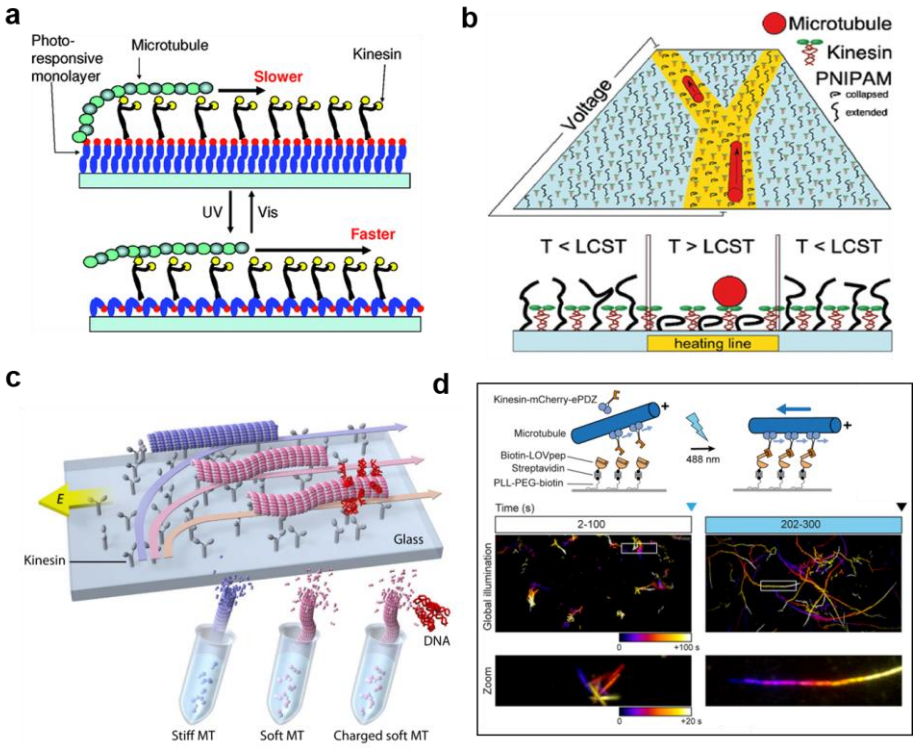

Figure 1.6 Schematic representations of **(a)** photocontrol of the mobility of MTs on a photoisomerizable monolayer surface.[81] **(b)** guiding direction of MTs by electrically heated polymer tracks on the substrate.[80] **(c)** controlling the trajectories of MTs under a given electric field.[67] **(d)** light-controlled MT propulsion where LOVpep domain of kinesin facilitates the controlled MT gliding upon blue light illumination.[82] Images are used with permissions from ref. 67, 80, 81, 82.

Several methods have been developed to control the motility of MTs driven by kinesin in *in vitro* through electric field manipulation,[77] heat-responsive polymer tracks utilization[78] and also

magnetic field application[79]. Besides, the control on MT gliding has been achieved using a light-to-heat converting layer in combination with heat-responsive polymers that compact upon heating and allow access of MTs to surface-attached motors.[80] Furthermore, photosensitive switches fused to inhibitory peptides have been used to control kinesin dependent motility with light. [81] However, the majority of these methods require extensive surface alterations or complicated molecular engineering, leaving simultaneous spatial-temporal and systematic control of force generation on non-predefined patterns underdeveloped. (**Figure 1.6a-b**) Some methods also limit the control of motility of MT only one destination; without an active control where all MT behave in the same manner and glide toward the same destination. Yokokawa et al. established a bottom-up methodology to control the gliding of MT to two different destinations as a highly efficient MT sorter under a single external field.[67] They developed both the electrical and the mechanical properties of MTs altering the stiffness simultaneously to control the gliding directions. In addition to the bottom-up designs of the MT electrical and mechanical properties, they took a top-down approach to design a microfluidic device that separates MTs according to measured radii of trajectory curvatures (**Figure 1.6c**). This integrated approach allowed to guide two types of MTs toward two different destinations, it requires complicated molecular engineering and difficult to integrate two properties in the MTs of the same system.

To control the MT gliding spatiotemporally, Kapitein *et al*. reported on local activation of MT gliding by direct light-inducible recruitment of kinesins to the surface ((**Figure 1.6b**)).[82] The interactions were based on tunable, light-controlled interacting protein tags (TULIPs) to reversibly control local protein recruitment *in vitro*. The recombinant protein was generated by fusing TULIPs to induce local heterodimerization under the control of blue light (λ=480 nm). Their approach allowed spatiotemporal control of MT gliding on homogeneously coated surfaces providing an adaptive platform to manipulate MT motility.

In this study, I explored a simple method to control the motility of biomolecular motor based microrobot without interrupting the interactions of MT-kinesin as well as complex surface modification. These approaches could be effective from studying the basic properties of motor proteins to the exploration of collective behaviors of self-organized systems.

Alongside with many applicable features of self-propelled biomolecular motors, they can exhibit self-propelling in collective behavior as groups.[83,84] Controlling their collective behaviors, a new dimension could open in the field of biomolecular motor based microrobotics as swarm robotics.[13] Developing a swarm robot at the molecular level would provide a new concept to understand and utilize the swarming phenomenon that is observed in nature.

1.4 Utilization of biomolecular motor system in artificial swarming

Swarming, one of the most fascinating phenomena in nature is a collective behavior exhibited by the self-propelled living organisms e.g. colonies of bacteria and ants, school of fish, or flocks of birds etc.[85–88] (**Figure 1.7**) The swarming pattern is generally emerged by the mutual interaction among the nearest neighbors moving with almost the same motion and direction in a dispersed manner. Three types of interactions such as attraction, repulsion and alignment are prerequisites for swarm formation.[89,90] Instead of having a sophisticated controller for a whole swarm system, local interactions among many unsophisticated single entities play a vital role in the emergence of such swarms.[91]

The self-organization of thousands to unlimited individual objects give rise to the emergent functions like parallelism, robustness, scalability and flexibility.[92] Parallelism enables the sharing of tasks by generating groups, robustness benefits to ensure that tasks are performed properly, and flexibility permits the swarm to respond instantaneously to their environments. This coordinated manner is facilitated to solve complex problems and to complete tasks for the living system that transcend individual capabilities. For example, a colony of ants can collectively achieve complex tasks such as constructing nests and gathering large prey; herrings

Figure 1.7 Swarming of living organisms in nature as fish school, bird flocks, honeybee swarms and ant colony (from left). Courtesy: https://en.wikipedia.org/wiki/Swarm_behaviour.

swimming in a grid can successfully capture very alert and evasive copepods in a synchronized way.[93,94]

They interact within a definite range by altering their direction of motion involving an effective alignment. The dynamic organization of the single entities into a large pattern and again dispersion into single entities retaining their individuality makes the whole system unique to work in a more sophisticated manner.[95]

Recent advancements in microrobotics ensure two major advantages in swarming of the microrobots: since microrobots are fabricated mostly from the molecular parts and their size is limited within the micro-scale.[13] Besides, allowing small individuals to interact with each other and produce a more complex, collective task, which is difficult for a single entity. This, in turn, further facilitates an opportunity to employ a large number of robots to work in a concerted fashion. Self-propelled biomolecular motor systems have been particularly promising for realizing such artificial swarming because of their small size, efficiency, and scalability. Recent studies have demonstrated some aspects of swarming behavior by controlling the mutual interactions of the propelled filaments using associated proteins,[96] depletion agents,[84] crowding effects,[97,98] or ligand–receptor-based crosslinking.[99–101] These interactions lead to the emergence of fascinating swarm patterns, such as bundles, spools, vortex lattices, zigzag patterns as well as circular or polar patterns(**Figure 1.8**). [102–105]

Self-assembly of moving MTs has been developed and vastly studied based on the *in vitro* motility assay by using strong non-covalent interaction e.g., streptavidin-biotin interaction or by using some kinds of cytoskeletal filament related proteins.[99,103,106,107] By using this method, a wide variety of assembled structures was obtained e.g. bundle, network, and ring-shaped structures that differ in size or shape. It was found that stiffer MTs with high bending rigidity favored the production of linear bundles while larger and longer bundles require more building blocks i.e; higher initial density of MTs. On the other hand, MT spools assembled from longer and flexible one is an example of such non-equilibrium structures, capable of storing bending energies on the order of 10^5 kT.[108,109] Phase diagram of ordered structures has thoroughly investigated and determined by changing the experimental conditions such as the density of MTs and the strength of interaction of streptavidin/biotin.[103]

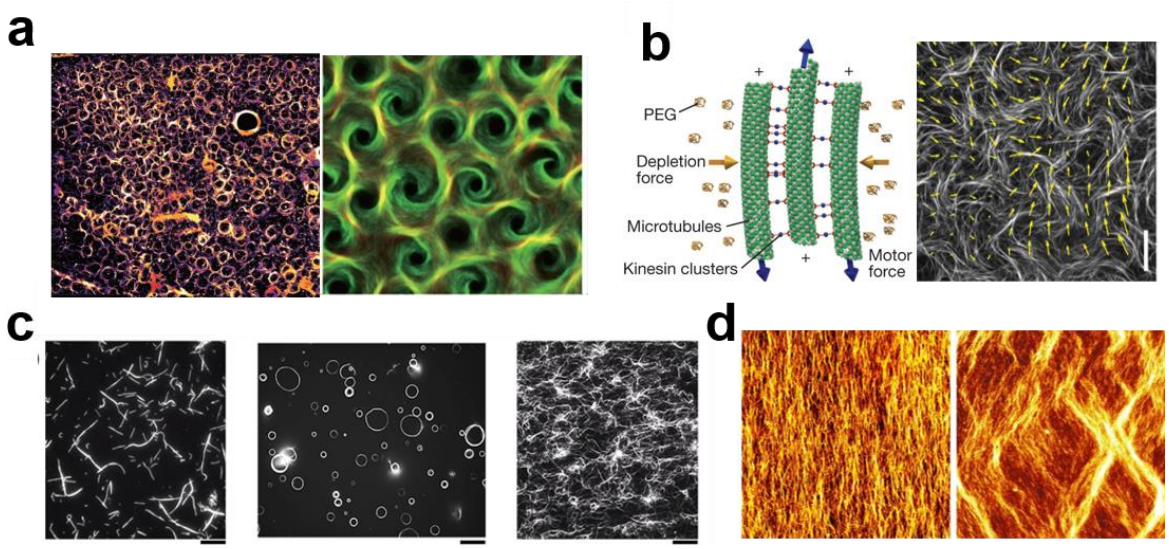

Figure 1.8 (a) Large sale vortex formation of collectively moving microtubules (b)Fluorescence image of an active microtubule network, scale bar: 80 μm. **(c)** Fluorescence microscopy images of MT bundles, rings, and networks produced in active self-assembly using streptavidin-biotin interaction. Scale bar: 10 μm. (d) Zigzag pattern formation of MTs under cyclic stretching stimuli. Images are used with permissions from ref. 102-105.

However, control over their collective behavior through a programmable manner is required to open an extensive opportunity for demonstrating tunable swarming with computing properties, which has not yet been achieved in these systems.[110] However, to get suitable linkers with the ability to combine with sufficient interaction strength, selectivity, reversibility, and capability to provide sensing and processing to the biomolecular motors systems have been always the biggest challenge.[111] In this way, a natural programmer DNA could be the most appropriate linker with all the capability to program swarming in the biomolecular motor system.

1.5 DNA as an information processor in artificial swarming

DNA, a versatile tool to store genetic information with high molecular recognition ability has enormous potential for molecular computing depending on base sequence information.[112,113] Biomolecular engineering mainly depends on the programmability of Watson-Crick base pairing combining with a decrease in the cost of synthesis. Structural simplicity and controllable binding interactions of DNA by four base units (adenine, (**A**), cytosine (**C**), guanine (**G**),

thymine (**T**)) result in a simple structure and predictable behavior.[114] (**Figure 1.9**) Other than these structural features two important and exclusive properties make DNA suitable for molecular level constructions such as molecular recognition and self-assembly.[115]

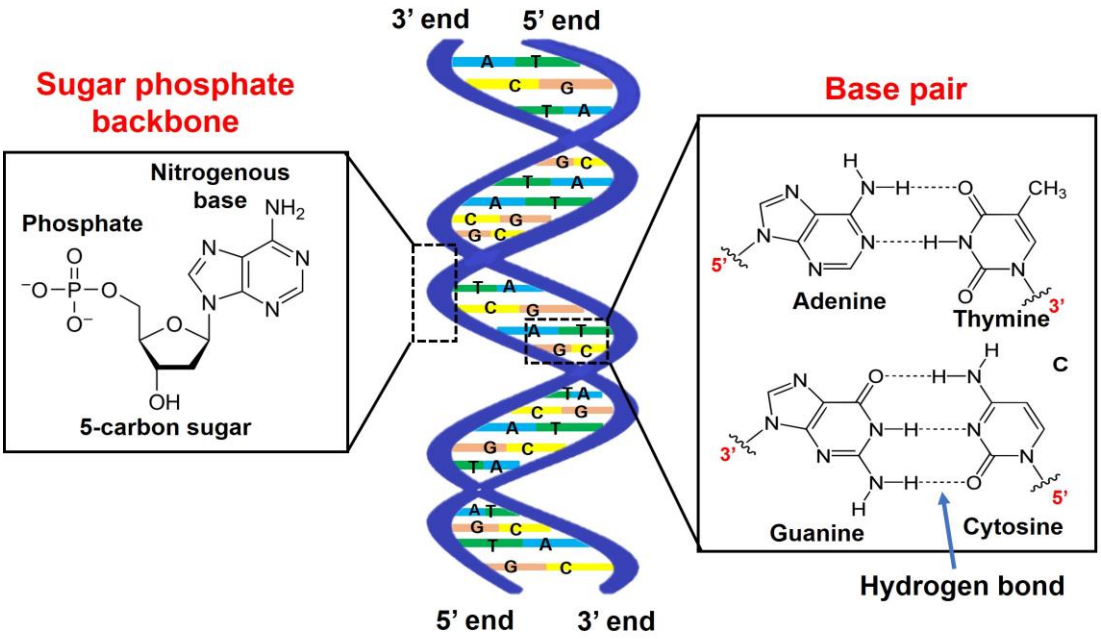

Figure 1.9 Schematic representation of the DNA double helix showing the sugar phosphate backbone and base pair.

The pioneering efforts of Seeman in DNA nanotechnology[116–121] and the revolutionizing work of Rothemond on DNA origami[122–124] paved the way to enable the rational design of DNA nanostructures. Adleman demonstrated the use of DNA to perform logical operations by solving a complex mathematical problem using only DNA oligonucleotides.[113] The self-assembly behavior of DNA was further computed to design different logical operations for engineering complex structures and exploit their functions. This attractive phenomenon of programming of DNA was further used for engineering the self-assembly of different building blocks to enhance their functionalities with higher-ordered structures. DNA programming was also successfully applied in DNA template self-assembly of other functional materials like nanoparticles and proteins.[125] Higher-order structures that originate from the specific and reversible DNA-directed self-assembly of microscopic building blocks hold great promise for future technologies. Applications of these self-assembly strategies span from photonics and plasmonics to

biosensing and gene therapy.[126–128] Moreover, the same self-assembly strategy has been applied to compliant Brownian units, including emulsion droplets, lipid vesicles, time dependent assembly of functional clusters that result in rationally designed mesoscopic structures.[129] The concept of molecular robotics is also rooted in DNA molecular computing and then facilitated by the development of DNA origami.[33] The first step in molecular robotics was the development of DNA walkers, which have developed from being non-autonomous to being capable of directed but brief motion on the one-dimensional track.[11,130] These walkers are powered by energy derived from DNA hybridization, consuming fuel oligonucleotides as they move from one binding site to another on a DNA-modified surface.

DNA has been used in combination with biomolecular motors either as a glue to assemble motors into multimers, or to connect motors to DNA origami scaffold, or being conjugated to MTs for cargo loading/unloading.[65,72,111,131] In spite of extensive studies on DNA based microrobotics, before 2018 there was no such report of DNA programmed swarming of biomolecular motor based microrobots.[13,30]

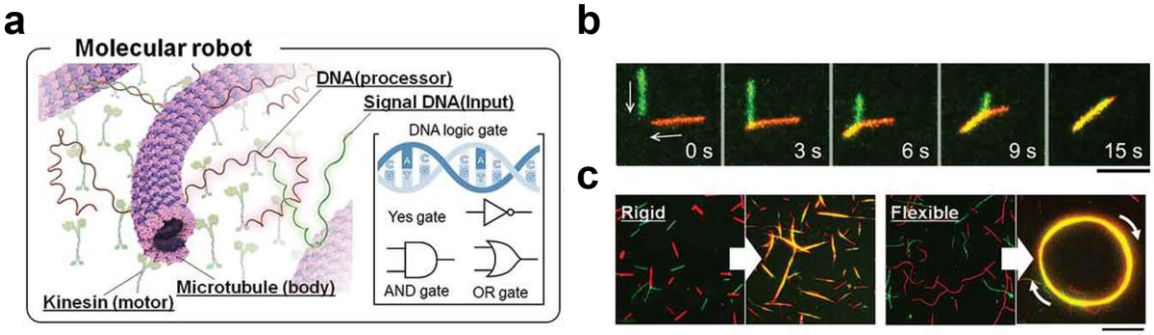

Figure 1.10 Swarming of molecular robots (a) MTs are conjugated with single-strand photoresponsive DNA with a complementary sequence. (b) Swarming formation of gliding MTs on a kinesin coated substrate through self-organization due to the hybridization of complementary DNA sequences. (c) The pattern of swarm can be tuned by simply changing the mechanical properties of MTs. Scale bar: 20 μm. Images are used with permissions from ref. 8.

For the first time, biomolecular motor based microrobot 'molecular robot' was constructed using DNA as information processor where DNA can program the swarming in a reversible manner to form 'molecular swarm robot'(**Figure 1.10**).[13,30] Swarming of molecular robots was realized by utilizing the molecular recognition ability of DNA in controlling local interactions

between molecular robots. DNA-based computation was used not only for swarm formation, but also for dissociation of the swarms into single molecular robots. The input signal of dissociation DNA prompted the groups of molecular robots to separate into single robots through strand displacement reaction of the complementary DNA of neighbor robots. But these systems limits the reversible regulation of the swarming. By incorporating photosensitive azobenzene moiety into DNA strands, the swarm formation by molecular robots and dissociation of swarms was controlled using light.

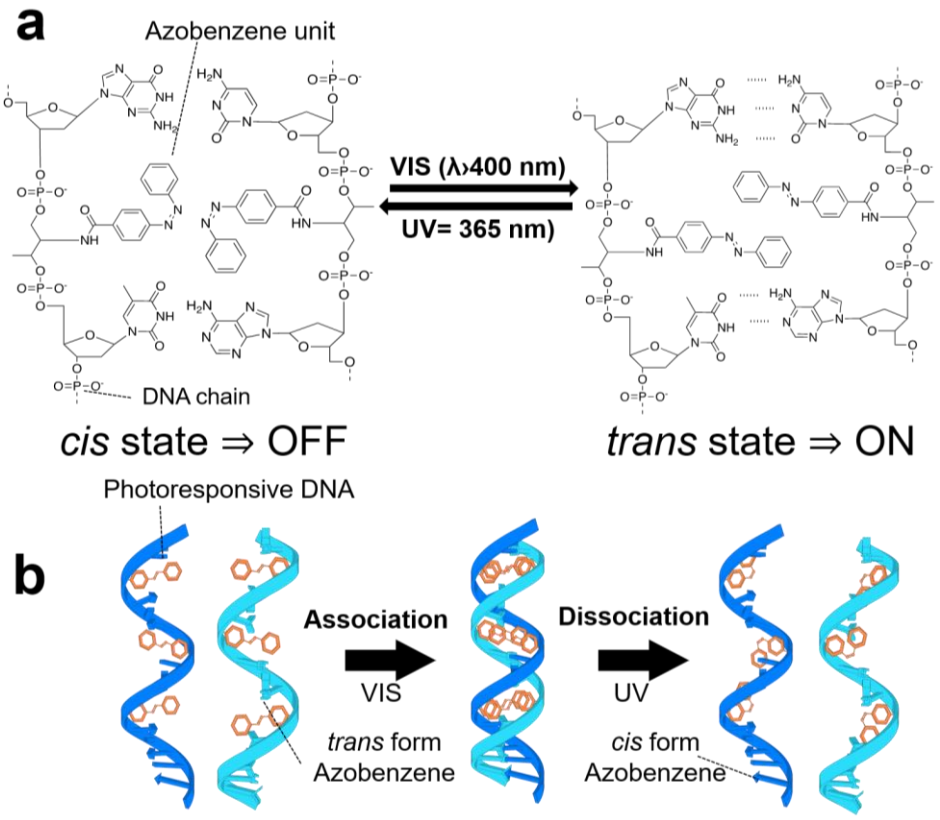

Figure 1.11 Association and dissociation of DNA duplex in response to light. (a) Reversible hydrogen bonding of photoresponsive DNA (*p*DNA) by light-induced *cis–trans* isomerization of azobenzene (b) DNA duplex formation and dissociation under VIS-UV light irradiation.

Azobenzene is the photoresponsive molecule which undergoes isomerization under UV-VIS light. If azobenzene is incorporated to the DNA strand, under VIS light it converted to the planar *trans* form which intercalates the DNA base sequences **(Figure 1.11)**. The intercalated

planar azobenzene stabilizes the duplex through the stacking mechanism. Under UV light the *trans* form converts to the cis form. In the *cis* form, the non-planar azobenzene destabilizes the DNA duplex and facilitates the duplex dissociation. After modification of the azobenzene incorporated DNA to the MT, the swarming of the MTs was regulated in a reversible manner in response to light.

However, the direct control over swarming of the biomolecular motor system was demonstrated by assisting the chemical and physical signal of DNA, still there are some limitations to well-control the system in a specific time and region and apply this system for further applications. Physical signal of DNA has further advancements over the chemical signal such as non-invasiveness, spatiotemporal precision-accuracy, stability and so on.[132,133] Therefore, in this study, I addressed a detailed, systematic and spatiotemporal regulation of the swarming of the molecular robot. But the main challenge is to let the molecular swarm robot work.

1.6 Applications of molecular swarm robot in active transport

It has been always a challenge to construct a micro-sized robot at a molecular level with the ability to work miniaturing the macro robot.[134] Modern-day factory assembly lines often feature robots that pick up, transport and unload components in a programmed manner.[135] The transport of molecules, supramolecular complexes, and nano- or microparticles by a molecular robot could be a prime application in nanotechnology and also in bioengineering and healthcare.[6,18–20,20,21,38,134,136]

The idea of manipulating molecular cargo similarly has to date only been explored using chemical synthetic atoms or biological building blocks. Leigh et al. reported on a molecular robot that could selectively transport molecular cargo in either direction between two spatially distinct, chemically similar sites on a molecular platform.[17] Each robot can manipulate a single molecule and is made up of just 150 carbon, hydrogen, oxygen and nitrogen atoms **(Figure 1.12a)**.

Xie et al. reported on microrobot swarm formation from the colloidal particles energized by external magnetic fields.[26] A variety of intriguing microrobotic swarm was exhibited ranging from dynamic self-organization to coherent motion; i.e. liquid, chain, vortex, and ribbon that enabled fast and reversible transformations between them **(Figure 1.12c)**. The reconfigurable

microrobot swarms provide versatile collective modes to address environmental variations or multitasking requirements by passage through narrow channels (chain formation), coordinated handling of large loads (vortex formation), and large-area synchronized manipulation (ribbon formation). However, these chemically powered microrobots could limit its further application in a nanotechnological engineered system, which could be improved by using natural molecular devices.

A cargo sorting DNA molecular robot was reported recently with the ability toerform autonomous cargo transport using three modular building blocks.[12] The robot explored a two-dimensional testing ground on the surface of DNA origami, could pick up multiple cargos from unordered locations, and delivered each type to a specified destination until all cargo molecules are sorted into two distinct piles **(Figure 1.12b)**.

But the slow-motion and poor efficiency of cargo sorting are the main drawbacks of this system which could be achieved by integrating motor proteins and launching simple communication between the robots for performing even more sophisticated tasks.[12] With more effort in developing modular and collective microrobots, and with simple and systematic approaches, molecular robots could eventually be easily programmed like macroscopic robots but working in microscopic environments.

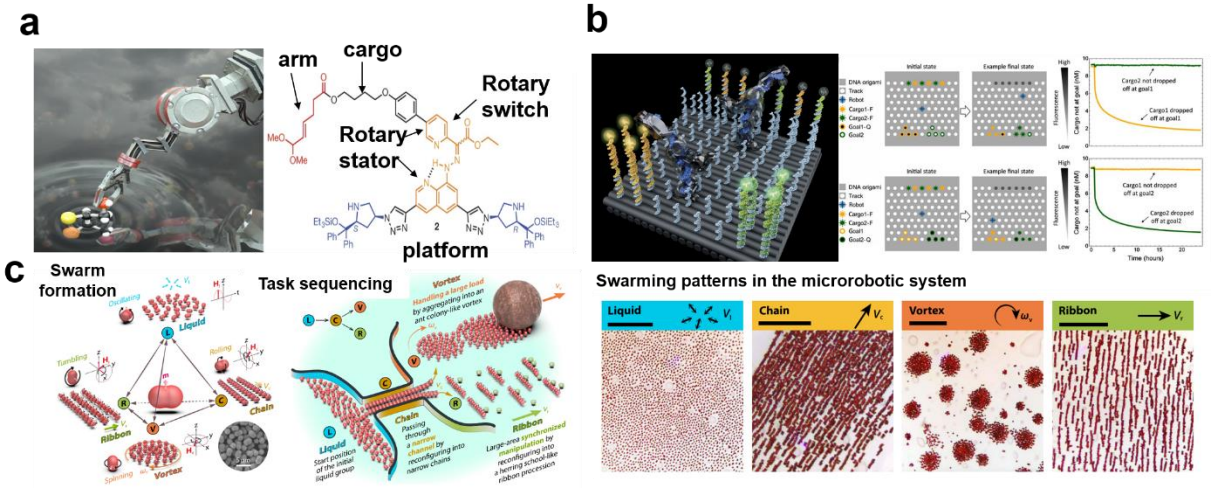

Figure 1.12 (a) The first molecular robot which can move molecule as cargo[17] **(b)** The cargo sorting DNA robot which can pick up two different types of cargo and deliver into the desired

location[12] **(c)** The magnetic microrobot swarm which can exhibit liquid, chain, vortex and ribbon-like collective behaviors.[26] Images are used with permissions from 12, 17 and 26.

No direct control of cargo loading, transportation and unloading by molecular swarm robot had been addressed yet except for the biomolecular motor based active transport system instead. Biological motors (e.g. kinesins, dyneins) can transport cargoes (e.g., vesicles, proteins) without external stimuli along MTs by using the energy of ATP hydrolysis within eukaryotic cells (*in vivo*).[61] Because of these amazing biological capabilities of autonomous loading/unloading and transport of specified cargoes, there is considerable interest in incorporating kinesins and MTs into artificially created (*in vitro*) transporters and actuators in nanometer- or cell-scale systems and applications.[62,63] Such a system assisted to create highly miniaturized on-chip systems such as molecular sorters, molecular sensors, and molecular communication systems.[64]

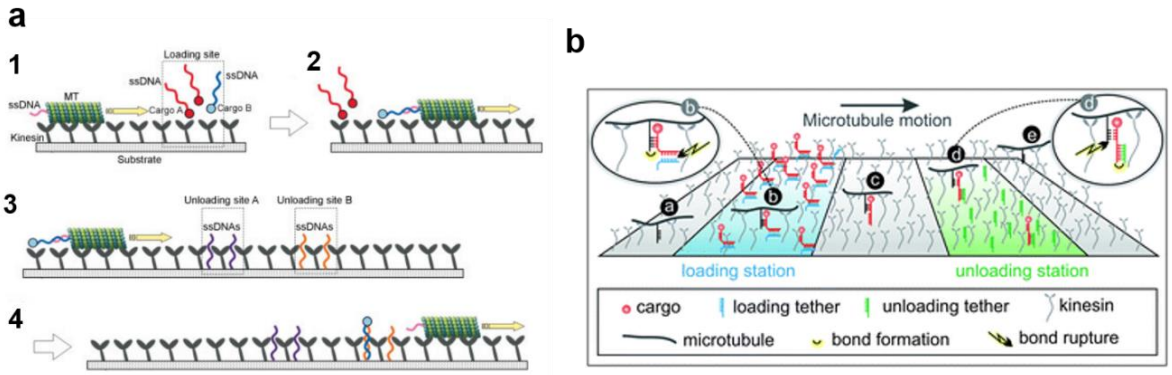

Figure 1.13 Cargo transport by the biomolecular motor system in *in vitro*. **(a)** Schematic diagram of a molecular transport system where MT labeled with DNA glided on kinesin surface and load a complementary DNA modified cargo[72] **(b)** Cargo pick-up from loading station, transport and discharge at unloading station by biomolecular motor based molecular shuttles.[73]. Images are used with permissions from ref. 72 and 73.

Cargoes can be attached to the kinesin-gliding MT tracks using different strategies in i*n vitro system*. Many tried to utilize the avidin-biotin or antigen-antibody bindings for cargo attachment but these bindings could limit the cargo unloading owing to their strong non-covalent interaction.[65–69] There were several reports on the external stimuli such as UV exposure,[66] ligand supplementation,[70] restriction enzyme digestion,[71] or temperature fluctuation to unload cargoes from gliding MTs, which restricts the autonomous behavior. The utilization of DNA hybridization took one step further in the reconstituted autonomous molecular transport system.

Hiyama et al. reported on an autonomous molecular transport system that loaded/unloaded specified cargoes using DNA hybridization and transported them using the reverse geometry of MT motility on kinesins (**Figure 1.13a**).[72] For achieving the directional transport of cargoes, preconfigured microlithographic tracks were used for controlling the transport direction of cargoes loaded onto gliding MTs.

Vogel et al. first demonstrated the cargo loading/unloading on one integrated surface by preparing two patterns with different surface functionalities to ensure the spatial separation of loading and unloading chemistries (**Figure 1.13b**).[73] A DNA functionalized MT passed the cargo loading station where the cargo was immobilized using double-stranded DNA in a zipper geometry, then attached the cargo with shearing geometry. Then cargo was transported to the unloading station by gliding MT and unloaded the cargo to the unloading station *via* shearing geometry.

Despite several extensive studies on the cargo transport system, cargo loading/unloading efficiency was found very low in the existing systems. Another disadvantage is the cargo loss caused by spontaneous dissociation of cargo from the MT which decreases the efficiency of cargo transport.[73–75] Utilization of single MTs limits the loading-unloading efficiency and cargo transport for a long distance in these biomolecular motor based cargo transport system or molecular shuttle system. Again these systems lack of spatiotemporal control of cargo unloading and cargo accumulation in a specific area. So the limitations of the biomolecular motor based active transport has inspired the utilization of molecular swarm robot in the further application in nanotechnology as an efficient molecular cargo transport system.[130]

1.6 Dissertation outline

In this dissertation, the development of a photoregulated molecular swarm robot combining a self-propelled biomolecular motor system with DNA and utilize them as a molecular cargo carrier system have been studied in detail. The results have been summarized in 5 chapters including general introduction and concluding remarks.

In **chapter 1**, the purpose of this dissertation and the background of this study are described. The development of microrobots in the field of robotics and its applications are also reviewed.

In **chapter 2**, the construction of photoregulated microrobot and the effect of light on their persistency of motion are addressed. Molecular robots were constructed using cellular proteins like MTs and kinesins as the actuators, DNAs as the information processors, and azobenzenes as the photosensors. Persistency of motion of robots was reversibly regulated by light without interrupting the interaction between MT and kinesins. Besides, photoresponsive DNA (*p*DNA) was utilized as a shield for MTs against damage by UV irradiation.

In **chapter 3**, the development of photoregulated swarming of microrobots are described. Complementary DNA conjugated microrobots exhibit swarming in response to the visible-UV light in a reversible manner. The effect of related physicochemical parameters was systematically investigated on the molecular swarm robot. Varying different physicochemical parameters, molecular swarm robot was regulated responding to the light signal. Again, swarming was regulated in local regions using photomasks through the UV light source.

In **chapter 4**, the formation of a photoregulated molecular swarm robot as a cargo transporter is revealed. How they load, transport and unload cargoes efficiently responding to the photo signal are also described.

In **chapter 5**, all the important results and future aspects of this research work have been summarized in the concluding remarks.

REFERENCES

1. Boden, M. *et al.* Principles of robotics: regulating robots in the real world. *Conn. Sci.* **29**, 124–129 (2017).

2. Yang, G. Z. *et al.* The grand challenges of science robotics. *Sci. Robot.* **3**, 3, 14, eaar7650 (2018).

3. Critchlow, A. K. Introduction to robotics. New York:Macmillan Publishing Co (1985).

4. Koren, Y. Robotics for Engineers. (2014). doi:10.1109/TSMC.1986.289270

5. Ricotti, L. & Menciassi, A. Nanotechnology in biorobotics: Opportunities and challenges. *J. Nanoparticle Res.* **17**, 1–10 (2015).

6. Ceylan, H., Giltinan, J., Kozielski, K. & Sitti, M. Mobile microrobots for bioengineering applications. *Lab Chip* **17**, 1705–1724 (2017).

7. Sato, Y., Hiratsuka, Y., Kawamata, I., Murata, S. & Nomura, S. I. M. Micrometer-sized molecular robot changes its shape in response to signal molecules. *Sci. Robot.* **2**, (2017).

8. Kabir, A. M. R., Inoue, D. & Kakugo, A. Molecular swarm robots: recent progress and future challenges. *Sci. Technol. Adv. Mater.* **21,** 323-332**,** 1 (2020).

9. Breguet, J. M., Driesen, W., Kaegi, F. & Cimprich, T. Applications of piezo-actuated micro-robots in micro-biology and material science. *Proc. 2007 IEEE Int. Conf. Mechatronics Autom. ICMA 2007*, 57–62 (2007). doi:10.1109/ICMA.2007.4303516

10. Hagiya, M., Konagaya, A., Kobayashi, S., Saito, H. & Murata, S. Molecular robots with sensors and intelligence. *Acc. Chem. Res.* **47**, 1681–1690 (2014).

11. Muscat, R. A., Bath, J. & Turberfield, A. J. A programmable molecular robot. *Nano Lett.* **11**, 982–987 (2011).

12. Thubagere, A. J. *et al.* A cargo-sorting DNA robot. *Science*, **357**, 6356, eaan6558 (2017).

13. Keya, J. J. *et al.* Control of swarming of molecular robots. *Sci. Rep.* **8**, 1–10 (2018).

14. Hara, Y., Maeda, S., Yoshida, R. & Hashimoto, S. Development of novel self-oscillating molecular robot fueled by organic acid. *2009 IEEE/RSJ Int. Conf. Intell. Robot. Syst.*

IROS 2009 2223–2227 (2009). doi:10.1109/IROS.2009.5354793

15. Kassem, S., Lee, A. T. L., Leigh, D. A., Markevicius, A. & Solà, J. Pick-up, transport and release of a molecular cargo using a small-molecule robotic arm. *Nat. Chem.* **8**, 138–143 (2016).

16. Nakakuki, T. Control system with biochemical reaction network and its application to molecular robotics. *5th International Symposium on Advanced Control of Industrial Processes (ADCONIP2014)*, 301-306 (2014).

17. Kassem, S. *et al.* Stereodivergent synthesis with a programmable molecular machine. *Nature*, **549**, 374–378 (2017).

18. Donald, B. R., Levey, C. G., McGray, C. G., Paprotny, I. & Rus, D. An untethered, electrostatic, globally controllable MEMS micro-robot. *J. Microelectromechanical Syst.* **15**, 1–15 (2006).

19. Corradi, P., Menciassi, A. & Dario, P. Space Applications of Micro-Robotics : a Preliminary Investigation of Technological Challenges and Scenarios. *Proc. 5th Round Table Micro/Nano Technol. Space, Noordwijk, Netherlands* (2005).

20. Li, J. *et al.* Development of a magnetic microrobot for carrying and delivering targeted cells. *Sci. Robot.* **3**, 1–12 (2018).

21. Xu, T., Yu, J., Yan, X., Choi, H. & Zhang, L. Magnetic actuation based motion control for microrobots: An overview. *Micromachines* **6**, 1346–1364 (2015).

22. Das, S., Steager, E. B., Stebe, K. J. & Kumar, V. Simultaneous control of spherical microrobots using catalytic & magnetic actuation. *Int. Conf. Manip. Autom. Robot. Small Scales, MARSS 2017 - Proc.* (2017). doi:10.1109/MARSS.2017.8001924

23. Hess, H. & Saper, G. Engineering with Biomolecular Motors. *Acc. Chem. Res.*, 51, 12, 3015–3022 (2018).

24. Van Den Heuvel, M. G. L. & Dekker, C. Motor Proteins at Work for Nanotechnology. *Science*, 317, 5836, 333-336, (2006).

25. Hess, H. & Bachand, G. D. Biomolecular motors. *Mater. Today*, **8**, 22–29 (2005).

26. Xie, H. *et al.* Reconfigurable magnetic microrobot swarm: Multimode transformation, locomotion, and manipulation. *Sci. Robot.* **4**, eaav8006 (2019).

27. Chowdhury, S., Jing, W. & Cappelleri, D. J. Controlling multiple microrobots: recent progress and future challenges. *J. Micro-Bio Robot.* **10**, 1–11 (2015).

28. Choi, Y. *et al.* High information capacity DNA-based data storage with augmented encoding characters using degenerate bases. *Sci. Rep.* **9**, 1–7 (2019).

29. Mc Laughlin, C. K., Hamblin, G. D. & Sleiman, H. F. Supramolecular DNA assembly. *Chem. Soc. Rev.* **40**, 5647–5656 (2011).

30. Keya, J. J. *et al.* DNA-assisted swarm control in a biomolecular motor system. *Nat. Commun.* **9**, 453 (2018).

31. Crespi, V., Galstyan, A. & Lerman, K. Top-down vs bottom-up methodologies in multi-agent system design. *Auton. Robots* **24**, 303–313 (2008).

32. Hagiya, M., Aubert-Kato, N., Wang, S. & Kobayashi, S. Molecular computers for molecular robots as hybrid systems. *Theor. Comput. Sci.* **632**, 4–20 (2016).

33. Hagiya, M., Konagaya, A., Kobayashi, S., Saito, H. & Murata, S. Molecular robots with sensors and intelligence. *Acc. Chem. Res.* **47**, 1681–1690 (2014).

34. Mariani, G. *et al.* Integration of molecular machines into supramolecular materials: Actuation between equilibrium polymers and crystal-like gels. *Nanoscale* **9**, 18456–18466 (2017).

35. Kim, H. *et al.* Micro manipulation using magnetic microrobots. *J. Bionic Eng.* **13**, 515–524 (2016).

36. Aghakhani, A., Yasa, O., Wrede, P. & Sitti, M. Acoustically powered surface-slipping mobile microrobots. *Proc. Natl. Acad. Sci. U. S. A.* **117**, 3469–3477 (2020).

37. Lu, X. *et al.* A Human Microrobot Interface Based on Acoustic Manipulation. *ACS Nano* **13**, 11443–11452 (2019).

38. Zhang, S. *et al.* The optoelectronic microrobot: A versatile toolbox for micromanipulation. *Proc. Natl. Acad. Sci. U.S.A.*, **116**, 14823–14828 (2019).

39. Li, D., Liu, Y., Yang, Y. & Shen, Y. Chemically Self-propelled 3D-printed Microbots. *2018 International Conference on Manipulation, Automation and Robotics at Small Scales (MARSS). IEEE*, 1–4 (2018).

40. Murata, S., Konagaya, A., Kobayashi, S., Saito, H. & Hagiya, M. Molecular robotics: A new paradigm for artifacts. *New Gener. Comput.* **31**, 27–45 (2013).

41. Alberts, B. The Cell as a Collection of Protein Machines: Preparing the Next Generation of Molecular Biologists. *Cell* **92**, 291–294 (1998).

42. Engelhart, M. D., Moughamian, H. & Walsh, J. A. Book Reviews : Book Reviews. *Educ. Psychol. Meas.* **30**, 187–187 (1970).

43. Fletcher, D. a & Mullins, R. D. Cell mechanisms and cytoskeleton. *Nature*, **463**, 485–492 (2010).

44. Dickinson, R. B., Caro, L. & Purich, D. L. Force Generation by Cytoskeletal Filament End-Tracking Proteins. *Biophys. J.* **87**, 2838–2854 (2004).

45. Hess, H. & Bachand, G. D. Biomolecular motors. *Mater. Today* **8**, 22–29 (2005).

46. Weisenberg, R. C. Microtubule Formation in vitro in Solutions Containing Low Calcium Concentrations. *Science*, **177**, 4054, 1104–1105 (1972).

47. Zhang, R. & Nogales, E. A new protocol to accurately determine microtubule lattice seam location. *J. Struct. Biol.* **192**, 245–254 (2015).

48. Pampaloni, F. *et al.* Thermal fluctuations of grafted microtubules provide evidence of a length-dependent persistence length. *Proc. Natl. Acad. Sci. U.S.A.*, **103**, 10248–10253 (2006).

49. Bachand, G. D., Spoerke, E. D. & Stevens, M. J. Microtubule-based nanomaterials: Exploiting nature's dynamic biopolymers. *Biotechnol. Bioeng.* **112**, 1065–1073 (2015).

50. Howard, J. The Movement of Kinesin Along Microtubules. *Annu. Rev. Physiol.* **58**, 703–729 (1996).

51. Schnitzer, M. J. & Block, S. M. Kinesin hydrolyses one ATP per 8-nm step. *Nature*, **388**, 386–390 (1997).

52. Coy, D. L., Wagenbach, M. & Howard, J. Kinesin takes one 8-nm step for each ATP that it hydrolyzes. *J. Biol. Chem.* **274**, 3667–3671 (1999).

53. Hirokawa, N., Noda, Y., Tanaka, Y. & Niwa, S. Kinesin superfamily motor proteins and intracellular transport. *Nat. Rev. Mol. Cell Biol.* **10**, 682–696 (2009).

54. Diez, S. & Howard, J. Nanotechnological applications of biomolecular motor systems. *La Phys. au Canada* **65**, 7–12 (2009).

55. Sugita, S., Sakamoto, N., Ohashi, T. & Sato, M. Characterization of Motility Properties of Kinesin-Driven Microtubules Towards NanoScale Transporter: Focusing on Length of Microtubules and Kinesin Density. *J. Biomech. Sci. Eng.* **3**, 510–519 (2008).

56. Keya, J. J., Kabir, A. M. R. & Kakugo, A. Synchronous operation of biomolecular engines. *Biophys. Rev.* **12**, 401–409 (2020).

57. Korten, T., Tavkin, E., Scharrel, L., Kushwaha, V. S. & Diez, S. An automated in vitro motility assay for high-throughput studies of molecular motors. *Lab on a Chip*, **18**, 3196–3206 (2018).

58. Spudich, J. A., Kron, S. J. & Sheetz, M. P. Movement of myosin-coated beads on oriented filaments reconstituted from purified actin. *Nature,* **315**, 584–586 (1985).

59. Przibill, M. J. & Hu, E. J. Yeast activators stimulate plant gene expression. *Nature*, **334**, 141–157 (1988).

60. Kron, S. J., & Spudich, J. A., Fluorescent Actin Filaments Move on Myosin Fixed to a Glass Surface. *Proc. Natl. Acad. Sci. U.S.A.*, **83**, 6272–6276 (2020).

61. Dinu, C. Z., Chrisey, D. B., Diez, S. & Howard, J. Cellular motors for molecular manufacturing. *Anat. Rec.* **290**, 1203–1212 (2007).

62. Diez, S., Helenius, J. H. & Howard, J. Biomolecular Motors Operating in Engineered Environments. In Protein Science Encyclopedia, A.R. Fersht (Ed.), (2008). doi:10.1002/9783527610754.bt03

63. Hess, H. Engineering Applications of Biomolecular Motors. *Annu. Rev. Biomed. Eng.*, 13, 429-450 (2011).

64. Hiyama, S., Gojo, R., Shima, T., Takeuchi, S. & Sutoh, K. Biomolecular-motor-based nano- or microscale particle translocations on DNA microarrays. *Nano Lett.* **9**, 2407–2413 (2009).

65. Agarwal, A., Katira, P. & Hess, H. Millisecond curing time of a molecular adhesive causes velocity-dependent cargo-loading of molecular shuttles. *Nano Lett.* **9**, 1170–1175 (2009).

66. Hess, H. & Vogel, V. Molecular shuttles based on motor proteins: Active transport in synthetic environments. *Rev. Mol. Biotechnol.* **82**, 67–85 (2001).

67. Isozaki, N. *et al.* Control of molecular shuttles by designing electrical and mechanical properties of microtubules. *Sci. Robot.* **2**, 1–11 (2017).

68. Ramachandran, S., Ernst, K. H., Bachand, G. D., Vogel, V. & Hess, H. Selective loading of kinesin-powered molecular shuttles with protein cargo and its application to biosensing. *Small* **2**, 330–334 (2006).

69. Isozaki, N. *et al.* Control of microtubule trajectory within an electric field by altering surface charge density. *Sci. Rep.* **5**, 1–8 (2015).

70. Kato, K., Goto, R., Katoh, K. & Shibakami, M. Microtubule-cyclodextrin conjugate: Functionalization of motile filament with molecular inclusion ability. *Biosci. Biotechnol. Biochem.* **69**, 646–648 (2005).

71. Koshland, D. E. The structural basis of negative cooperativity: Receptors and enzymes. *Curr. Opin. Struct. Biol.* **6**, 757–761 (1996).

72. Hiyama, S. *et al.* Autonomous loading, transport, and unloading of specified cargoes by using DNA hybridization and biological motor-based motility. *Small* **4**, 410–415 (2008).

73. Schmidt, C. & Vogel, V. Molecular shuttles powered by motor proteins: Loading and unloading stations for nanocargo integrated into one device. *Lab Chip* **10**, 2195–2198 (2010).

74. Früh, S. M., Steuerwald, D., Simon, U. & Vogel, V. Covalent cargo loading to molecular shuttles via copper-free ‘click chemistry’. *Biomacromolecules* **13**, 3908–3911 (2012).

75. Hiyama, S., Gojo, R., Shima, T., Takeuchi, S. & Sutoh, K. Biological motor-based pick-and-move manipulations of nano- or micro-scale particles on a DNA microarray. *Proc. Conf. MicroTAS 2009 - 13th Int. Conf. Miniaturized Syst. Chem. Life Sci.* 857–859 (2009).

76. Yokokawa, R. *et al.* Unidirectional transport of kinesin-coated beads on microtubules oriented in a microfluidic device. *Nano Lett.* **4**, 2265–2270 (2004).

77. Van Den Heuvel, M. G. L., De Graaff, M. P. & Dekker, C. Molecular sorting by electrical steering of microtubules in kinesin-coated channels. *Science.* **312**, 910–914 (2006).

78. Van Den Heuvel, M. G. L., Butcher, C. T., Smeets, R. M. M., Diez, S. & Dekker, C. High rectifying efficiencies of microtubule motility on Kinesin-coated gold nanostructures. *Nano Lett.* **5**, 1117–1122 (2005).

79. Mahajan, K. D. *et al.* Steering microtubule shuttle transport with dynamically controlled magnetic fields. *Nanoscale* **8**, 8641–8649 (2016).

80. Schroeder, V., Korten, T., Linke, H., Diez, S. & Maximov, I. Dynamic guiding of motor-driven microtubules on electrically heated, smart polymer tracks. *Nano Lett.* **13**, 3434–3438 (2013).

81. Rahim, M. K. A., Fukaminato, T., Kamei, T. & Tamaoki, N. Dynamic photocontrol of the gliding motility of a microtubule driven by kinesin on a photoisomerizable monolayer surface. *Langmuir* **27**, 10347–10350 (2011).

82. Tas, R. P. *et al.* Guided by Light: Optical Control of Microtubule Gliding Assays. *Nano Lett.* **18**, 7524–7528 (2018).

83. Saito, A. *et al.* Understanding the emergence of collective motion of microtubules driven by kinesins: role of concentration of microtubules and depletion force. *RSC Adv.* **7**, 13191–13197 (2017).

84. Inoue, D. *et al.* Depletion force induced collective motion of microtubules driven by kinesin. *Nanoscale* **7**, 18054–18061 (2015).

85. Pearce, D. J. G., Miller, A. M., Rowlands, G. & Turner, M. S. Role of projection in the control of bird flocks. *Proc. Natl. Acad. Sci. U.S.A.* **111**, 10422–10426 (2014).

86. Couzin, I. D., Krause, J., James, R., Ruxton, G. D. & Franks, N. R. Collective memory and spatial sorting in animal groups. *J. Theor. Biol.* **218**, 1–11 (2002).

87. Reynolds, C. W. Flocks, herds, and schools: A distributed behavioral model. *Proc. 14th Annu. Conf. Comput. Graph. Interact. Tech.* **21**, 25–34 (1987).

88. Aoki, I. A Simulation Study on the Schooling Mechanism in Fish. *Nippon Suisan Gakkaishi* **48**, 1081–1088 (1982).

89. D'Orsogna, M. R., Chuang, Y. L., Bertozzi, A. L. & Chayes, L. S. Self-propelled particles with soft-core interactions: Patterns, stability, and collapse. *Phys. Rev. Lett.* **96**, 10, 104302 (2006).

90. Walker, A. W. Intestinal alkaline phosphatase in serum of patients on maintenance haemodialysis. *Clin. Chim. Acta* **55**, 399–405 (1974).

91. Ramos, V., Fernandes, C. & Rosa, A. C. Computational chemotaxis in ants and bacteria over dynamic environments. *2007 IEEE Congress on Evolutionary Computation*, 1109-1117, (2007).

92. Bibic, S. M., Cipu, E. C. & Buiu, C. A bioinspired mathematical model for a robotic swarm to discriminate between self and nonself robots. *2015 19th International Conference on System Theory, Control and Computing (ICSTCC)* 279–284 (2015). doi:10.1109/ICSTCC.2015.7321306

93. Wilson, E. O. The Sociogenesis of Insect Colonies. *Science.* **228**, 1489-1495, (1985).

94. Gelblum, A. *et al.* Ant groups optimally amplify the effect of transiently informed individuals. *Nat. Commun.* **6**, (2015).

95. Schaller, V. *et al.* Frozen steady states in active systems. *Sci. SEE Comment.* **108**, (2011).

96. Schaller, V. *et al.* Crosslinking proteins modulate the self-organization of driven systems. *Soft Matter* **9**, 7229–7233 (2013).

97. Kraikivski, P., Lipowsky, R. & Kierfeld, J. Enhanced ordering of interacting filaments by molecular motors. *Phys. Rev. Lett.* **96**, 1–4 (2006).

98. Schaller, V., Weber, C., Semmrich, C., Frey, E. & Bausch, A. R. Polar patterns of driven

filaments. *Nature* **467**, 73–77 (2010).

99. Hess, H. *et al.* Molecular self-assembly of 'nanowires' and 'nanospools' using active transport. *Nano Lett.* **5**, 629–633 (2005).

100. Tamura, Y. *et al.* Dynamic self-organization and polymorphism of microtubule assembly through active interactions with kinesin. *Soft Matter* **7**, 5654–5659 (2011).

101. Kumar, S. *et al.* Sensing protein antigen and microvesicle analytes using high-capacity biopolymer nano-carriers. *Analyst* **141**, 836–846 (2016).

102. Sumino, Y. *et al.* Large-scale vortex lattice emerging from collectively moving microtubules. *Nature* **483**, 448–452 (2012).

103. Kabir, A. M. R. & Kakugo, A. Study of active self-assembly using biomolecular motors. *Polym. J.* **50**, 1139–1148 (2018).

104. Inoue, D. *et al.* Adaptation of Patterns of Motile Filaments under Dynamic Boundary Conditions. *ACS Nano* **13**, 11, 12452-12460 (2019). doi:10.1021/acsnano.9b01450

105. Sanchez, T., Chen, D. T. N., Decamp, S. J., Heymann, M. & Dogic, Z. Spontaneous motion in hierarchically assembled active matter. *Nature*, **491**, 431–434 (2012).

106. Whitesides, G. M. & Grzybowski, B. Self-assembly at all scales. *Science* **295**, 5564, 2418–2421 (2002).

107. Idan, O. *et al.* Nanoscale transport enables active self-assembly of millimeter-scale wires. *Nano Lett.* **12**, 240–245 (2012).

108. Lam, A. T. *et al.* Cytoskeletal motor-driven active self-assembly in in vitro systems. *Soft Matter* **12**, 988–997 (2016).

109. Lam, A. T., Curschellas, C., Krovvidi, D. & Hess, H. Controlling self-assembly of microtubule spools via kinesin motor density. *Soft Matter* **10**, 8731–8736 (2014).

110. Yigit, B., Alapan, Y. & Sitti, M. Programmable Collective Behavior in Dynamically Self-Assembled Mobile Microrobotic Swarms. *Adv. Sci.* **6**, 6, 1801837 (2019).

111. Wollman, A. J. M., Sanchez-Cano, C., Carstairs, H. M. J., Cross, R. A. & Turberfield, A.

J. Transport and self-organization across different length scales powered by motor proteins and programmed by DNA. *Nat. Nanotechnol.* **9**, 44–47 (2014).

112. Turelli, M. *et al.* 1. **99**, 1196–1202 (2011).

113. Adleman, L. M. Molecular Computation of Solutions to Combinatorial Problems Author (s): Leonard M . Adleman Published by : American Association for the Advancement of Science Stable URL : https://www.jstor.org/stable/2885489 JSTOR is a not-for-profit service that help. *Science.* **266**, 1021–1024 (1994).

114. Crick F. C. and Watson J. D., The structure of DNA. *Cold Spring Harbor symposia on quantitative biology*, Cold Spring Harbor Laboratory Press, **18,** 123-132. (1953).

115. Lehn, J. M., Mascal, M., Decian, A. and Fischer, J. Molecular recognition directed self-assembly of ordered supramolecular strands by cocrystallization of complementary molecular components. *J. Chem. Soc. Chem. Commun.* **479**, 479–481 (1990).

116. Robinson, B. H. and Seemant, N. C. *Biophysical journal*, **51**, 4, 611-626 (1987).

117. Kallenbach N., Ma R. and Seeman N. C. An immobile nucleic acid junction constructed from oligonucleotides, *Nature.* **305**, 829-831 (1983).

118. Chen, J. and Seeman, N. C. Dock-Bregeon, A. C. et a. *Jacquier. A. Dujon, B. Biochim.* **50**, 133–139 (1987).

119. Seeman, N. C. Biochemistry and structural DNA nanotechnology: An evolving symbiotic relationship. *Biochemistry* **42**, 7259–7269 (2003).

120. Zhang, Y. & Seeman, N. C. Construction of a DNA-Truncated Octahedron. *J. Am. Chem. Soc.* **116**, 1661–1669 (1994).

121. Tsu-Ju, F. & Seeman, N. C. DNA Double-Crossover Molecules. *Biochemistry* **32**, 3211–3220 (1993).

122. Rothemund, P. W. K., Papadakis, N. & Winfree, E. Algorithmic self-assembly of DNA Sierpinski triangles. *PLoS Biol.* **2**, 12, e424 (2004).

123. Maune, H. T. *et al.* Self-assembly of carbon nanotubes into two-dimensional geometries using DNA origami templates. *Nat. Nanotechnol.* **5**, 61–66 (2010).

124. Rothemund, P. W. K. Folding DNA to create nanoscale shapes and patterns. *Nature* **440**, 297–302 (2006).

125. Li, H., Park, S. H., Reif, J. H., LaBean, T. H. & Yan, H. DNA-Templated Self-Assembly of Protein and Nanoparticle Linear Arrays. *J. Am. Chem. Soc.* **126**, 418–419 (2004).

126. Zheng, Y. B., Kiraly, B., Weiss, P. S. & Huang, T. J. Molecular plasmonics for biology and nanomedicine. *Nanomedicine* **7**, 751–770 (2012).

127. Liu, N. & Liedl, T. DNA-Assembled Advanced Plasmonic Architectures. *Chem. Rev.* **118**, 3032—3053 (2018).

128. Shen, B., Kostiainen, M. A. & Linko, V. DNA Origami Nanophotonics and Plasmonics at Interfaces. *Langmuir* **34**, 14911–14920 (2018).

129. Parolini, L., Kotar, J., Di Michele, L. & Mognetti, B. M. Controlling Self-Assembly Kinetics of DNA-Functionalized Liposomes Using Toehold Exchange Mechanism. *ACS Nano* **10**, 2392–2398 (2016).

130. Lund, K. *et al*. Molecular robots guided by prescriptive landscapes. *Nature* **465**, 206–209 (2010).

131. Schmidt, C. & Vogel, V. Molecular shuttles powered by motor proteins: Loading and unloading stations for nanocargo integrated into one device. *Lab Chip* **10**, 2195–2198 (2010).

132. Chen, K. & Chen, X. Design and Development of Molecular Imaging Probes. *Curr. Top. Med. Chem.* **10**, 1227–1236 (2010).

133. Thang, D. C., Wang, Z., Lu, X. & Xing, B. Precise cell behaviors manipulation through light-responsive nano-regulators: Recent advance and perspective. *Theranostics* **9**, 3308–3340 (2019).

134. Abbott, J. J., Nagy, Z., Beyeler, F. & Nelson, B. J. Robotics in the Small, Part I: Microbotics. *IEEE Robot. Autom. Mag.* **14**, 92–103 (2007).

135. Kassem, S., Lee, A. T. L., Leigh, D. A., Markevicius, A. & Solà, J. Pick-up, transport and release of a molecular cargo using a small-molecule robotic arm. *Nat. Chem.* **8**, 138–

143 (2016).

136. Fischer, T., Santa, K. & Fatikow, S. Sensor system and powerful computer system for controlling a microrobot-based micromanipulation station. *J. Micromechanics Microengineering* **7**, 256–258 (1997).

CHAPTER 2

Photoregulated trajectories of DNA conjugated microrobots

ABSTRACT

Self-propelled biomolecular motor systems i.e. microtubule (MT)-kinesin and MT-dynein are promising as actuators and have been successfully used in various fields including molecular robotics, nanotransportation, molecular computation and so on. But controlling the motion e.g. velocity, direction and persistency of the gliding biomolecular motors have remained a challenging task for such sophisticated applications in engineered environments. In this chapter, I describe the persistency control of MTs driven by kinesin in a non-invasive manner employing a photoresponsive DNA. The persistence of motion of photoresponsive DNA conjugated MTs, characterized as path persistence length, increases and decreases upon UV and visible light irradiation respectively. This could be accounted for by UV and visible light-induced *cis-trans* isomerization of azobenzene moiety incorporated in the DNA. Besides, photoresponsive DNA can be utilized as a shield for MTs against damage by photoirradiation. This work would widen the applications of the biomolecular motor system MT-kinesin/dynein in nanotechnology which relies on the motion of MTs.

2.1 INTRODUCTION

Biomolecular motor systems e.g. microtubule-kinesin/dynein are the smallest natural machines with high energy efficiency and specific power.[1–3] Because of the attractive features they have been utilized as a micro-actuator in molecular transportation,[4–9] molecular robotics,[10–14] molecular computing,[15,16] fabrication of artificial molecular muscle,[17] etc. In these applications, controlling the motion of the filamentous microtubules (MTs), driven by kinesin/dynein utilizing the chemical energy of ATP, is crucial. The utilization of photoirradiation has appeared a promising methodology to control the motion of MTs. The velocity of MTs has been reversibly regulated by employing photoisomerization of an azobenzene monolayer or activation of ATP using photoresponsive switches.[18–21] On the other hand, by tuning the interaction between MTs and kinesins using light-controlled interacting protein tags, MT motion was regulated under photoirradiation.[22] However, regulating the persistency in the motion of kinesin/dynein driven MTs without interrupting their mutual interaction has remained challenging yet.

In this chapter, I described the first example of controlling the persistency of motion of the MTs by photoirradiation, without sacrificing their interaction with kinesins. My strategy was based on the change of the polarity of azobenzene moiety incorporated DNA (*p*DNA) to control the motion of the MTs. Thus the construction of *p*DNA conjugated MTs was performed as photoregulated microrobots followed by the *in vitro* motility assay on the kinesin coated surface. Azobenzene undergoes *cis-trans* isomerization upon irradiation by ultraviolet (UV)-visible (VIS) light[21,23] and facilitates change in polarity of DNA.[24,25] The effect of photoisomerization of azobenzene have applied to *p*DNA to control the motility of MTs. They were driven on the kinesin coated surface and investigated by characterizing the path persistence length of the gliding MTs.[26–28] The path persistence length of *p*DNA modified MTs was found to alter upon irradiation with UV-VIS light irradiation without affecting the velocity of the MTs. The reversible regulation of persistency in the motion of gliding MTs and the shielding against photodamage were also addressed in the chapter. This work would provide the ability of MTs to navigate simply by responding to any light source and consequently would widen applications of the biomolecular motor in nanotechnology.

2.2 RESULTS & DISCUSSION

2.2.1 Preparation of *p*DNA conjugated MTs and *in vitro* motility assay

Azide labeled microtubules (MTs) were polymerized from the azide labeled tubulin in the presence of GMPCPP (guanosine-5´-[(β, γ)-methyleno] triphosphate, sodium salt). Then microrobots were prepared by conjugating photoresponsive azobenzene incorporated DNA (*p*DNA) to MTs through a copper-free click reaction where *p*DNA was labeled with DBCO (dibenzocyclooctyne) at the 5-end to react with azide functionalized MT (**Figure 2.1a**). Prior to the conjugation of *p*DNA, MTs were modified with the fluorescent dye ATTO550 to allow visualization of the MTs using a fluorescence microscope. The name of the *p*DNA sequence was mentioned in **Figure 2.1b** where Z represents the azobenzene moiety.

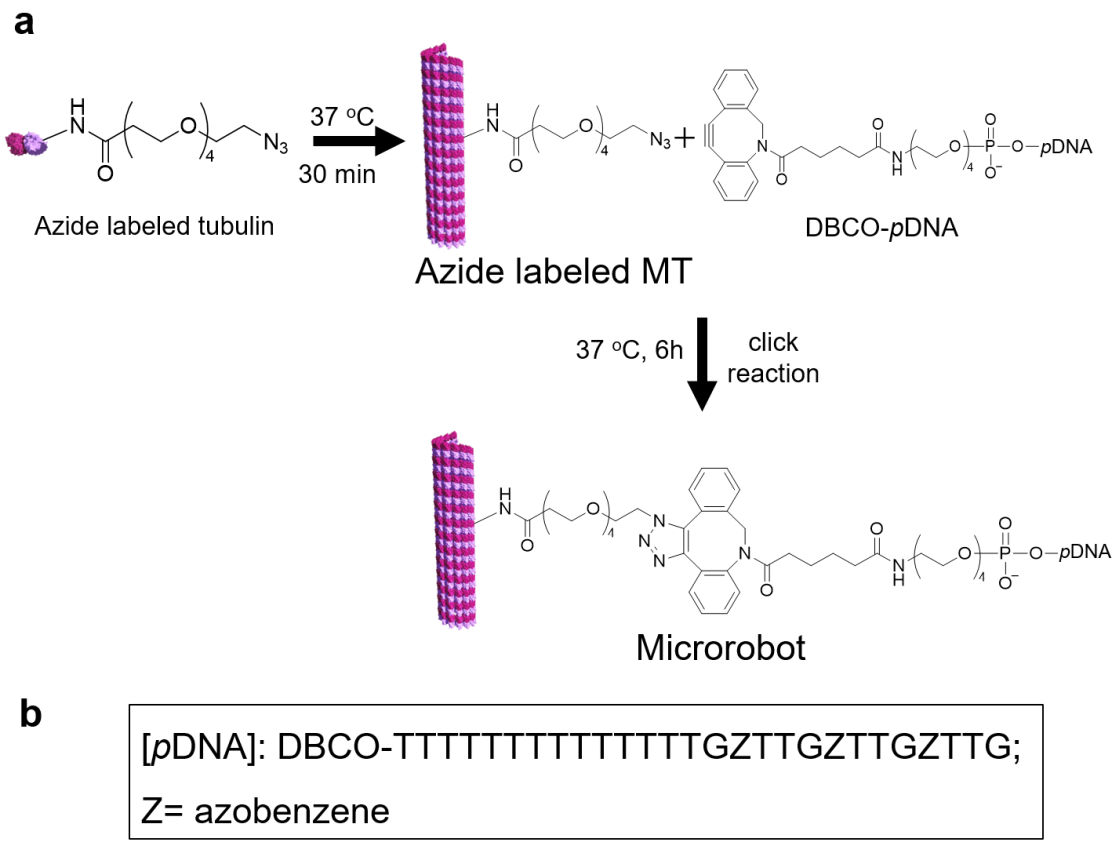

Figure 2.1 Preparation of *p*DNA conjugated microrobot and regulation of their trajectories by photoirradiation. **(a)** Polymerization of azide labeled MT from azide labeled tubulin and then conjugation of DBCO-*p*DNA to azide functionalized MTs by azide-alkyne cycloaddition reaction. **(b)** The sequence of the *p*DNA strand used to conjugate to MTs where Z shows the azobenzene moiety in DNA. The DNA was modified with dibenzocyclooctyne (DBCO) at the 5´ end.

The success of the *p*DNA conjugation to MTs was confirmed from the absorption spectrum of *p*DNA to tubulin which was shown in **Figure 2.2(b)**.

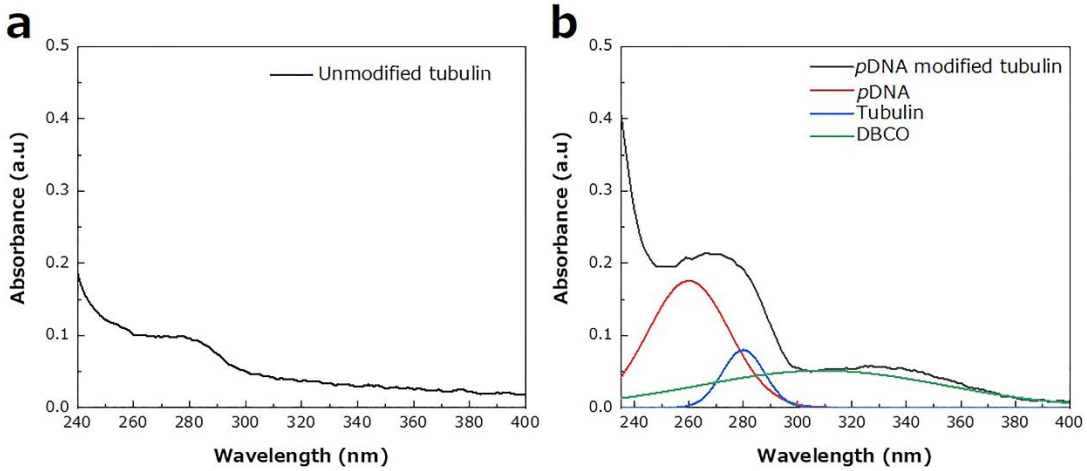

Figure 2.2 Estimation of the labeling ratio of *p*DNA to MTs in microrobot. **(a)** The representative absorption spectrum of unmodified MTs. **(b)** Representative deconvoluted absorption spectra of *p*DNA conjugated MTs. The labeling ratio of *p*DNA to tubulin dimers was determined after estimating the concentrations of *p*DNA and tubulin from their absorption maxima.

After the comparison of the absorption spectrum of unmodified MTs (**Figure 2.2a**), successful preparation of *p*DNA modified MTs can be confirmed from **Figure 2.2b**. From the absorption spectrum the labeling ratio of *p*DNA to tubulin was estimated to be 91.0%.

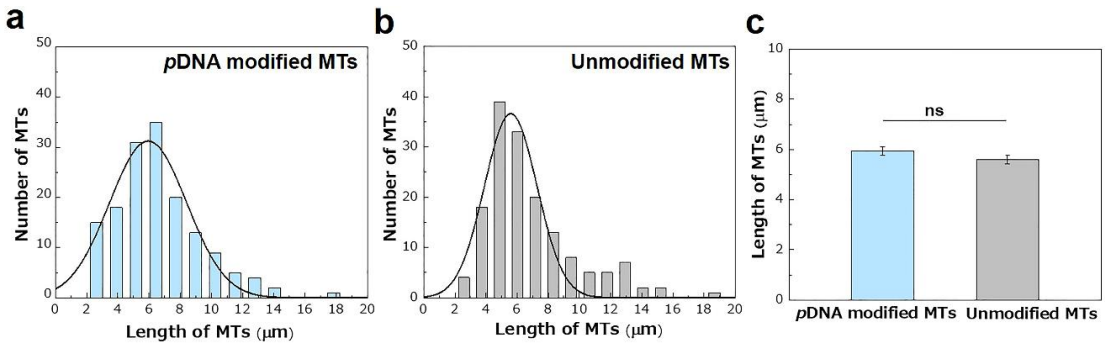

Figure 2.3 Distribution of length of **(a)** *p*DNA modified and **(b)** unmodified MTs. **(c)** Mean lengths of *p*DNA modified and unmodified MTs were not significantly different as obtained from the result of Student's t-test. ns: non-significant. Error bar: standard error. The number of MTs considered for analysis was 153 and 157 for *p*DNA modified and unmodified MTs respectively. The fitted curves are represented by the solid lines (R^2=0.95 and 0.90 for *p*DNA modified and unmodified MTs respectively).

As length of MTs may affect their rigidity the length of *p*DNA modified MTs was compared with that of unmodified MTs,[27,29,30] The length distributions of *p*DNA modified MTs and unmodified MTs were given in **Figure 2.3**. The distributions of lengths of MT were fitted to the Gaussian equation ($\boldsymbol{y = Ae^{\frac{-(x-b)^2}{c^2}}}$) for normal distribution. The mean MT length obtained from the fitting was 5.9±0.2 µm and 5.6±0.2 µm for *p*DNA modified and unmodified MTs respectively. No significant difference in the length of *p*DNA modified MTs (6.8 ±2.9 µm) and unmodified MTs (6.6± 2.8 µm) was confirmed.

Then the *p*DNA modified MTs were driven by kinesins on a substrate in the presence of ATP. The velocity was observed as 513 ± 12 nm/s whereas the velocity of the MTs without DNA modification was 452± 17 nm/s. (**Figure 2.4**) This result indicates that conjugation of *p*DNA to MTs may affect the interaction of MTs with kinesins. The surface of MTs is rich in carboxyl groups, providing a net negative charge along the MT surface. Besides, DNA is also negatively charged due to the phosphate ions. The presence of negative charge in both the *p*DNA and MTs is likely to alter the electrostatic interaction between MTs and kinesins' motor domains. This might be a reason for the higher velocity of the *p*DNA modified MTs than the unmodified MTs, confirmation of which requires further investigation in the future.

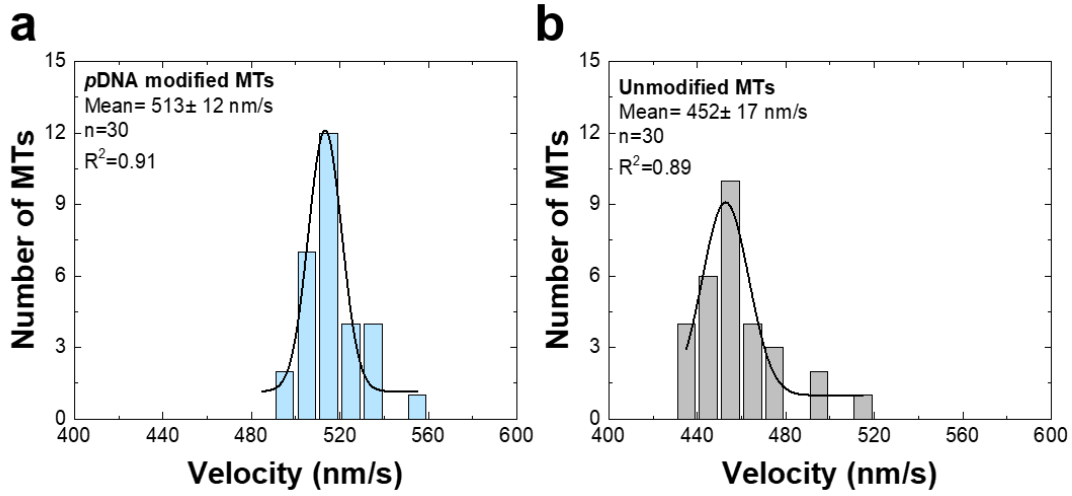

Figure 2.4 Distribution of velocity of **(a)** *p*DNA modified and **(b)** unmodified MTs Error bar: standard deviation. The number of MTs considered for analysis was 30 in each case. The curves are fitted by Gaussian equation ($\boldsymbol{y = Ae^{\frac{-(x-b)^2}{c^2}}}$) for normal distribution; the fitted curve was represented by the black colored solid lines.

2.2.2 Photo-regulation of the motion of the *p*DNA conjugated microrobots

To regulate the motion of the gliding MTs, visible (VIS) and ultraviolet (UV) light was irradiated on the robots which are schematically shown in **Figure 2.5.**

Path persistence length is used as a parameter for the evaluation of the persistency in motion. The path persistence length of *p*DNA modified and unmodified MTs was estimated by measuring the end-to-end and contour length of their trajectories that is the path along which the MTs travelled on kinesins. The path persistence lengths were estimated using the following equation (1):

$$\boldsymbol{R^2 = 2{L_P}^2\left[\left(\frac{L}{L_P} - 1\right) + exp\left(\frac{-L}{L_P}\right)\right]} \qquad (1)$$

where R is the end-to-end distance, L is the contour length of the trajectories of MT, and L_p represents the path persistence length of MTs. From the fitting of the data of R and L, the L_p of *p*DNA modified and unmodified MTs were evaluated to be 110.7±8.8 μm and 658.5±19.3 μm respectively.

Thus, the observed difference in L_p of *p*DNA modified MTs and unmodified MTs was not due to any difference in their length. The lower value of L_p of *p*DNA modified MTs agrees

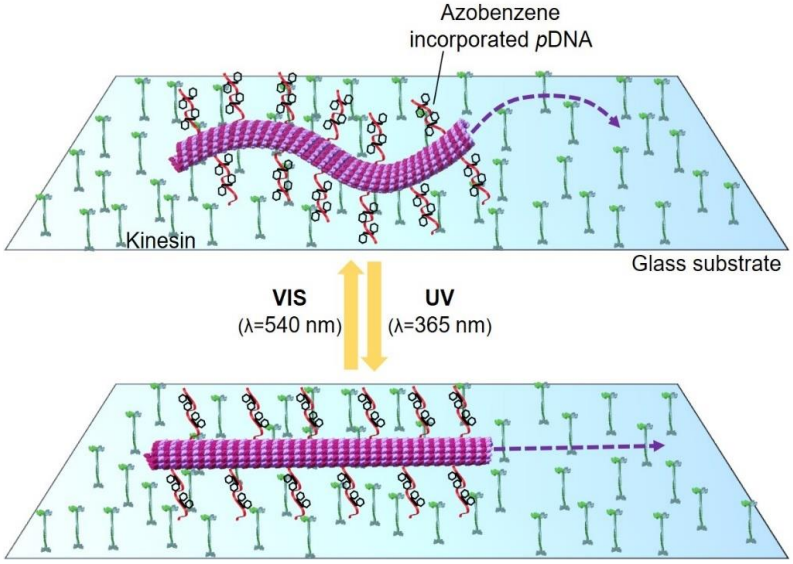

Figure 2.5 Schematic representation shows change in moiton of *p*DNA conjugated MTs, moving on a kinesin coated substrate, upon UV-VIS light irradiation. The purple colored arrow showed the gliding direction of MT. The azobenzene moiety in *p*DNA undergoes isomerization from *trans*-to-*cis* and *cis-to-trans* state upon illumination with UV (wavelength, λ= 365 nm and intensity, I= 0.13 mW/cm^2) and VIS light (λ= 540 nm and I= 0.11 mW/cm^2) respectively.

well with a previous report in which L_p of MTs was reported to decrease upon DNA conjugation to MTs.[13]

Next, in order to investigate the effect of photoisomerization of azobenzene in *p*DNA on the path persistence length of MTs, the gliding MTs were irradiated with UV light for 100 s using a photoirradiation system (details in **section 2.4**). The wavelength (λ) of the UV light was 365 nm whereas the intensity (*I*) of the light was 0.13 mW/cm^2.

The power of the UV light was enough to induce photo-isomerization of azobenzene in *p*DNA which can be observed from **Figure 2.6**.

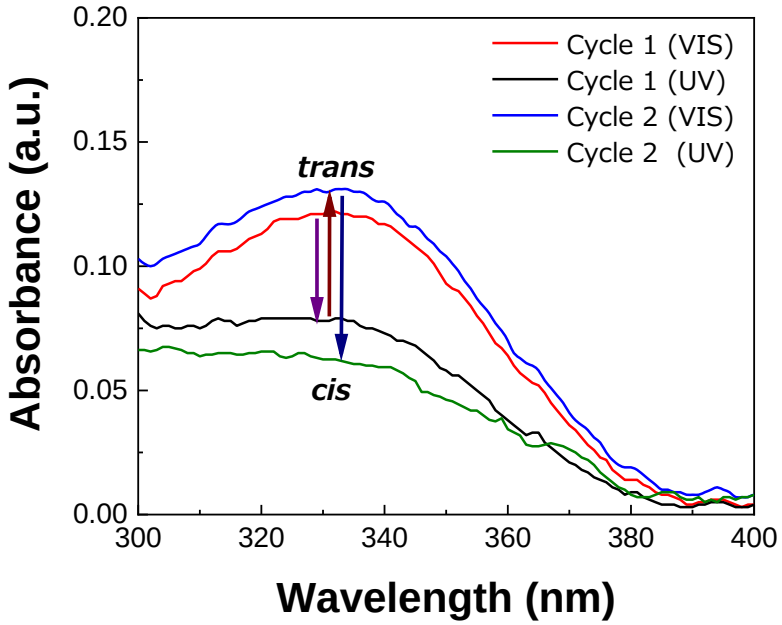

Figure 2.6 Absorption spectra of azobenzene in *p*DNA. After 100 s of VIS light irradiation the azobenzene in *p*DNA isomerized into trans state (red line). Upon irradiation with UV light azobenzene returend to the *cis* state (black line). After cycle 1, first VIS and then UV light was irradiated consecutively for 100 s. Experimental conditions: 20 µM *p*DNA, 100 mM NaCl, 10 mM phosphate buffer, pH 7.0.

The trajectories of *p*DNA modified MTs were found affected by UV light which was shown by the temporal color code projections in **Figure 2.7**.

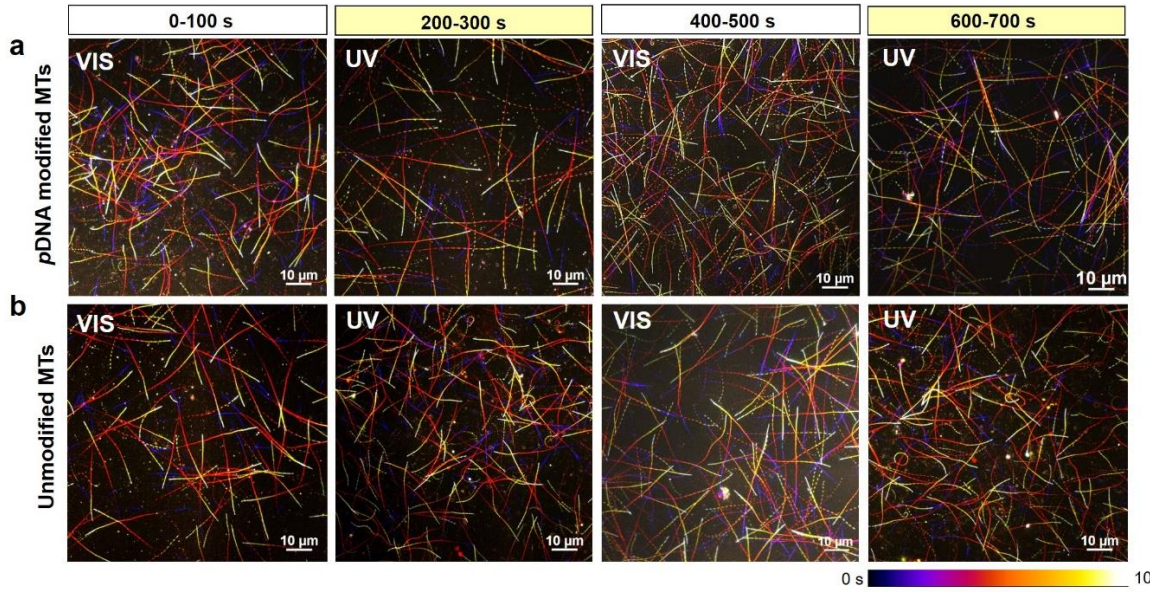

Figure 2.7 Reversible regulation of persistency in motion of MTs by *p*DNA conjugation and UV light irradiation. **(a)** Temporal color-coded maximum projections of *p*DNA modified and **(b)** unmodified MTs for 100 second interval frames in the absence (white box) and presence (yellow box) of UV irradiation. The color code denotes the traveled distance of MTs with time.

Upon UV light irradiation, the L_p of *p*DNA modified MTs increased to 563.2± 9.7 μm from 110.7 ±8.8 μm as shown in **Figure 2.8b**. This increase in L_p took place when the azobenzene in *p*DNA was in the *cis* state. The non-planar *cis* isomer of azobenzene was known to be hydrophilic whereas the planar *trans* isomer is hydrophobic.[31] This difference in hydrophilicity of the two isomers of azobenzene directly affected the conjugate.[24,32]

When the UV irradiation was turned off, and VIS light was turned ON, the *cis* isomer of azobenzene was recovered from the *trans* isomer under VIS light (**Figure 2.8c**). This *cis*-to-*trans* conversion of azobenzene in *p*DNA allowed the L_p of *p*DNA conjugated MTs to return to the initial value (114.1± 15.0 μm). The L_p of the *p*DNA conjugated MTs increased to 566.0 ± 7.6 μm when the gliding MTs were shined by UV light again (**Figure 2.8d**).

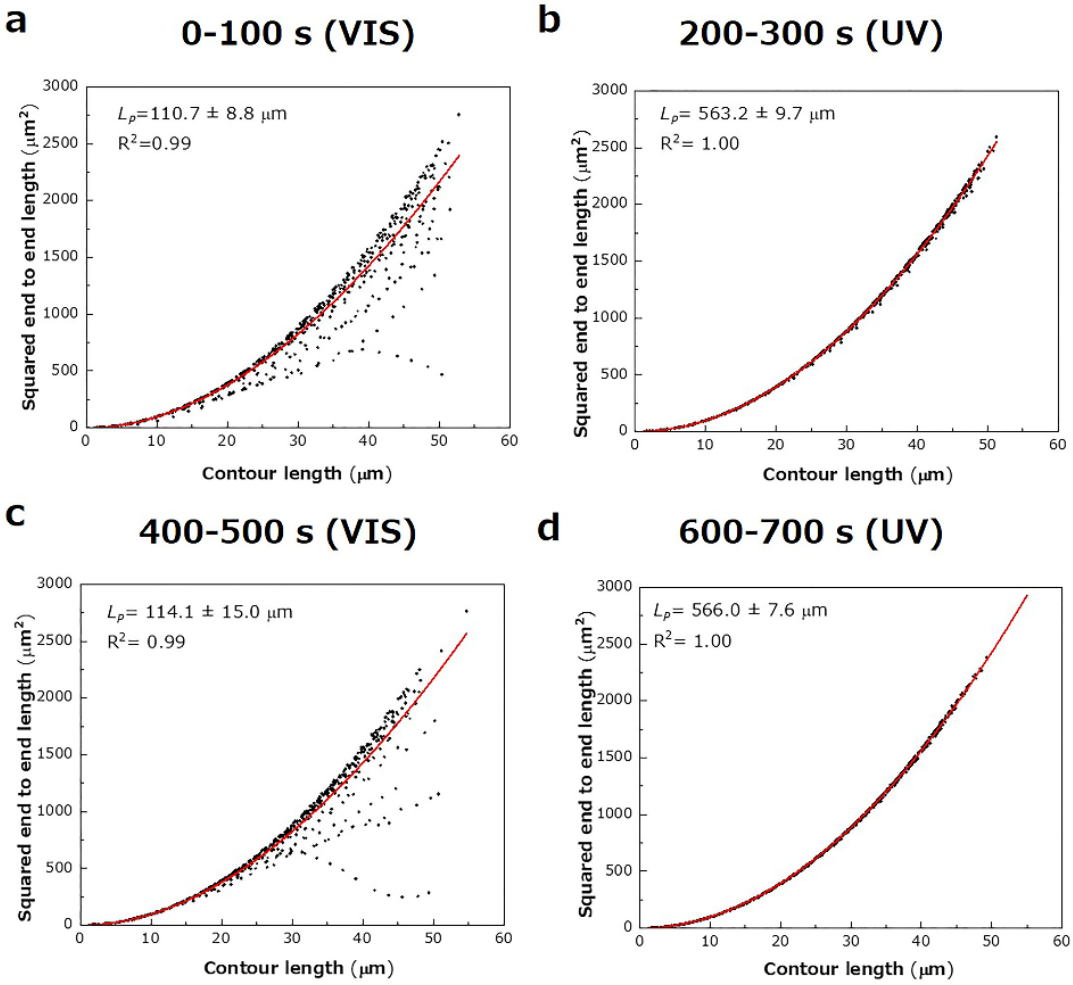

Figure 2.8 Estimation of the path persistence length (*Lp*) of *p*DNA modified MTs where the MTs were irradiated with **(a)** VIS irradiation (0-100 s); **(b)** UV irradiation (200-300 s); **(c)** VIS irradiation (400-500 s) and **(d)** UV irradiation (600-700 s).

Based on these results it is evident that the L_p of MTs could be repeatedly regulated simply through photoiomerization of azobenzene in the *p*DNA. Despite the change in L_p of the *p*DNA modified MTs upon UV and VIS light irradiation, velocity of the MTs was not noticeably affected. The average velocity of *p*DNA MTs in the four consecutive cycles discussed above were 516 ± 12 nm/s, 496 ± 14 nm/s, 479±29 nm/s and 464±18 nm/s respectively (**Figure 2.9b**). These results indicate that the repeated changes in L_p of *p*DNA conjugated MTs upon UV-VIS light irradiation was independent of the velocity of MTs

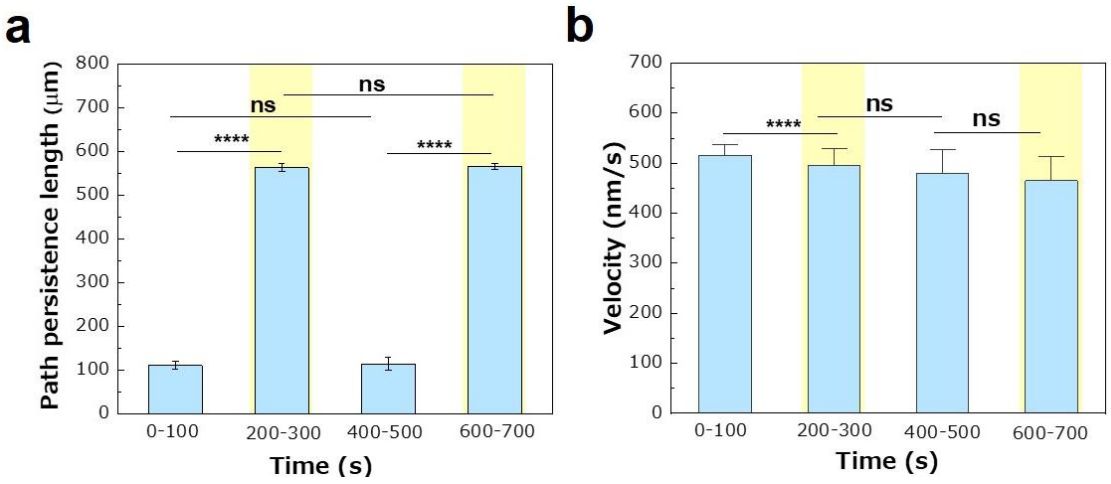

Figure 2.9 (a) Path persistence length, L_p and **(b)** average velocity of *p*DNA modified MTs in the absence and presence (yellow shaded column) of UV light. Error bar: standard deviation. The cycle was repeated two times. In each case more than 45 MT tracks were analyzed for estimating the L_p. Statistical analysis using Student's t-test confirmed significant difference between the two data sets at P<0.0001 indicated by **** and non-significant difference indicated by **ns.**

2.2.3 Effect of light on the motion of gliding unmodified MTs

As *p*DNA modified MTs was affected by the UV irradiation, it was important to observe the effect on the unmodified MTs. Unlike the *p*DNA modified MTs, the L_p of unmodified MTs drastically decreased from 658.5±19.3 µm to 65.2 ± 7.6 µm upon UV irradiation which is shown in **Figure 2.10**.

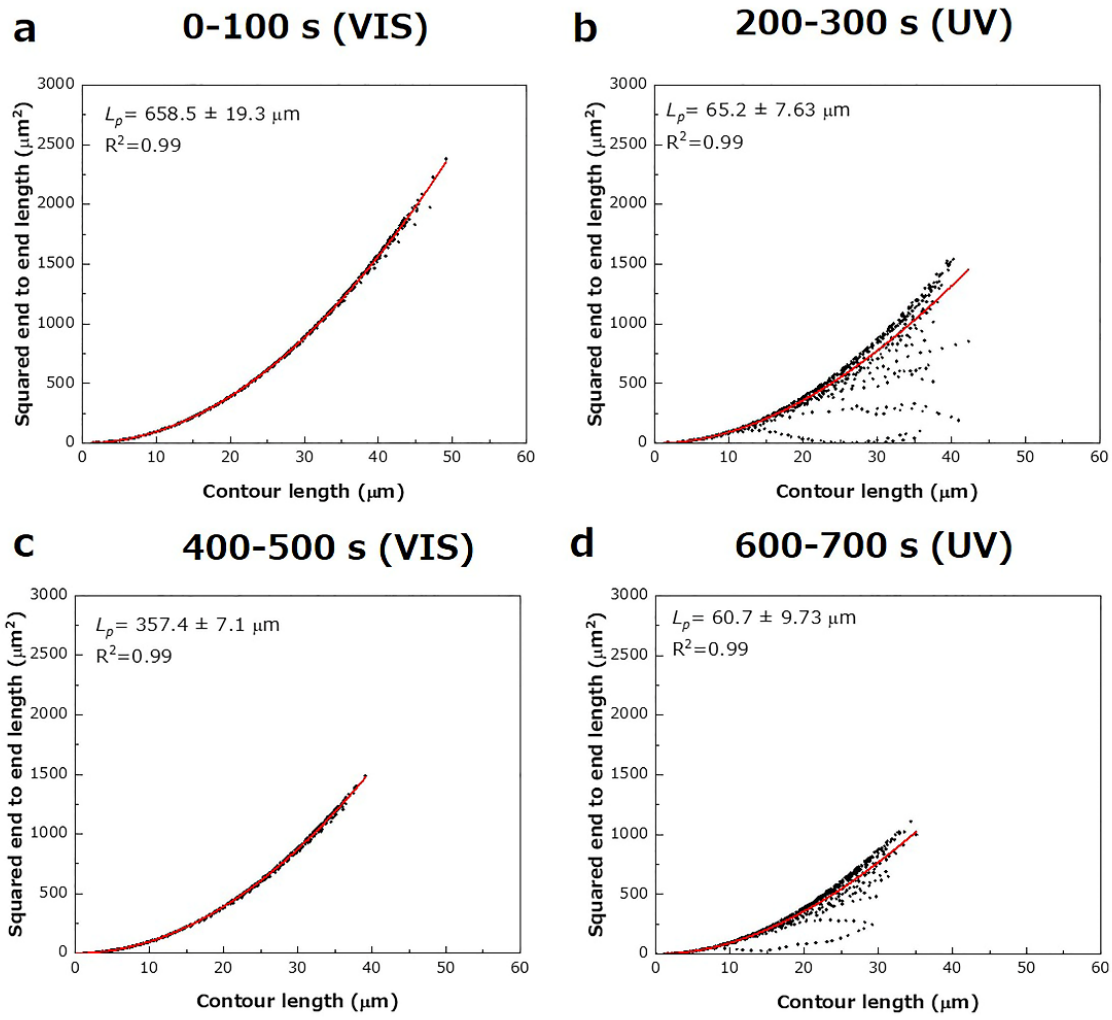

Figure 2.10 Estimation of the path persistence length (*Lp*) of unmodified MTs where the MTs were irradiated with: **(a)** VIS irradiation (0-100 s); **(b)** UV irradiation (200-300 s); **(c)** VIS irradiation (400-500 s) and **(d)** UV irradiation (600-700 s). The data were fitted using equation 1.

When the UV irradiation was turned off, the L_p increased to 357.4 ± 7.1 µm which is almost half of the L_p estimated before UV irradiation (**Figure 2.11a**). The L_p of unmodified MTs decreased further to 60.7 ± 9.7 µm when the MTs were subjected to another dose of the UV

irradiation. To understand the obvious failure in the restoration of L_p for the unmodified MTs, the velocity of the unmodified MTs was investigated after every cycle of photo-irradiation (**Figure 2.11b**).

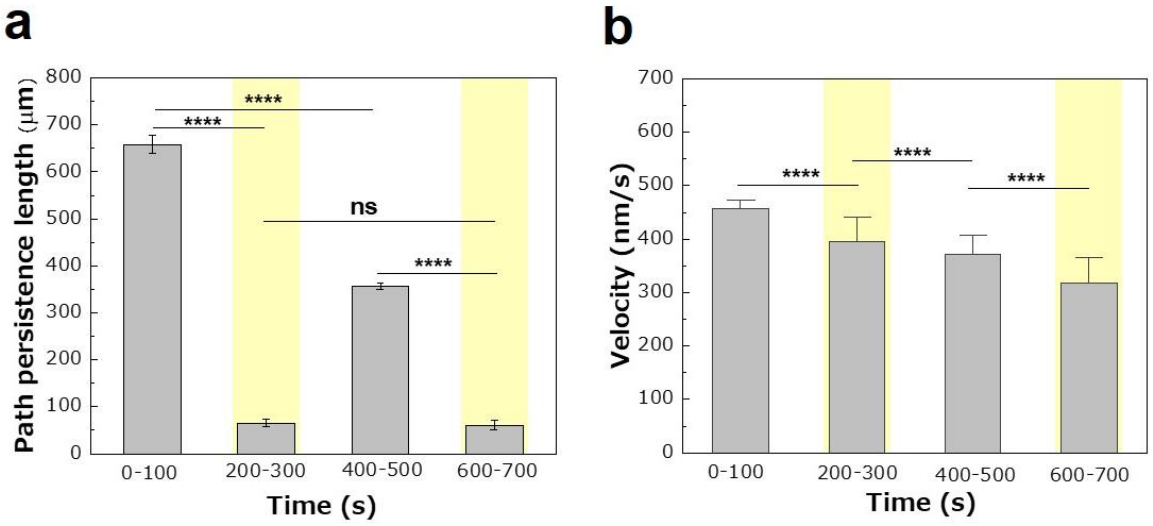

Figure 2.11 (a) Path persistence length, L_p and **(b)** average velocity of unmodified MTs in the absence and presence (yellow shaded column) of UV light. Error bar: standard deviation. The cycle was repeated two times. In each case, 50 MT tracks were analyzed for estimating the L_p. Statistical analysis using Student's t-test confirmed a significant difference between the two data sets at P<0.0001 indicated by **** and non-significant differences indicated by **ns**.

The velocities of the unmodified MTs gradually decreased upon consecutive irradiation of UV-VIS light (457± 17 nm/s, 394 ± 19 nm/s, 370 ± 17 nm/s and 318.44 ± 21 nm/s). Irradiation of MTs by UV light is known to induce conformational changes in MT structure.[33] Such changes can result in depolymerization or fragmentation of MTs through the removal of tubulin dimers,[34,35] the units assembling MT, may decrease the rigidity of MT. The observed decrease in velocity of MTs in the absence of *p*DNA under UV light irradiation can be accounted for by damage of these MTs.[36,37]

2.2.4 UV shielding effect of *p*DNA against UV damage

*p*DNA modified and unmodified MTs were sequentially exposed to altering irradiation of VIS-UV light twice and the velocity of those MTs was investigated using kinesins that were not exposed to UV-VIS light in these processes (**Figure 2.12**).

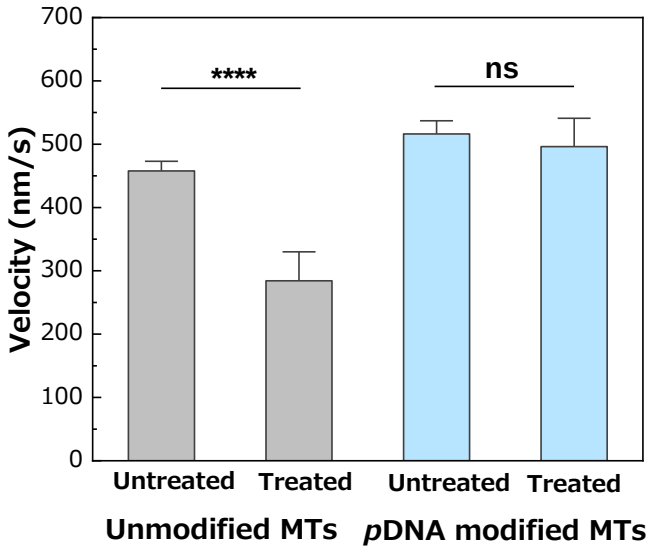

Figure 2.12 Average velocity of unmodified MTs and *p*DNA modified MTs after sequential treatment with VIS-UV-VIS-UV light irradiation for 100 sec ('Treated') and untreated period ('Untreated'). UV and VIS light were applied to MTs keeping the MTs in a nitrogen atmosphere. Observation of the motility of MTs was carried out by exposing the MTs to VIS light (λ=540 nm) using an epifluorescence microscope. Error bar: standard deviation.

The velocity of unmodified MTs that were exposed to photoirradiation before the velocity measurement was 284.3±26.7 nm/s whereas the velocity of untreated and unmodified MTs was 457.7±17.5 nm/s. The velocity of the photo-treated unmodified MTs was similar to that observed for MTs that were treated in four consecutive cycles by UV-VIS light while they were driven by kinesins (**Figure 2.11b**). These results confirm that UV light t caused the damage to MTs and consequently decreased the velocity of MTs.[33–35,38]

This could be further supported by time lapse fluorescence microscopy images in which breakage of kinesin driven treated unmodified MTs is evident (**Figure 2.13a**). On the contrary, the velocity of *p*DNA modified MTs that were exposed to photoirradiation prior to the velocity measurement remained similar to that untreated *p*DNA modified MTs as confirmed by non-significant differences in statistical analysis (Student's t-test, $P < 0.0001$).

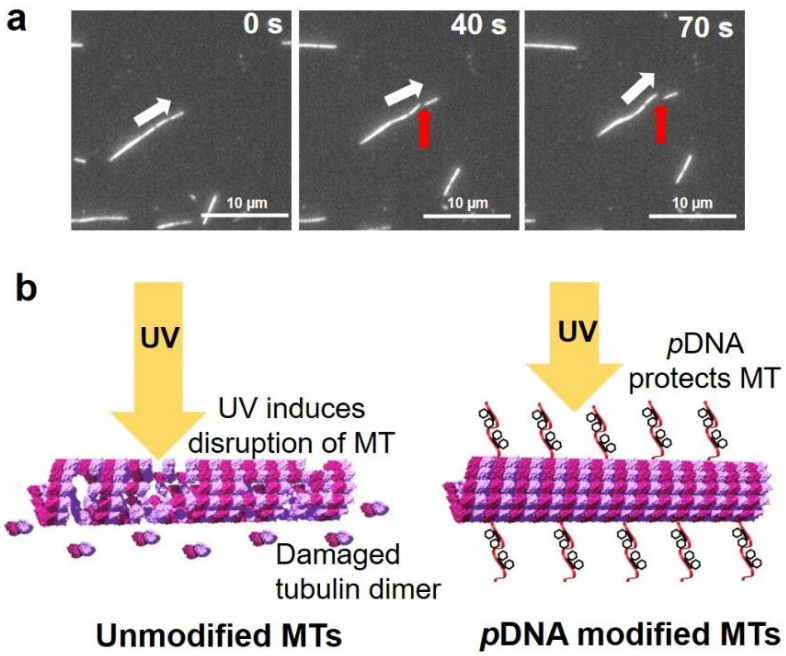

Figure 2.13 (a) Time lapse fluorescence microscopy images show breakage of a photo treated unmodified MT during its movement on kinesins. The white arrow indicates the direction of movement of the MT whereas the red arrows indicate the breaking of the MT. **(b)** Schematic representation shows the effect of UV light on the stability of *p*DNA modified MTs and unmodified MTs. *p*DNA serves as a shield for MTs against UV irradiation and protects MTs from photodamage and breaking, whereas unmodified MTs are prone to degradation when exposed to UV light.

The result from **Figure 2.12** suggests that the *p*DNA modified MTs did not undergo damage by UV light as observed for the unmodified MTs. In the case of *p*DNA modified MTs the UV light might have been absorbed by the azobenzene moiety in DNA to initiate the *trans* to *cis* isomerization which is schematically shown in **Figure 2.13b.**[39] Another possibility is to consider photoinduced electron transfer from MTs to azobenzene or DNA that may suppress the photodamage of MTs, confirmation of which requires future investigation.[40,41]

2.3 CONCLUSIONS

In conclusion, *p*DNA can be used as the non-invasive stimuli to regulate the motion of the MTs on the kinesin coated surface. The repeated UV-VIS light irradiation can reversibly control the motion of MTs. Besides, *p*DNA is found effective in protecting MTs from the harmful effect of UV light. These findings would be important for other biomolecules where protecting them from UV induced damage is crucial for their applications in harsh environments.[42,43] This work will advance the ability to control persistency in the motion of kinesin driven MTs which in turn is expected to contribute to the study of collective behavior exhibited by self-propelled particles or active matters. [44–46] This may also accelerate the ongoing development in molecular robotics and their swarming.[10,12] Moreover, the demonstrated ability to control the trajectory of MTs should contribute to molecular transportation[4,47] and computation[10,15] which depend on the persistence in the motion of MTs. The outcomes in this work are expected to promote further development of phototactic molecular robots which would be able to self-align or navigate by responding to any light source .[48,49]

2.4 MATERIALS & METHODS

2.4.1 Purification of tubulin and kinesin

Tubulin was purified from the porcine brain using high-concentration PIPES buffer (1 M PIPES, 20 mM EGTA, and 10 mM $MgCl_2$) and preserved in BRB80 buffer (80 mM PIPES, 1 mM EGTA, 2 mM $MgCl_2$, pH maintained to 6.8 using KOH) at -80 °C.[1] Recombinant kinesin-1 consisting of the first 573 amino-acid residues of human kinesin-1 was prepared as described in the literature[2]. Azide labeled tubulin was prepared using N_3-PEG_4-NHS following an established protocol of tubulin labeling with a fluorescent ATTO550 dye[3]. The concentration of tubulin was determined by measuring the absorbance at 280 nm using a UV spectrophotometer (Nanodrop 2000c).

2.4.2 Design and preparation of DNA sequences

The sequence of *p*DNA used in this work was TTTTTTTTTTTTTTGZTTGZTTGZTTG ($T_{12}(TTG)_4Z_3$; Z is azobenzene). *p*-DNA strand was purchased from Hokkaido System Science Co. Ltd. The *p*-DNA was modified at the 5′ end with dibenzocyclooctyne (DBCO). Quality control of all the synthesized DNA was performed by polyacrylamide gel electrophoresis (PAGE). Characterization of the *p*-DNA strands was carried out by LC-ESI-MS spectroscopy.

2.4.3 Preparation of microtubules (MTs)

MTs were polymerized from a mixture of azide labeled tubulin and Atto 550 labeled tubulin in which the concentration of tubulin was 70 µM. Molar ratio between azide labeled tubulin and ATTO 550 labeled tubulin was adjusted to 4:1. Then the tubulin mixture in polymerization buffer was incubated at 37 °C for 30 min to form MTs. 1 µL of 4×BRB80 buffer (80 mM PIPES, 1 mM EGTA, 1 mM $MgCl_2$, 1 mM GMPCPP, pH~6.8) and 0.5 µL of 1 mM taxol (in DMSO) were added to the MT solution just after polymerization to stabilize the MTs. Copper free click reaction was carried out by adding 3.5 µL DBCO conjugated *p*DNA (500 µM) to 5 µL MT solution (56 µM) and incubating at 37 °C for 6 h.[4] Cushion buffer (100 µL of BRB80 buffer supplemented with 60% glycerol) was used to separate the MTs by centrifugation at 201,000 × g (S55A2-0156 rotor, Hitachi) for 1 h at 37 °C. After removing the supernatant, the pellet of *p*DNA-conjugated MTs was washed with 100 µL BRB80P (BRB80 supplemented with 1 mM taxol) and resuspended in 15 µL of BRB80P buffer.

2.4.4 Measurement of the labeling ratio of *p*DNA to MTs

The *p*DNA conjugated MTs were depolymerized to *p*DNA conjugated tubulins by keeping the MTs on ice overnight. The absorption spectrum of the *p*DNA conjugated tubulin dimers was measured using a spectrophotometer (NanoDrop™ 2000c, Thermo Fisher Scientific Inc.) and deconvoluted using the normal distribution function with Microsoft Excel (Windows Edition, Microsoft Corporation) with peaks at 260 nm and 280 nm. The concentrations of *p*DNA and tubulin dimers were calculated from the Beer-Lambert law using the molar extinction coefficient of tubulin dimers (115,000 L mol^{-1} cm^{-1}) and *p*DNA (230,000 L mol^{-1} cm^{-1}) from which the labeling ratio was determined (Figure S1).

2.4.5 Gliding assay of MTs on a kinesin coated substrate

A microfluidic channel was constructed using two glass cover slides of 40×50 mm^2 and 18×18 mm^2 (MATSUNAMI Inc.) adhered together by parafilm as a spacer with a channel pattern cut off. Prior to preparing the channel the glass slides were plasma treated for 3 min by a plasma etcher (SEDE-GE; Meiwafosis) to make it hydrophilic. The channel pattern was designed using Brother Canvas Workspace software on the parafilm and cut by Brother ScanNCut printer. The flow cell was prepared setting the designed parafilm on the large cover glass and then the small slide glass on the top and then heating at 70 ^{o}C. The flow cell was filled with 5 μL casein buffer (BRB80 buffer supplemented with 0.5 mg mL^{-1} casein). After incubating for 3 min, 0.8 μM kinesin solution was introduced into the flow cell and incubated for 5 min. After washing the flow cell with 5 μL of wash buffer (BRB80 buffer supplemented with 1 mM DTT, 10 μM taxol), 5 μL of ATTO550-labeled MT (*p*DNA modified or unmodified) solution was introduced and incubated for 2 min, followed by washing with 10 μL of wash buffer. The motility of MTs was initiated by applying 5 μL ATP buffer (wash buffer supplemented with 5 mM ATP, 4.5 mg mL^{-1} D-glucose, 50 U mL^{-1} glucose oxidase, 50 U mL^{-1} catalase, and 0.2% methylcellulose (w/v). The time of ATP addition was set as 0 h. Soon after the addition of ATP buffer, the flow cell was placed in an inert chamber system (ICS)[5] and the MTs were monitored after 30 min of ATP addition using an epifluorescence microscope at room temperature (25 °C). The samples were illuminated with a 100 W mercury lamp and visualized by an epifluorescence microscope (Eclipse Ti, Nikon) using an oil-coupled Nikon Plan Apo 60× objective (N.A.=1.4). UV cut-off filter blocks (TRITC: EX 540/25, DM565, BA605/55; Nikon) were used in the optical path of the microscope. Images were captured using a cooled-CMOS camera (NEO sCMOS, Andor) connected to a PC. In order to observe the effect of UV on the motility of MTs,

Nikon super high-pressure Hg lamp was used as a light source which passed through a UV1A filter (EX 365-10, DM400, BA390; Nikon). The beam is expanded and steered into the microscopic objective lens. The intensity of UV light is measured as 0.13 mW/cm^2 by Thorlabs power meter (PM100). Movie was captured for 100 s taking each frame in 4 s interval. There was rest time of 100 s and then the next movie was captured under UV irradiation. This cycle was repeated twice for both the *p*DNA modified and unmodified MTs.

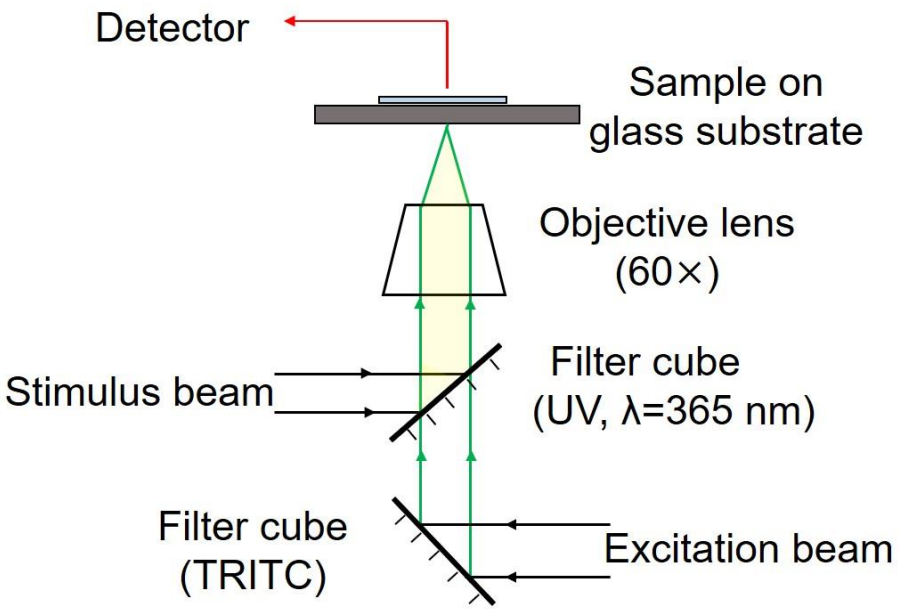

Figure 2.14 Schematic representation of the experimental setup used to apply UV to kinesin driven MTs during observation of the MTs using a fluorescence microscope.

2.4.6 Data Analysis

The fluorescence microscopy images were analyzed by NIS- Elements BR software (Nikon) and Fiji 1.52J software (National Institutes of Health, USA). The velocity of the gliding MTs was measured using the ImageJ plugin 'MTrackJ' (https://imagej.net/MTrackJ). The temporal color coded projection of the of the gliding MTs in Figure 3a was prepared using the ImageJ plugin 'Temporal color code' (https://imagej.net/Temporal-Color_Code). Statistical analysis and graphs were performed with the software OriginPro Version 2019, OriginLab, USA. Mann-Whitney test and two-tailed Student's t-test were used to compare the normality and significance of the two groups of data where applicable.

2.5 SUPPLEMENTAL INFORMATION

Table 1 Estimation of the labeling ratio of *p*DNA to tubulin dimers

In feed concentration of *p*DNA (µM)	**Concentration of tubulin dimers (µM)**	**Concentration of *p*DNA in tubulin dimers (µM)**	**Labeling ratio of *p*DNA to tubulin dimers (%)**
500	14	13	91.02

2.6 REFERENCES

1. Hess, H. & Bachand, G. D. Biomolecular motors. *Mater. Today* **8**, 22–29 (2005).
2. Van Den Heuvel, M. G. L. & Dekker, C. Motor proteins at work for nanotechnology. *Science,* **317**, 333–336 (2007).
3. Diez, S., Helenius, J. H. & Howard, J. Biomolecular motors operating in engineered environments. *Protein Sci. Encycl.* 1–18 (2008). doi:10.1002/9783527610754.bt03
4. Hess, H., Clemmens, J., Qin, D., Howard, J. & Vogel, V. Light-controlled molecular shuttles made from motor proteins carrying cargo on engineered surfaces. *Nano Lett.* **1**, 235–239 (2001).
5. Brunner, C., Wahnes, C. & Vogel, V. Cargo pick-up from engineered loading stations by kinesin driven molecular shuttles. *Lab Chip* **7**, 1263–1271 (2007).
6. Schmidt, C. & Vogel, V. Molecular shuttles powered by motor proteins: Loading and unloading stations for nanocargo integrated into one device. *Lab Chip* **10**, 2195–2198 (2010).
7. Ramachandran, S., Ernst, K. H., Bachand, G. D., Vogel, V. & Hess, H. Selective loading of kinesin-powered molecular shuttles with protein cargo and its application to biosensing. *Small* **2**, 330–334 (2006).
8. Steuerwald, D., Früh, S. M., Griss, R., Lovchik, R. D. & Vogel, V. Nanoshuttles propelled by motor proteins sequentially assemble molecular cargo in a microfluidic device. *Lab Chip* **14**, 3729–3738 (2014).
9. Agarwal, A., Katira, P. & Hess, H. Millisecond curing time of a molecular adhesive causes velocity-dependent cargo-loading of molecular shuttles. *Nano Lett.* **9**, 1170–1175 (2009).
10. Keya, J. J. *et al.* DNA-assisted swarm control in a biomolecular motor system. *Nat. Commun.* **9**, 453 (2018).
11. Hagiya, M., Konagaya, A., Kobayashi, S., Saito, H. & Murata, S. Molecular robots with sensors and intelligence. *Acc. Chem. Res.* **47**, 1681–1690 (2014).
12. Keya, J. J. *et al.* Control of swarming of molecular robots. *Sci. Rep.* **8**, 1–10 (2018).
13. Isozaki, N. *et al.* Control of molecular shuttles by designing electrical and mechanical properties of microtubules. *Sci. Robot.* **2**, 1–11 (2017).
14. Hagiya, M., Aubert-Kato, N., Wang, S. & Kobayashi, S. Molecular computers for molecular robots as hybrid systems. *Theor. Comput. Sci.* **632**, 4–20 (2016).
15. Nicolau, D. V. *et al.* Parallel computation with molecular-motor-propelled agents in

nanofabricated networks. *Proc. Natl. Acad. Sci. U. S. A.* **113**, 2591–2596 (2016).

16. Dinu, C. Z., Chrisey, D. B., Diez, S. & Howard, J. Cellular motors for molecular manufacturing. *Anat. Rec.* **290**, 1203–1212 (2007).
17. Matsuda, K. *et al.* Artificial smooth muscle model composed of hierarchically ordered microtubule asters mediated by dna origami nanostructures. *Nano Lett.* **19**, 3933–3938 (2019).
18. Rahim, M. K. A., Fukaminato, T., Kamei, T. & Tamaoki, N. Dynamic photocontrol of the gliding motility of a microtubule driven by kinesin on a photoisomerizable monolayer surface. *Langmuir* **27**, 10347–10350 (2011).
19. Kumar, K. R. S., Amrutha, A. S. & Tamaoki, N. Spatiotemporal control of kinesin motor protein by photoswitches enabling selective single microtubule regulations. *Lab Chip* **16**, 4702–4709 (2016).
20. Kumar, K. R. S., Kamei, T., Fukaminato, T. & Tamaoki, N. Complete ON/OFF photoswitching of the motility of a nanobiomolecular machine. *ACS Nano* **8**, 4157–4165 (2014).
21. Merino, E. & Ribagorda, M. Control over molecular motion using the cis-trans photoisomerization of the azo group. *Beilstein J. Org. Chem.* **8**, 1071–1090 (2012).
22. Tas, R. P. *et al.* Guided by light: optical control of microtubule gliding assays. *Nano Lett.* **18**, 7524–7528 (2018).
23. HARTLEY, G. S. The cis-form of azobenzene. *Nature* **140**, 281 (1937).
24. Gu, R. *et al.* Photocontrolled micellar aggregation of amphiphilic DNA-azobenzene conjugates. *Colloids Surfaces B Biointerfaces* **135**, 126–132 (2015).
25. Kuzuya, A., Tanaka, K. & Komiyama, M. Photoswitching of site-selective RNA scission by sequential incorporation of azobenzene and acridine residues in a DNA oligomer. *J. Nucleic Acids* **2011**, (2011).
26. Nitta, T. & Hess, H. Dispersion in active transport by kinesin-powered molecular shuttles. *Nano Lett.* **5**, 1337–1342 (2005).
27. Van Den Heuvel, M. G. L., Bolhuis, S. & Dekker, C. Persistence length measurements from stochastic single-microtubule trajectories. *Nano Lett.* **7**, 3138–3144 (2007).
28. Isozaki, N. *et al.* Control of microtubule trajectory within an electric field by altering surface charge density. *Sci. Rep.* **5**, 1–8 (2015).
29. Pampaloni, F. *et al.* Thermal fluctuations of grafted microtubules provide evidence of a length-dependent persistence length. *Proc. Natl. Acad. Sci. U. S. A.* **103**, 10248–

10253 (2006).

30. Sugita, S., Sakamoto, N., Ohashi, T. & Sato, M. Characterization of motility properties of kinesin-driven microtubules towards nanoscale transporter: focusing on length of microtubules and kinesin density. *J. Biomech. Sci. Eng.* **3**, 510–519 (2008).
31. Freundlich, H. & Heller, W. The Adsorption of cis- and trans-Azobenzene. *J. Am. Chem. Soc.* **61**, 2228–2230 (1939).
32. Schumers, J. M., Fustin, C. A. & Gohy, J. F. Light-responsive block copolymers. *Macromol. Rapid Commun.* **31**, 1588–1607 (2010).
33. Zaremba, T. G., LeBon, T. R., Millar, D. B., Smejkal, R. M. & Hawley, R. J. Effects of ultraviolet light on the in vitro assembly of microtubules. *Biochemistry* **23**, 1073–1080 (1984).
34. Zamansky, G. B. & Chou, I. N. Environmental wavelengths of ultraviolet light induce cytoskeletal damage. *J. Invest. Dermatol.* **89**, 603–606 (1987).
35. Zamansky, G. B., Perrino, B. A. & Chou, I. N. Disruption of cytoplasmic microtubules by ultraviolet radiation. *Exp. Cell Res.* 195, 1, 269-273 (1991).
36. VanDelinder, V., Adams, P. G. & Bachand, G. D. Mechanical splitting of microtubules into protofilament bundles by surface-bound kinesin-1. *Sci. Rep.* **6**, 1–10 (2016).
37. Keya, J. J. *et al.* High-Resolution Imaging of a single gliding protofilament of tubulins by HS-AFM. *Sci. Rep.* **7**, 1–7 (2017).
38. Staxén, I., Bergounioux, C. & Bornman, J. F. Effect of ultraviolet radiation on cell division and microtubule organization in Petunia hybrida protoplasts. *Protoplasma* **173**, 70–76 (1993).
39. Asanuma, H., Liang, X., Yoshida, T. & Komiyama, M. Photocontrol of DNA duplex formation by using azobenzene-bearing oligonucleotides. *ChemBioChem* **2**, 39–44 (2001).
40. Kurian, P., Obisesan, T. O. & Craddock, T. J. A. Oxidative species-induced excitonic transport in tubulin aromatic networks: Potential implications for neurodegenerative disease. *J. Photochem. Photobiol. B Biol.* **175**, 109–124 (2017).
41. Heinlein, T., Knemeyer, J.-P., Piestert, O. & Sauer, M. Photoinduced electron transfer between fluorescent dyes and guanosine residues in DNA-hairpins. *J. Phys. Chem. B* **107**, 7957–7964 (2003).
42. Teresa, M., Petersen, S. & Prakash, G. UV light effects on proteins: from photochemistry to nanomedicine. *Mol. Photochem-Var. Asp.* 125-158 (2012).

43. Hahn, M. B., Smales, G. J., Seitz, H., Solomun, T. & Sturm, H. Ectoine interaction with DNA: influence on ultraviolet radiation damage. *Phys. Chem. Chem. Phys.* **70**, 6984–6992 (2020).
44. Inoue, D. *et al.* Depletion force induced collective motion of microtubules driven by kinesin. *Nanoscale* **7**, 18054–18061 (2015).
45. Saito, A. *et al.* Understanding the emergence of collective motion of microtubules driven by kinesins: role of concentration of microtubules and depletion force. *RSC Adv.* **7**, 13191–13197 (2017).
46. Wang, S. & Wolynes, P. G. On the spontaneous collective motion of active matter. *Proc. Natl. Acad. Sci. U. S. A.* **108**, 15184–15189 (2011).
47. Nitta, T. & Hess, H. Dispersion in active transport by kinesin-powered molecular shuttles. *Nano Lett.* **5**, 1337–1342 (2005).
48. Dai, B. *et al.* Programmable artificial phototactic microswimmer. *Nat. Nanotechnol.* **11**, 1087–1092 (2016).
49. Zhao, Y. *et al.* Soft phototactic swimmer based on self-sustained hydrogel oscillator. *Sci. Robot.* **4**, 33, eaax7112 (2019).
50. Castoldi, M. & Popov, A. V. Purification of brain tubulin through two cycles of polymerization – depolymerization in a high-molarity buffer. *Protein Expr. Purif.* **32**, 1, 83–88 (2003).
51. Case, R. B., Pierce, D. W., Hom-booher, N., Hart, C. L. & Vale, R. D. The Directional preference of kinesin motors is specified by an element outside of the motor catalytic domain. *Cell* **90**, 959–966 (1997).
52. Peloquin, J., Komarova, Y. & Borisy, G. Conjugation of fluorophores to tubulin. *Nat. Methods* **2**, 299–303 (2005).
53. Früh, S. M., Steuerwald, D., Simon, U. & Vogel, V. Covalent cargo loading to molecular shuttles via copper-free 'click chemistry'. *Biomacromolecules* **13**, 3908–3911 (2012).
54. Kabir, A. M. R., Inoue, D., Kakugo, A., Kamei, A. & Gong, J. P. Prolongation of the active lifetime of a biomolecular motor for in vitro motility assay by using an inert atmosphere. *Langmuir* **27**, 13659–13668 (2011).

CHAPTER 3

Photocontrol of the swarming of biomolecular motor based-microrobots

ABSTRACT

Swarming of microrobots has emerged as a new aspect in the field of microrobotics as it has overcome one of the major challenges to control the mutual interaction of a large number of microrobots. Swarming of a self-propelled biomolecular motor based microrobot was reported recently where interactions among thousands of motile microrobots were regulated in a highly programmable fashion by using DNA as a processor. However, precise control of this potential system is yet to be achieved to optimize the swarm behavior in a spatiotemporal manner. In this chapter, I addressed on the photoregulated swarming of microrobots in a reversible and spatiotemporal manner through the conjugation of complementary azobenzene incorporated DNA duplex. Swarming of the microrobots was systematically controlled by different physicochemical parameters of DNA e.g. length, concentration of DNA, labeling ratio of DNA to tubulin etc. Besides, swarming was regulated in local regions introducing different-sized photomasks in the UV light system. Reversibility of swarming was further controlled by changing wavelengths of light, the intensity of light and number of azobenzne in response to the UV irradiation. Moreover, the persistency of motion of the molecular swarm robot was also found to be altered under UV irradiation. Such a detailed study of precise control of swarming would provide new perceptions into developing a swarm robot system for further applications in engineering system.

3.1 INTRODUCTION

In nature, swarming of living organisms is fascinating for constructing large scale complex patterns with emergent functions.[1–3] Fish schools, ant colonies, and bird flocks are typical examples of swarming observed in nature. It enables the living organisms to obtain several advantages including parallelism, robustness and flexibility which are impossible to obtain by a single entity.[4,5] Inspired by the fascinating features of this natural system, a variety of artificial swarm robots that can show complex collective patterns or exhibit complex task sequencing have been reported. In macroscopic swarm robots it is difficult to have a large number of swarm units and control their interactions. On the other hand, micro-sized swarmrobots has been a big advantage as they enable to create a large number of robots and managing them to perform tasks coherently.[6–12]

However, controlling the local interactions of a large number of robots in a programmable manner has always been a major obstacle in the microrobotics for further applications.[6,13] The challenge was addressed recently with the construction of DNA programmed micro sized molecular robot where, DNA worked as information processor as well as sensor and self-propelled biomolecular motor system worked as actuator.[11,12] Though DNA can control the swarming of the robots successfully, controlling them in reversible and spatiotemporal manner are still lacking which has not been introduced yet. Incorporating a photoswitchable sensor into the processor could facilitate photo regulated swarming of the hybridization of the complementary sequences photoirradiation.[11,14–16]

Moreover, alongside with programming the swarming, understanding the effects of physicochemical parameters of the system are equally important to design complex behavior of molecular swarm robots.[17–19] To utilize the photoregulated microrobots with controlled swarm behavior, optimization of the related parameters of the system is essential which has not been explored yet. In the previos chapter, the motion of the microrobot was regulated by conjugation of single strand of photoresponsive azobenzene incorporated DNA (*p*DNA) in response to the photoirradiation.

Here, in this chapter, I introduced photoregulated swarming of the microrobots employing complementary *p*DNA through DNA duplex formation . Additionally, I explored the role of relevant physicochemical parameters in the reversible regulation of swarming of microrobots. I demonstrated the effect of concentration of DNA, length of DNA, number

of azobenzene in on the regulation of the swarming of microrobots. I furthermore investigated how the wavelength and intensity of light can control the swarming of MTs. A detailed understanding of the physicochemical parameters for the swarming system will enable us to expand the controllability and range of swarming behaviors. The knowledge may advance the development and optimization of the swarming of microrobots for the further applications in the field of molecular computation, robotics as well as nanotechnology.[20–23]

3.2 RESULTS AND DISCUSSION

3.2.1 Preparation of microrobots as swarm unit

Microrobots were prepared prior to the demonstration of the swarming by polymerization of azide labeled tubulin with GMPCPP (guanosine-5´-[(β, γ)-methyleno] triphosphate, sodium salt).[24] ATTO550 and ATTO488 labeled tubulins were added to the azide tubulins to allow the visualization by the epifluorescence microscopy.[25]

To control the microrobots by photoirradiation, azobenzene incorporated DNA (*p*DNA) was employed to modify the swarm units. This allowed ON/OFF switching of the swarming of the microrobots through UV-visible (VIS) light induced *cis-trans* isomerization of the azobenzene moiety, resulting in the change of melting temperature (*Tm*) of DNA hybridization (**Figure 3.1**).[14,15,26]

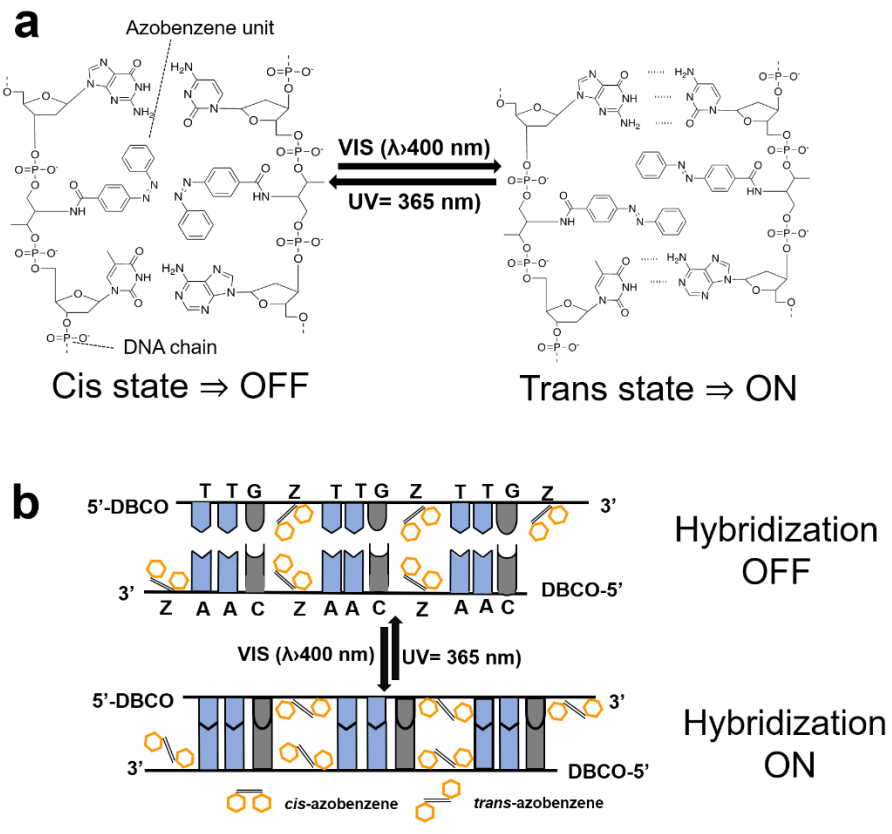

Figure 3.1 Schematic representation of **(a)** reversible hydrogen bonding of complementary *p*DNA by light induced *cis-trans* isomerization of azobenzene **(b)** sequence design of the photo regulated azobenzene tethered DNA.

From the simulation of the *Tm*, the *p*DNA sequences were designed by considering the base number and sequences that can construct microrobot in presence of input signals avoiding any undesired interactions at the working temperature (25 ^{o}C). The melting temperature (*Tm*) was measured for the DNA duplex (sequence given in **Table1**) which was shown in **Figure 3.2a**. For the *trans* form of the azobenzene in the DNA duplex, the *Tm* was 71 ^{o}C whereas for the *cis* form was <20 ^{o}C.

The photoisomerization of azobenzene in *p*DNA was confirmed from the UV-VIS absorbance spectra of DNA duplex where *trans* form of azobenzene converts to *cis* form after the UV irradiation (λ=365 nm). (**Figure 3.2b**)

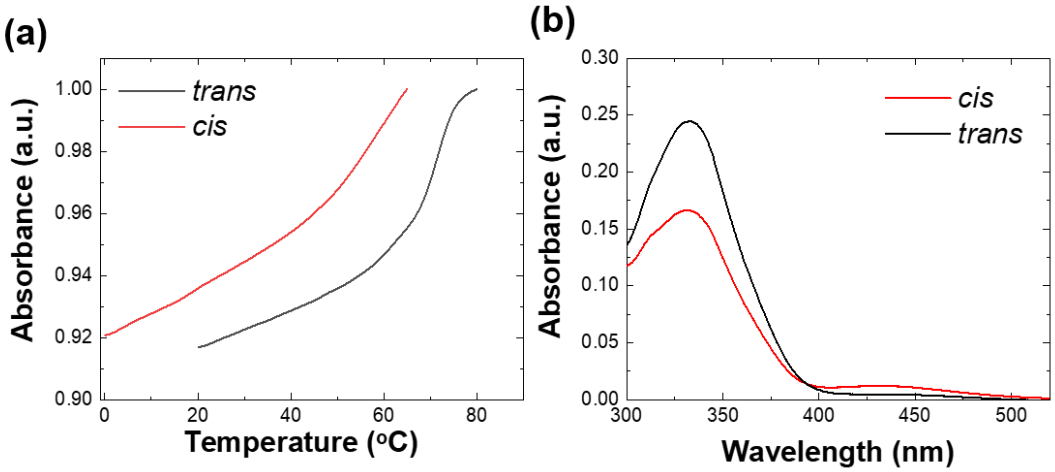

Figure 3.2 (a) Change of melting temperature (*Tm*) of *p*DNA duplex upon photoinduced isomerization of azobenzene in *trans*- (black line) and *cis*-form (red line). Conditions: 20 µM DNA, 100 mM NaCl, 10 mM phosphate buffer (pH 7.0) at 37 ^{o}C **(b)** Absorbance spectra of azobenzene in *p*DNA duplex.

Two complementary *p*DNAs (detailed sequence given in **Table2**) were selected to modify the MTs through copper free click reaction where they were labeled with DBCO (dibenzocyclooctyne) at the 5-end to react with azide functionalized MT (**Figure 3.3a**). ATTO550 and ATTO488 labeled tubulins were used to distinguish the microrobots as red (R)-swarm units and green (G) swarm units respectively which were shown in **Figure 3.3b**.

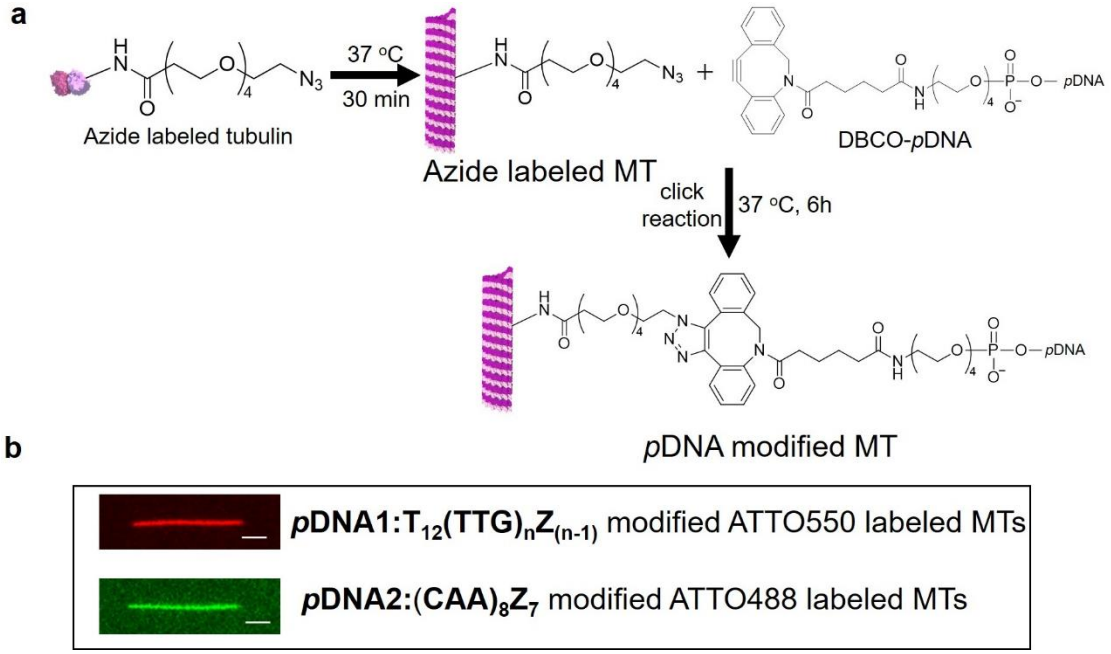

Figure 3.3 (a) Schematic diagram of preparation of swarm unit through conjugation of MT with *p*DNA by click reaction and **(b)** Fluorescence microscopic images of microrobot as swarm units, scale bar: 1 µm. The sequences of the *p*DNA were provided inside the box where n=2-8.

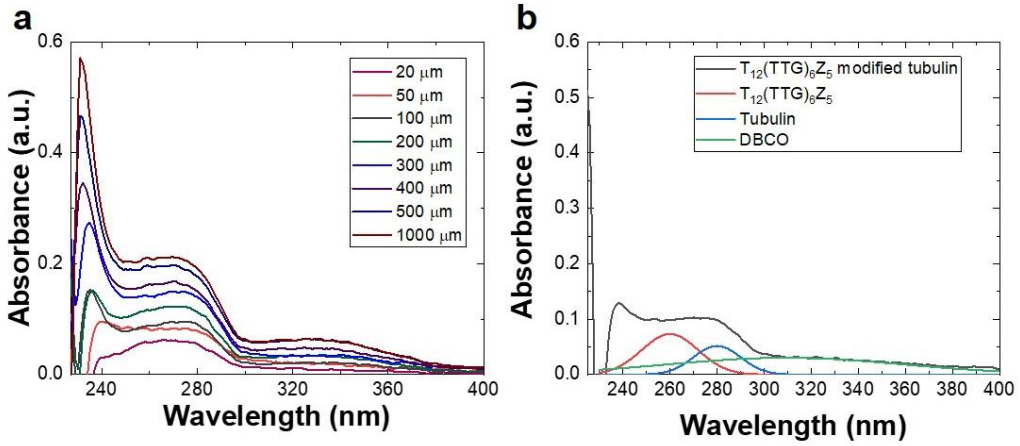

Figure 3.4 (a) UV-VIS absorption spectra of *p*DNA1 (n=6) conjugated MTs at various concentrations of *p*DNA1 as mentioned in the inset and evaluation of absorbance peaks of *p*DNA1, tubulin and DBCO by Gaussian distribution function. (a.u=arbitrary unit) **(b)** After conjugation of *p*DNA to MTs, the labeling ratio of *p*DNA to tubulin was determined using UV-visible spectrophotometer; the concentration of *p*DNA was 200 µM.

With increasing the *p*DNA concentration for conjugation, the labeling ratio was found to increase which can be clearly observed from **Figure 3.4a**. Each spectrum at different concentration was analyzed to determine the final concentration of *p*DNA conjugated MTs and the resulted labeling ratio (**Figure 3.4b**). The molar extinction of *p*DNA and labeling ratio of *p*DNA to tubulin were shown in **Table 3** and **Table 4** respectively.

The labeling ratio of *p*DNA to MTs was found ~40% from 200 µM DNA concentration which confirmed that 40% of total tubulin were labeled with minimum one single strand of *p*DNA.

3.2.2 Demonstration of swarming by active self-assembly of swarm units using photo-irradiation

Swarming of the two complementary *p*DNA modified microrobots was demonstrated under visible irradiation which is schematically shown in **Figure 3.5a.** Under the visible light, the *cis* to *trans* isomerization of the azobenzene units initiates the hybridization of the

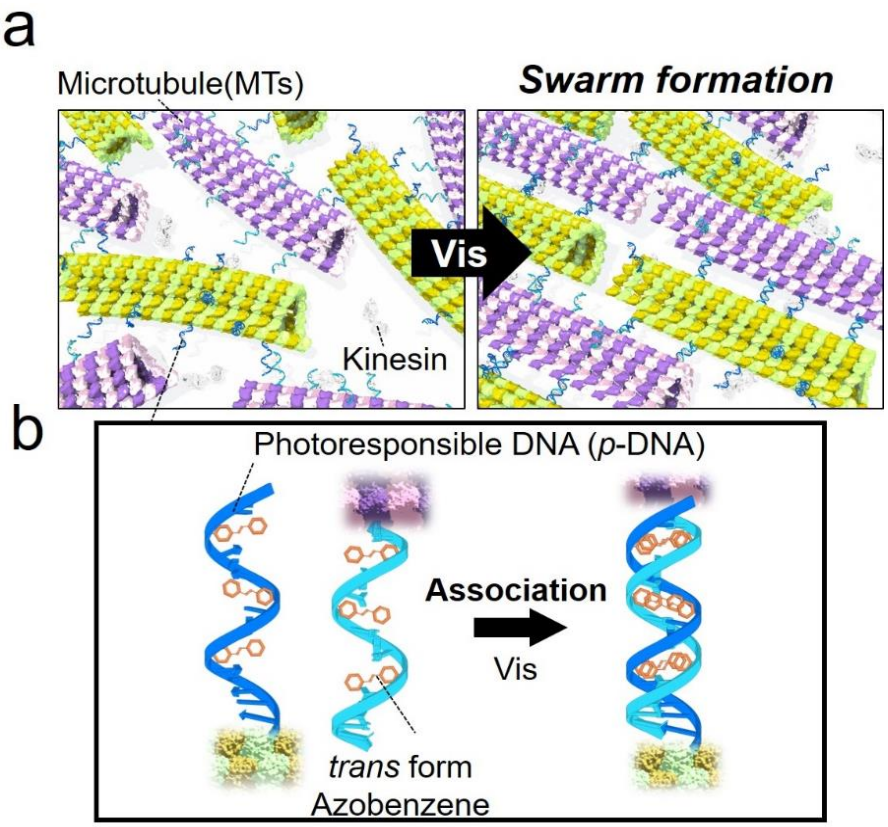

Figure 3.5 (a) Schematic diagram of swarm formation of complementary DNA modified MTs by photoirradiation. **(b)** DNA stabilization by trans isomerization of azobenzene.

complementary single strand of *p*DNA in an unzipping manner (**Figure 3.5b**). The planar *trans*-azobenzene intercalates between adjacent base pairs and stabilizes the DNA duplex by stacking interactions, whereas the nonplanar cis- azobenzene destabilizes it by steric hindrance.[14] The change in *Tm* observed upon isomerization is probably associated with changes in both the polarity and the structure of the azobenzene moiety.[27] The *trans* azobenzene is nonpolar and planar so that it favorably stacks with the adjacent DNA bases thus, the duplex is stabilized.[28] In contrast, the *cis* azobenzene is polar and nonplanar, making the duplex less stable.

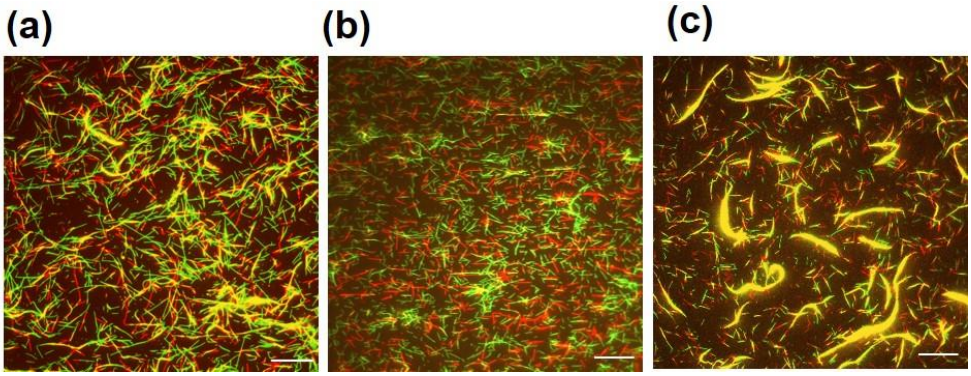

Figure 3.6 Fluorescence microscopic images of microrobots in different system: **(a)** microrobots were found to form aggregates in a static system. **(b)** no swarm formation was observed in an unfueled system (on a kinesin coated surface in the absence of ATP) **(c)** In the dynamic system, swarming of microrobots were formed on a kinesin coated surface in the presence of ATP. Scale bar: 20 µm.

Here to demonstrate swarming, individual swarm units were placed on a kinesin coated substrate at a density of ~36,000 per mm^2 area (density was measured in 0.04 mm^2 area) with almost an equal density of the two types of swarm units. The swarming was initiated after the addition of ATP under visible light which is favored by the active or dynamic self-assembly of swarm units using the driving force of molecular motor kinesin powered by ATP. It is to be mentioned that, in static condition i.e. in absence of ATP or kinesin swarming didn't take place but some aggregates were found to observe (**Figure 3.6a**).

These aggregates were mainly formed by the Brownian motion of swarm units in equilibrium condition while swarm units attached on the kinesin coated surface without ATP were restricted to move by Brownian or dynamic motion which even prevents the aggregate formation.

On the other hand, while gliding, the red and green MTs came close to each other, combined to form swarming (appearing yellow in the merged images), and continued moving on the substrate.[12] Swarming is preferentially formed by the unidirectional moving swarm units with similar velocity in active self-assembly process under visible light. They form swarm due to the DNA hybridization through the unzipping mode as DNA hybridization was facilitated due to the unidirectional movement of MTs just before the collision. However, for the MTs that collided while moving in the opposite direction, no successful swarm formation was observed. Besides, in the presence of ATP the length or width of the swarm robots increased due to the association of the small bundles. Despite the increase in the length of swarm robots, the molecular swarm robot exhibited translational motion with a velocity (0.51 ± 0.02 μm s^{-1}) close to that of single units (0.60 ± 0.05 μms^{-1}).

In order to optimize the swarm robotic system, I systematically investigated the effect of related physicochemical parameters on the swarming of microrobots in reponse to photo-irradiaiton. A detailed understanding of the physicochemical parameters of different components of the swarming system will enable to expand the controllability and range of swarming behaviors. The knowledge may advance the development of complex molecular devices utilizing swarming of biomolecular motor systems in a bottom-up manner giving rise to new emergent functions of microrobots. Varying the following parameters, light sensors such as the number of photoresponsive azobenzene molecules in the DNA sequences, length of DNA sequences, the intensity of light, regulating localized association and dissociation of MTs swarms responding to the light signal; spatiotemporal and well-control over molecular swarm robots could be further achieved. To compare the effect of these parameters, the association time was adjusted for 60 min after ATP addition at which association ratio reached a saturated value (~90%) under visible light. Kinesin concentration was fixed at 800.0 nM in all cases which were optimized by varying the concentration of kinesin. The effects of the relevant parameters on the swarming of molecular robots were systematically studied.

3.2.3 Effect of time on swarming through active self-assembly

Time dependent swarming was explored by the active self-assembly of microrobots to investigate the saturation of assembly formation and prolonged observation of this system. Thus, MTs were modified with the complementary *p*DNA strands individually and the labeling ratio of *p*DNA1 (n=6) to tubulin was estimated as 39% whereas for *p*DNA2 to tubulin was 31%. For driving the self-association in the non-equilibrium system, the kinesin concentration was used 800.0 nM with a density of red and green swarm units ~36,000 per mm^2 area. The fluorescence microscopic observation was performed just after the ATP addition using ICS with scavengers.[29] **Figure 3.7** shows the time lapse fluorescence images where the change in size and number of swarm groups can be clearly observed.

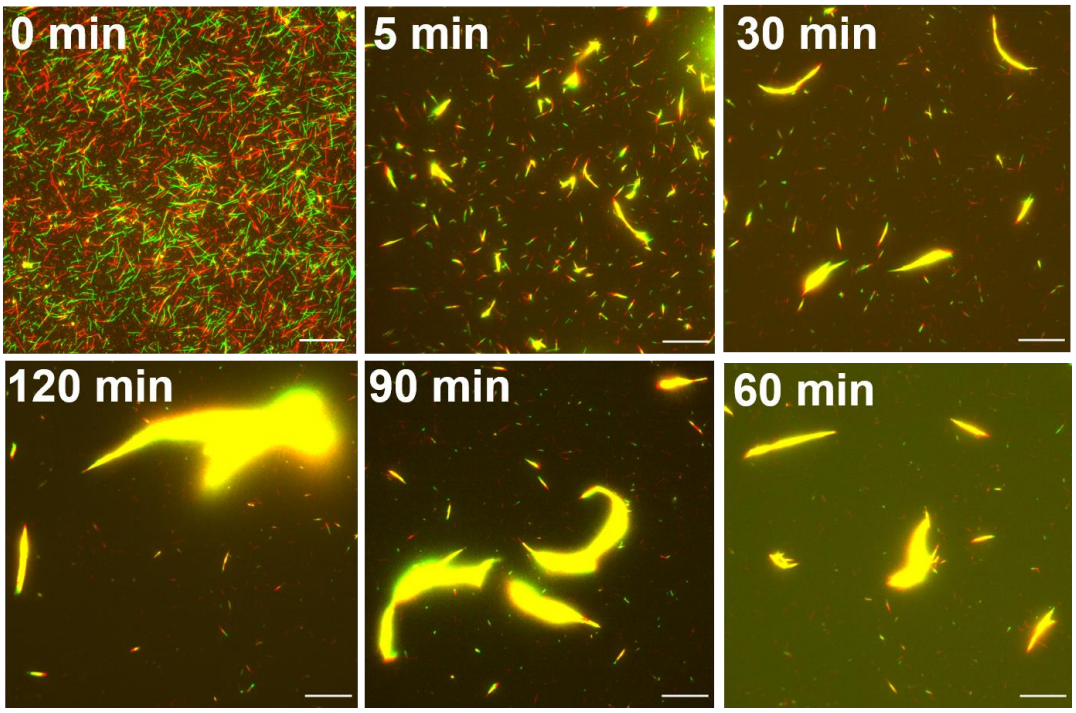

Figure 3.7 Time lapse fluorescence microscopy images showing the variation of size and number of swarm robots with time. Scale bar: 20 µm.

The association ratio increased with time and reached a plateau value (~90%) after 60 min of ATP addition under visible light which was shown in **Figure 3.8**.

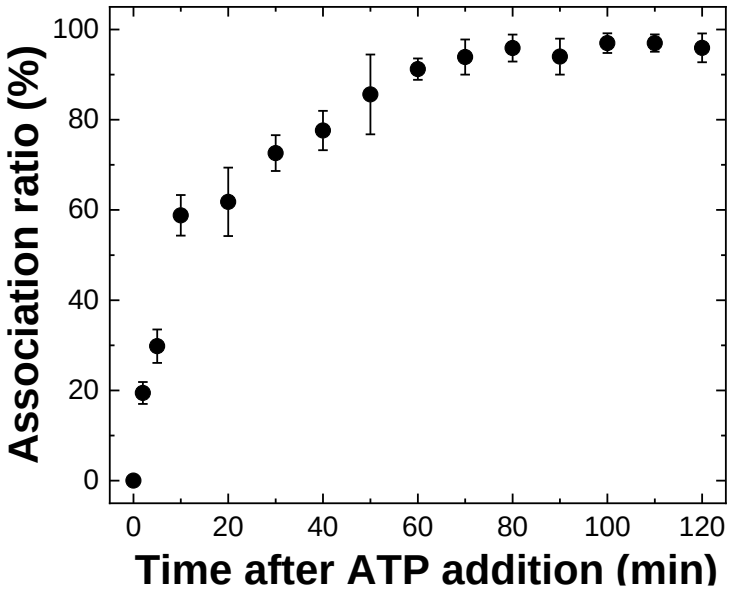

Figure 3.8 Association ratio of microrobots as swarm units with time after the addition of ATP in the system. Error bar: Standard deviation.

Upon collision of the red and green microrobots, swarm robots with an average size of ~10.28±5.29 µm were produced which was larger in size than the individual swarm units (average length of ~6.61± 2.89 µm) as shown in **Figure 3.9a**. Initially the number of bundles increases which then found to gradually decrease with time. The reason behind decreasing the bundle number can be understood from the fact that the size of the bundles or swarm robot increased which formed through the encountering of the small swarm robots (**Figure 3.9b**). Over time the size of the swarm robots increased as~33.91± 16.45 µm at 60 min and ~45.97 ± 32.41 µm at 120 min.

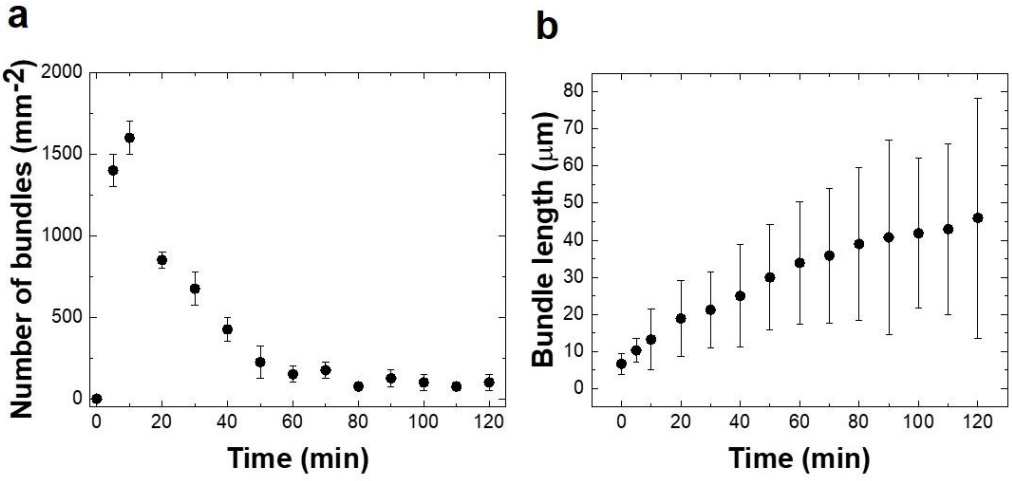

Figure 3.9 (a) Change in the number of swarm robots with time. **(b)** Variation of length of swarm robots over time. The number of swarm groups with translational motion increased initially just after ATP addition and then decreased with time. The association of swarm

groups into larger ones caused such a decrease in number which is ascribed to the change in their bundle length with time. Error bar: Standard deviation.

3.2.4 Effect of concentration of *p*DNA on swarming

A systematic investigation was performed to determine how the concentration of the *p*DNA1 affects the swarming of microrobots. Fixing the concentration of *p*DNA2 at 200 µM, the concentration of *p*DNA1 (n=3) was varied for MT modification from 20-500 µM. In the motility assay, the kinesin concentration was used as 800.0 nM for driving the self-

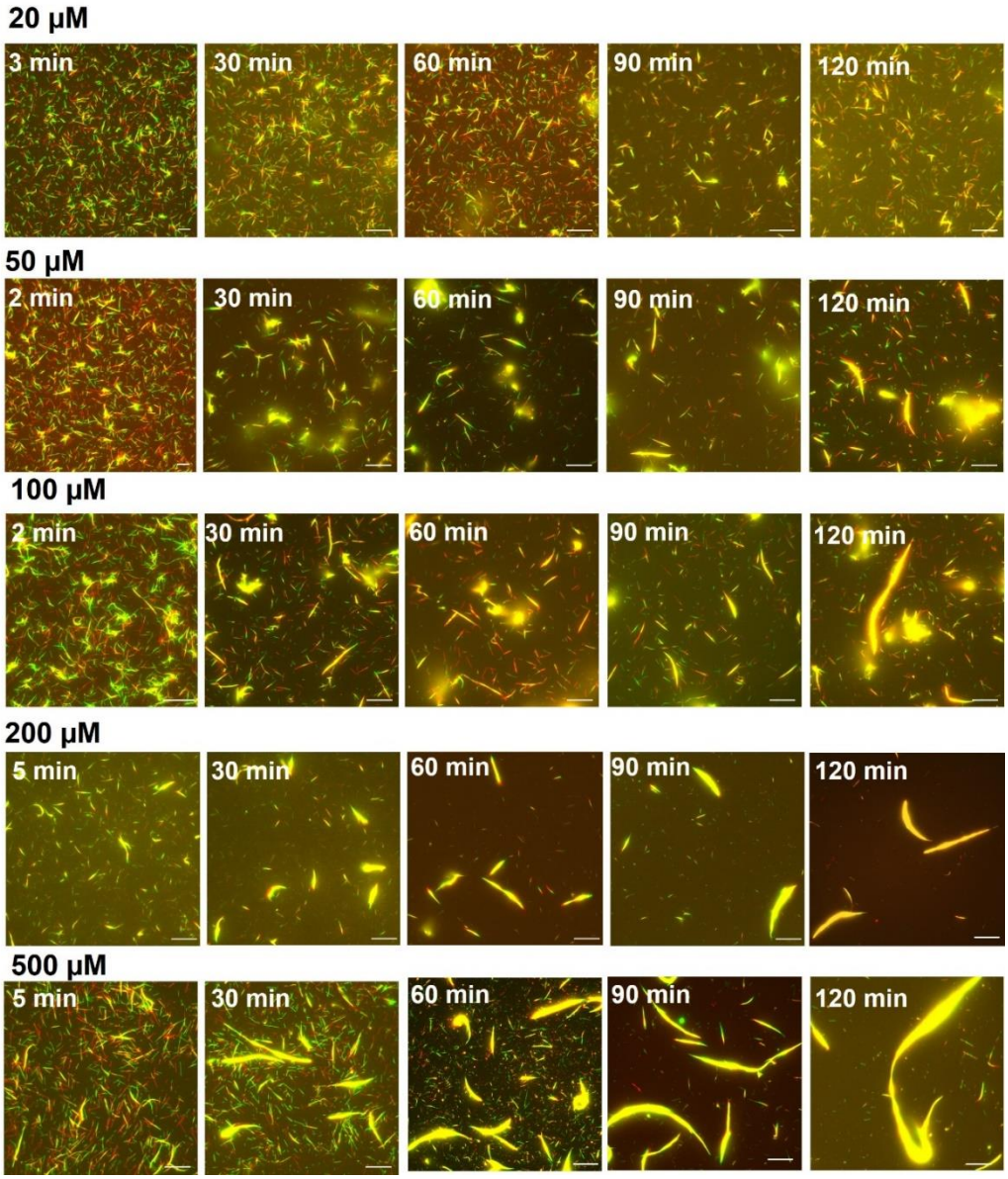

Figure 3.10 Fluorescence microscopy images of the swarming of microrobots affected by the concentration of *p*DNA1 (n=3). The concentration of the *p*DNA1 (n=3) used during experiments was mentioned in the inset. Scale bar: 20 µm.

assembly of red and green microrobots. An almost equal density of red and green microrobot (1:1 density ratio) was used in the experiments at which swarms with the highest association ratio and largest size were formed. The swarming of microrobots was observed by epifluorescence microscopy just after the ATP addition shown in **Figure 3.10**. The labeling ratio of *p*DNA1 to tubulin dimers was found to increase as the concentration of *p*DNA1 increased and reached ~62% at the concentration of 200 µM (**Figure 3.11a**).

Although MTs exhibited swarming with translational motion when the concentration of *p*DNA1 was 20 µM, more swarming was observed after increasing the concentration, which is evident from the corresponding association ratio (**Figure 3.11b**). Further increase in *p*DNA1 concentration (200–500 µM) brought no considerable change in the association ratio. This is occurred due to the high labeling ratio of DNA to tubulin dimers, the swarming among the microrobots increases which was confirmed from the yellow color and long bundle length of swarming which shows translation motion. From 200 µM of concentration, the self-assembly becomes saturated as can be clearly understood from their association ratio (**Figure 3.11b**).

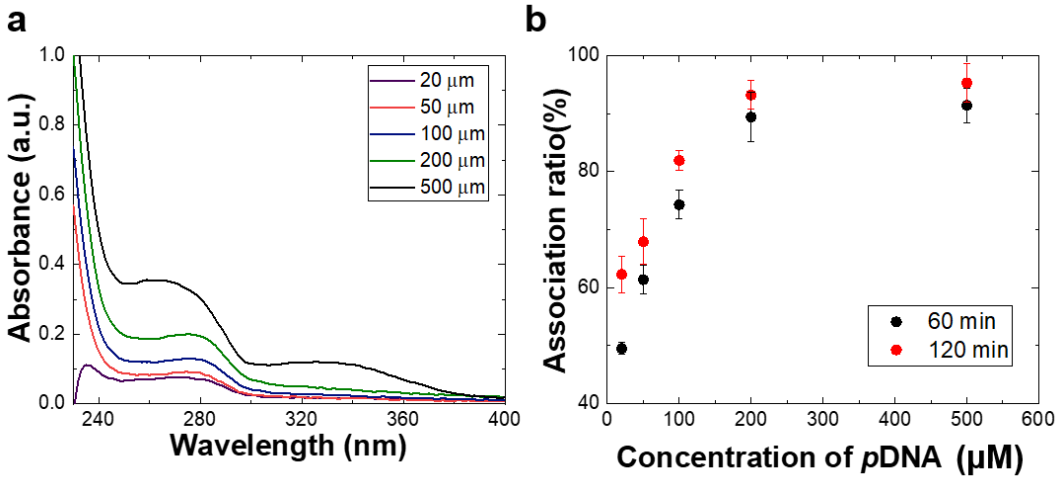

Figure 3.11 (a) Absorption spectra of DNA labeled tubulin changing the concentration of *p*DNA1 during preparation. **(b)** Change in association ratio of swarm units upon changing the concentration of *p*DNA1 (n=3). With increasing the concentration of *p*DNA1 (n=3), the association ratio rapidly increased and reached a plateau at 200 µM. Error bar: standard deviation.

3.2.5 Effect of length of *p*DNA on swarming

The stability of DNA double helix depends on the number of base sequences that change the melting temperature (*Tm*) of DNA hybridization. It is important to investigate the effect of length of DNA on the extent of swarming depending on the DNA hybridization strength at room temperature. To confirm the effect of length of DNA on the swarming of MTs, *p*DNA1 with different length ($T_{12}(TTG)_nZ_{(n-1)}$ where n =2–8) were designed (in **Table1**). Simulations predict how the melting temperature (*Tm*) increases with the increasing length of *p*DNA1. Depending on the feasibility of the hybridization of complementary DNA strands favored by their *Tm*, the length of *p*DNA1 can influence the DNA based self-assembly as found in the previous works. To investigate the effect of length in the system, MTs were modified with different lengths of *p*DNA1 maintaining almost the same labeling ratio of DNA to tubulin. The concentration of *p*DNA2 was kept the same in all the cases. The concentration and the labeling ratio of DNA to tubulin were mentioned in **Table5**. Complementary *p*DNA1 and *p*DNA2 conjugated MTs were loaded on a kinesin-coated surface at a combined density of ~50,000 mm^{-2}.

Upon addition of *p*DNA1 with the number of TTG base (n) smaller than 4, almost no swarming of MTs was observed ($T_{12}(TTG)_2Z_1$- $T_{12}(TTG)_3Z_2$) (**Figure 3.12**). In the case of n=4, ($T_{12}(TTG)_4Z_3$ modified MTs) where the total number of base pair is 12, microrobots started to form an association under visible light irradiation. While gliding, the red and green microrobots came close to each other and formed an association appearing yellow in the merged images, and continued moving. This may represent that increasing complementary base pair provided sufficient interaction energy which resulted in the increasing yellow colored swarms of MTs. Swarming of the microrobots was observed to increase with time combining the small swarm robots. Along with the thermodynamic feasibility, the swarm formation rate was also influenced by the length of *p*DNA1.

The increase of the extent of swarming with increasing the length of *p*DNA1 sequence can be easily understood from the change in their association ratio with time (**Figure 3.13 and 3.14**). TTG base sequences more than 4 are found to have high association ratio (~90–98%) and reach a plateau after 60 min of ATP addition.

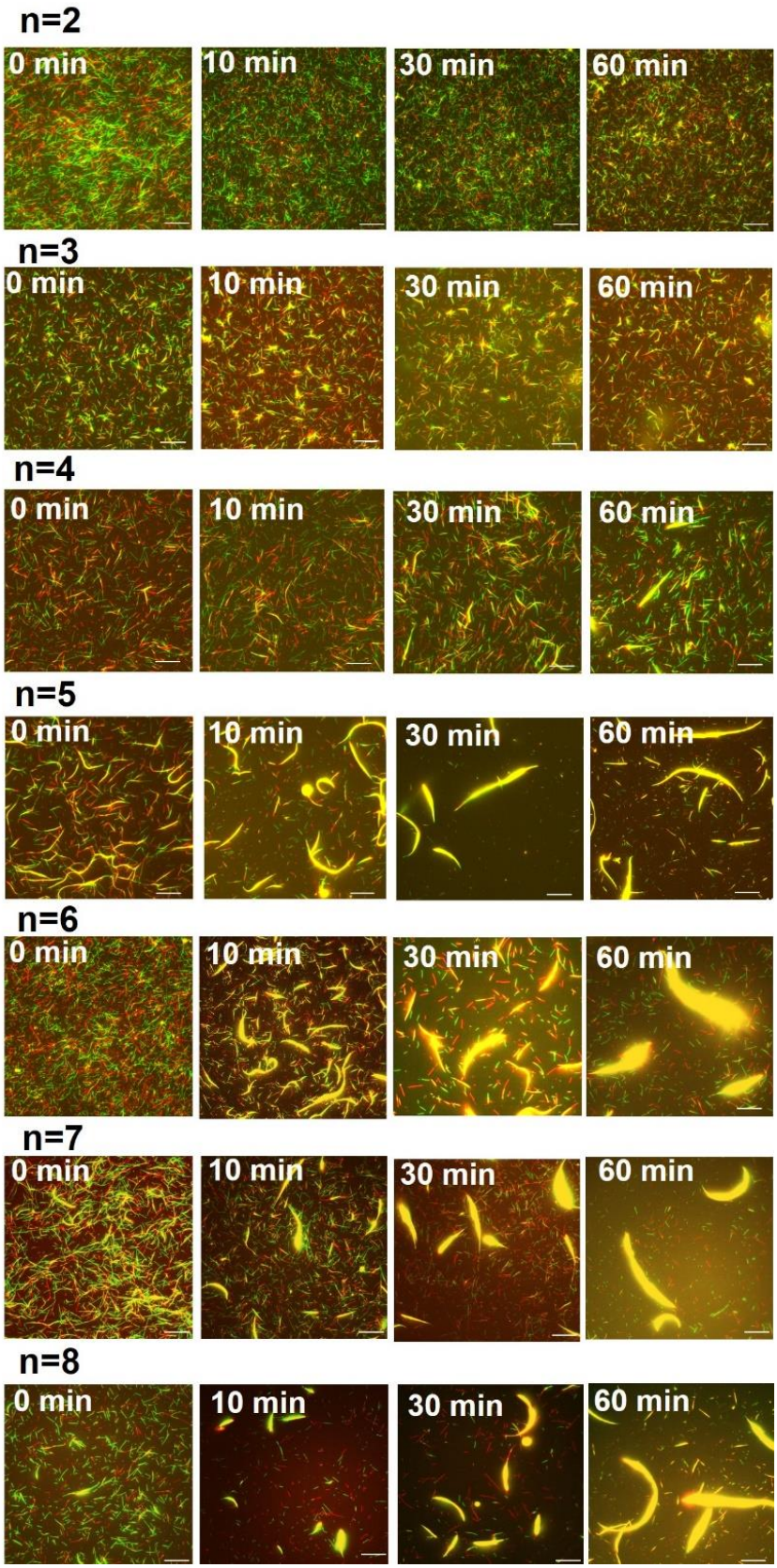

Figure 3.12 Fluorescence microscopy images of swarming of microrobots formed in presence of different lengths of *p*DNA1. 0 min indicates the time of ATP addition. Scale bar: 20 µm.

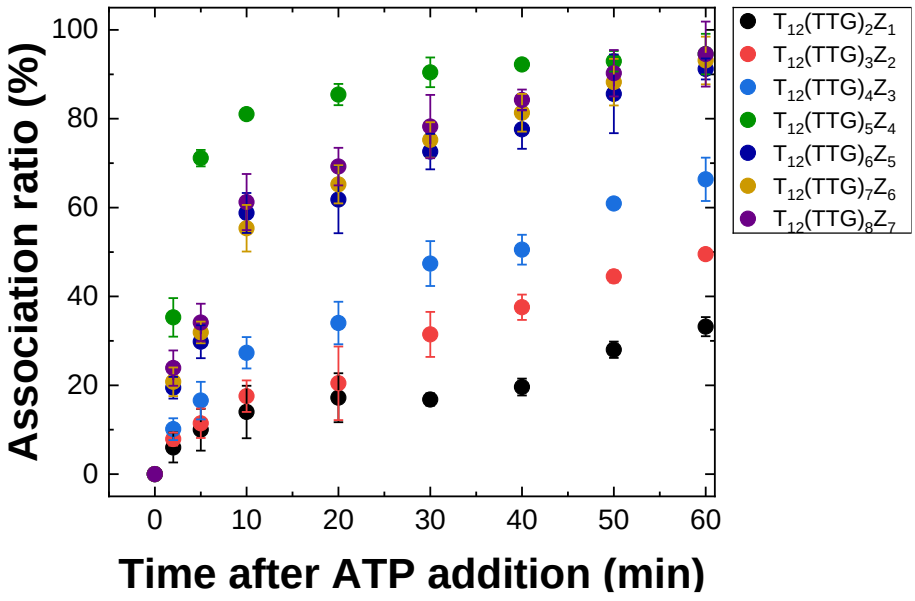

Figure 3.13 Association ratio of molecular swarm robot where red MTs modified with different lengths of $T_{12}(TTG)_nZ_{(n-1)}$; n = 2–8. The name of the base sequences was mentioned in the box positioned on the right of the plot. Error bar: standard deviation.

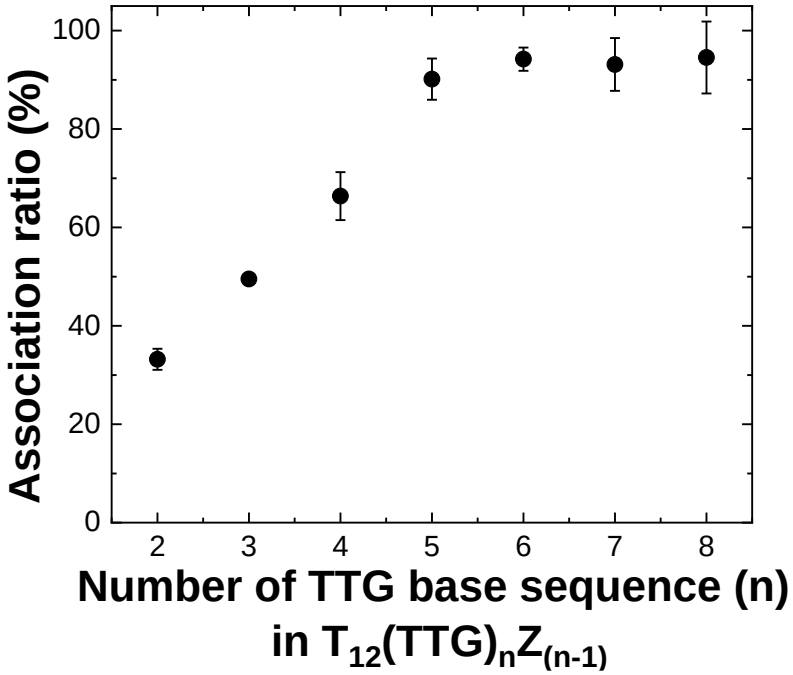

Figure 3.14 Variation of association ratio of molecular swarm robot with the number of TTG base sequences (n) formed after 60 min of ATP addition.

Thus, the kinetics of the self-association of swarm units can be controlled by designing the number of sequences of input DNA signals.

3.2.6 Reversible swarming of microrobots

To control swarming of the microrobots reversibly, photoresponsive molecule azobenzene was incorporated into the DNA sequences (in detail in section 3.2.2) which dissociate the swarm robot into single robots under UV light (**Figure 3.15a**). Under UV irradiation (λ=365 nm) *trans* form of azobenzene converts to *cis* form, the nonplanar *cis*-azobenzene destabilizes the DNA sequence by steric hindrance which breaks the hybridization of the DNA base pair (**Figure 3.15b**).

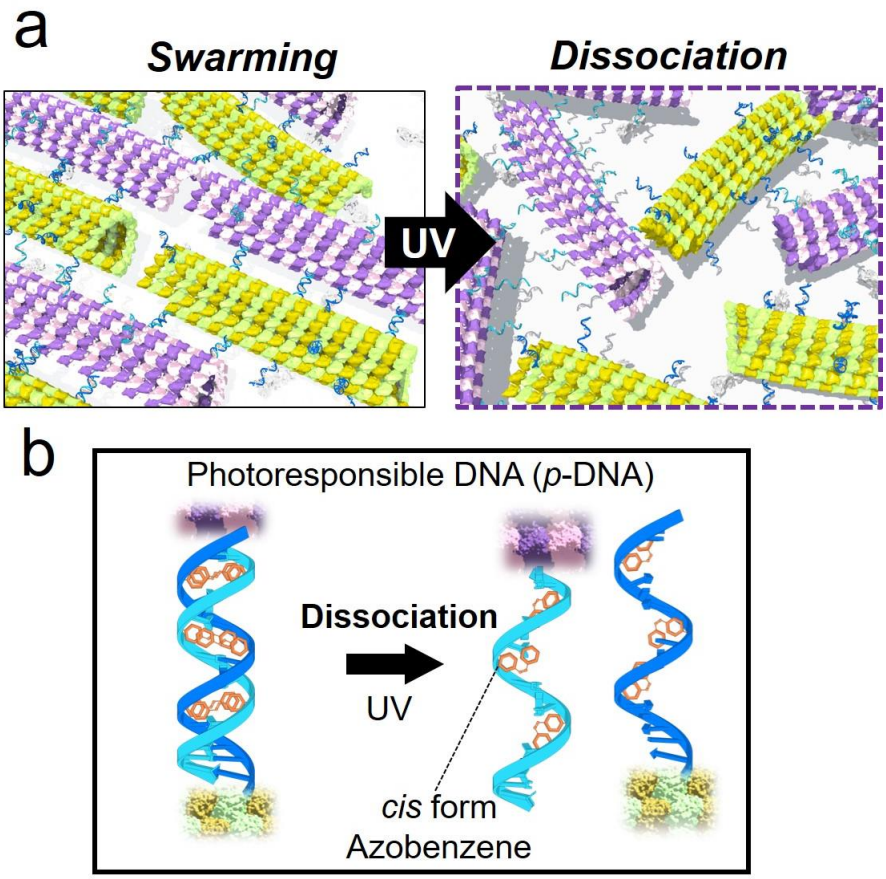

Figure 3.15 (a) Schematic diagram of reversible swarming of microrobots into complementary DNA modified single microrobots by UV irradiation (λ=365 nm). **(b)** Schematic illustration of DNA destabilization by *cis* isomerization of azobenzene under UV irradiation (λ=365 nm).

To investigate the effect of UV light on the swarming, UV light was irradiated directly on the swarm robot after 1 h of ATP addition and observed by epifluorescence microscopy. The intensity of the UV light was 0.59 mW/cm^2.

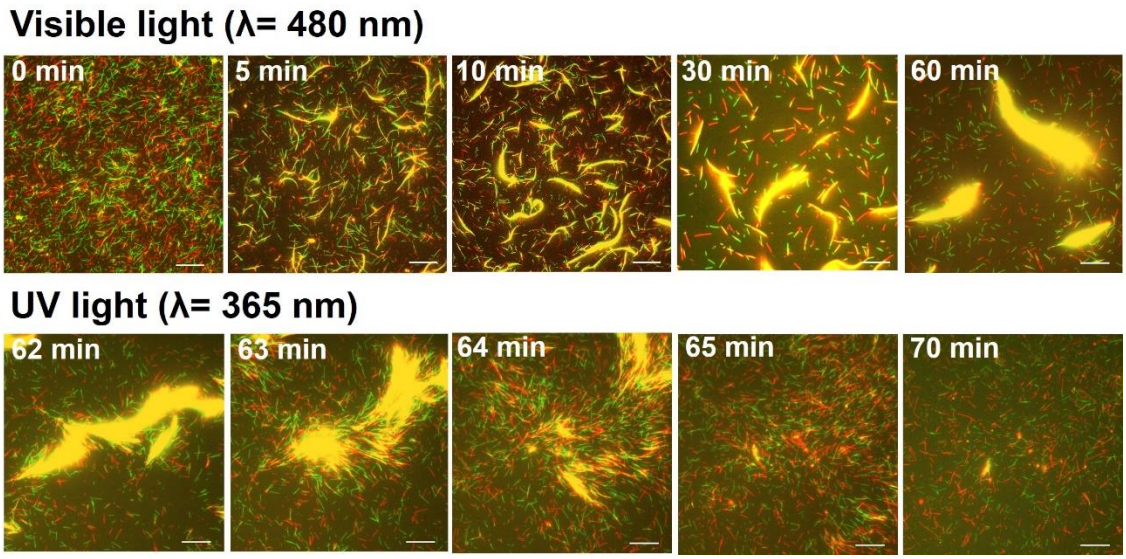

Figure 3.16 Time lapse fluorescence microscopic images of the swarm formation of microrobot under visible light and disscoiation of the molecular swarm robot into individual single microrobots after application of UV irradiation. Scale bar: 20 µm.

Under UV irradiation the *trans* form of azobenzene converts to *cis* form, which breaks the hybridization of the *p*DNA which allowed to dissociate the MTs individually. **Figure 3.16** shows the time lapse fluorescence microscopic images of the effect of visible-UV light on the swarming of microrobots. Visible light (λ>480 nm) was illuminated till 60 min of ATP

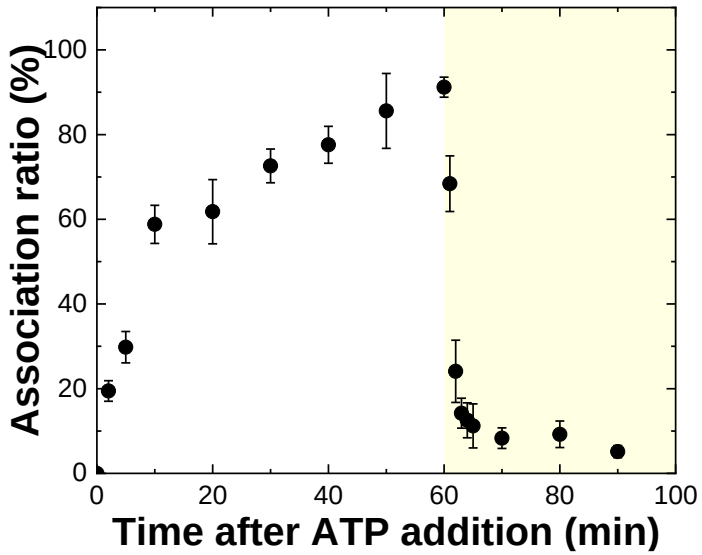

Figure 3.17 Variation of association ratio of the swarm robot under visible-UV irradiation. The yellow box indicates the effect under UV irradiation. Error bar: standard deviation.

addition and then UV light (λ=365 nm) was irradiated to observe the consequences of swarming.

The size of the bundle increased with time under visible irradiation as *cis* to *trans* isomerization of azobenzene in *p*DNA facilitates the hybridization of the complementary DNA as well as the association of the microrobots. But after UV irradiation to the *trans* form of the azobenzene converts to *cis* form which breaks the hydrogen bonding of the complementary DNA which allowed the reversible swarming or dissociation of the swarm robot into the single MTs. The dissociation into single MTs was quantified by a significant decrease in the association ratio in **Figure 3.17**. The association of the microrobots went to plateau after 60 min of ATP addition under visible light, but after UV irradiation the association ratio changes rapidly within 4 min.

To confirm that azobenzene incorporated DNA initiates the reversible swarming of the microrobots, the experiment was performed with the similar DNA sequences without azobenzene incorporation (control DNA or non *p*DNA) (sequences are given in SI **Table6**).

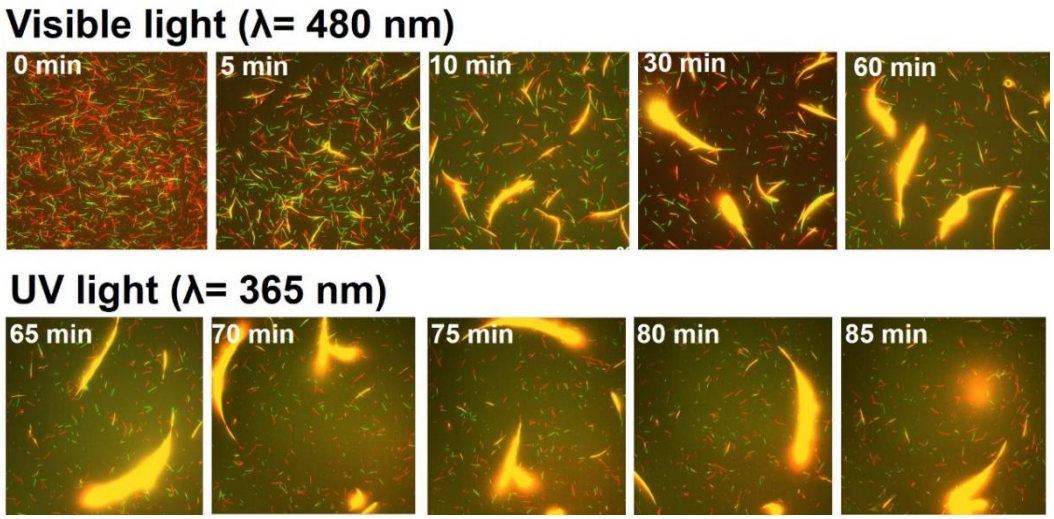

Figure 3.18 Time lapse fluorescence microscopic images of the effect of photoirradiation on the swarming of non *p*DNA (same DNA sequences without azobenzene incorporation) modified MTs. Scale bar: 20 µm.

From the fluorescence microscopic images in **Figure 3.18**, it was observed that the microrobots started to form swarming just after ATP addition under visible light. After 60 min of ATP addition UV light was irradiated constantly on the swarming of microrobots for 30 min. But no dissociation was observed under UV light. Besides, it was observed to increase the length of swarm robots associating small swarm robots even under UV

irradiation. So, light has no effect on the swarming of non *p*DNA modified MTs as azobenzene is the main factor to regulate the swarming reversibly.

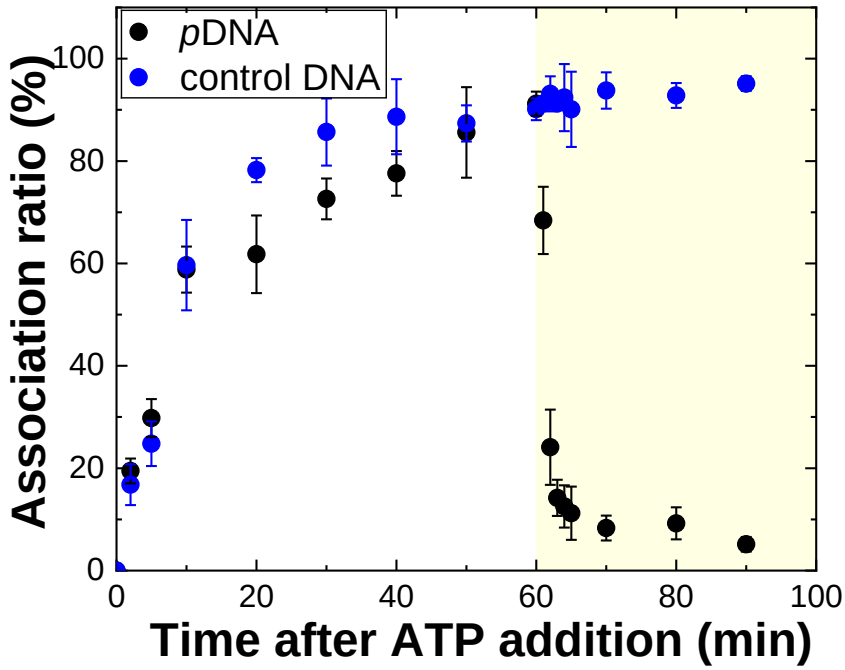

Figure 3.19 Variation of association ratio of the swarm robot under visible-UV irradiation. The yellow box indicates the effect under UV irradiation.

From the **Figure 3.19,** it can be said that the association ratio of the non *p*DNA modified MTs increased with time under both visible and UV irradiation. This result indicates that azobenzene acts as photosensor in the microrobots which can sense the wavelength of the light and program the association-dissociation of the actuators in the microrobot.

3.2.7 Effect of the number of azobenzenes in *p*DNA on reversible swarming

By introducing multiple azobenzenes in DNA, hybridization could be efficiently photo-regulated at constant temperature. To regulate the reversible swarming of the microrobots systematically, it is also necessary to understand the effect of the number of azobenzene in DNA. To investigate the effect of number of azobenzene in DNA on the reversible swarming of microrobot, the number of azobenzenes was varied in the $T_{12}(TTG)_nZ_{(n-1)}$ [where, n=2-8] sequence prior to swarm unit modification. The association ratio was

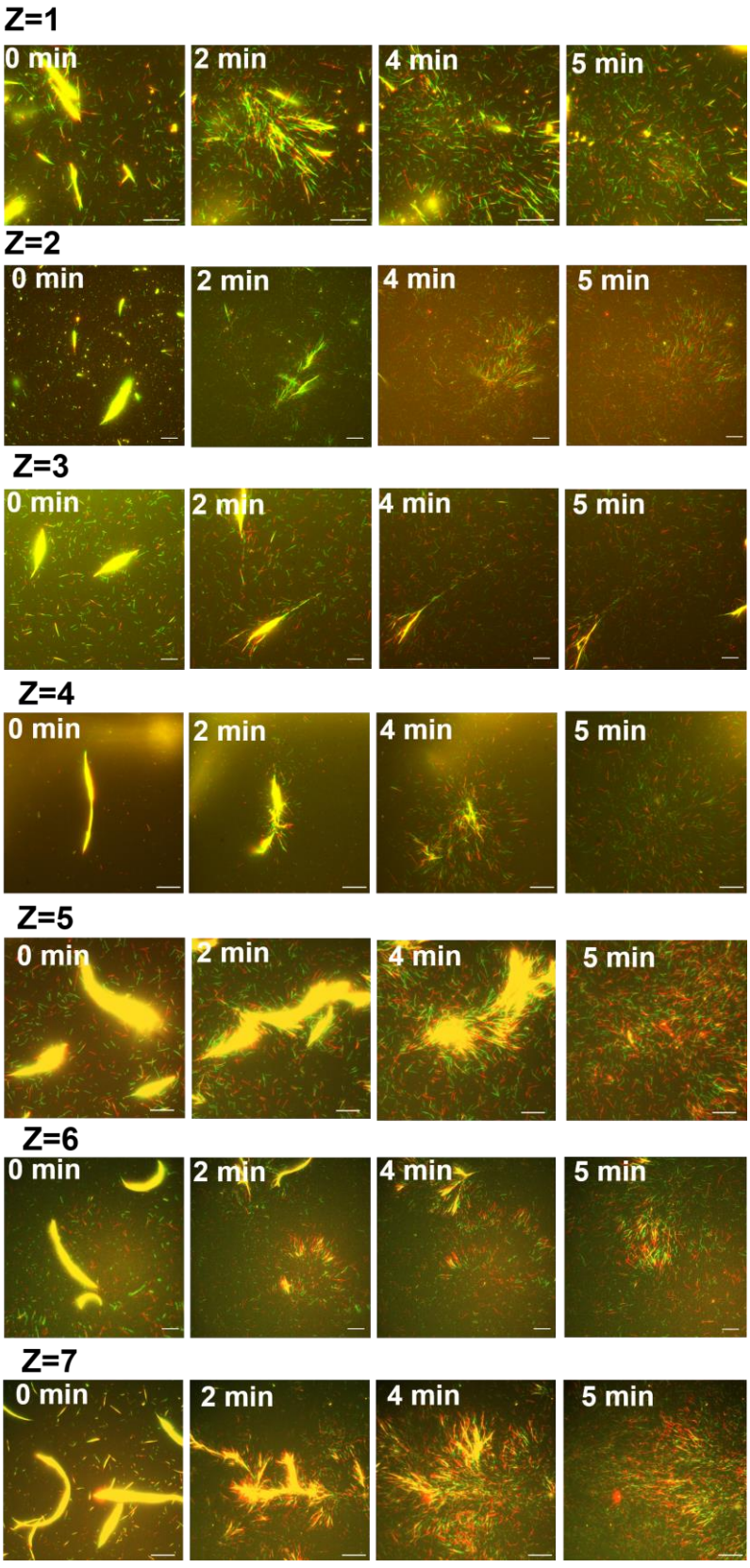

Figure 3.20 Time lapse fluorescence microscopy images showing reversible swarming of microrobots varying different number of azobenzene (Z) in $T_{12}(TTG)_nZ_{(n-1)}$. The images were captured after 60 min of ATP addition under UV light. Scale bar: 20 µm.

modification to get the maximum association ratio.

UV light was irradiated directly onto the swarm robot after 60 min of ATP addition. The intensity of the UV light was kept same for all the sequences as 0.59 mW/cm^2. **Figure 3.20** shows the time lapse fluorescence microscopic images of the reversible swarming of the molecular robot via dissociation into single MTs with increasing number of azobenzene (Z) in $T_{12}(TTG)_nZ_{(n-1)}$ strand.

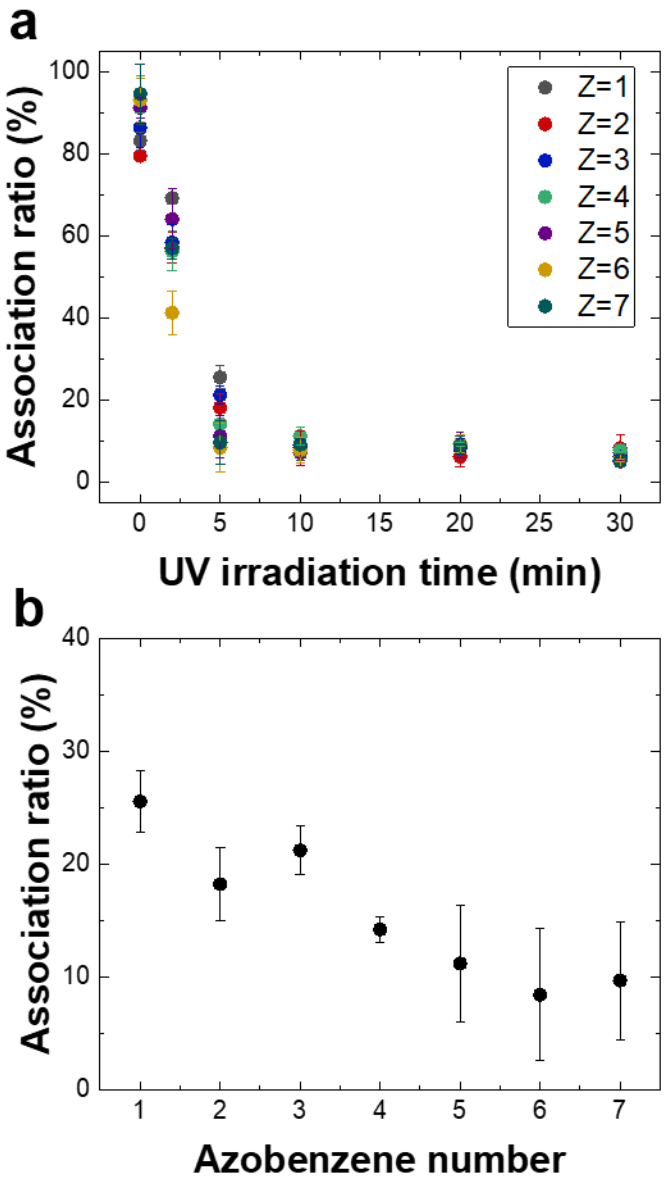

Figure 3.21 (a) Change in association ratio of swarm robots upon changing the number of azobenzenes in $T_{12}(TTG)_nZ_{(n-1)}$ under UV light. **(b)** The variation of the association ratio with the number of azobenzenes estimated after 5 min of UV irradiation. Error bar: Standard deviation.

With the UV irradiation the swarm robot started to dissociate and within 5 min the large swarm robot dissociated into the single microrobots as UV irradiation facilitates the dissociation by breaking the hybridization of the complementary DNA. After dissociation of the swarming robots, the single MTs retained their velocity and glided on the kinesin coated surface with a velocity of 0.6±0.1 μm/sec.

The variation of the association ratio of the microrobots was given in **Figure 3.21a** where it can be observed that the association ratio decreased drastically after the UV irradiation. Before UV irradiation, the association ratio of the microrobots was more than 80% in all cases. But after UV irradiation, the association ratio started to decrease very rapidly. The number of azobenzene can increase the efficiency of the reversible swarming of the microrobot. Here, it is important to mention that the dissociation also depends on the lengths of the swarm robots though the association ratio was almost same in every case.

From **Figure 3.21b,** it can be commented that with the number of azobenzenes, the dissociation ratio of the microrobots increases with time of UV irradiation. After 5 min of UV irradiation, for the higher number of azobenzene in DNA, the association ratio changed to ~10%. So, it indicates that the higher number of azobenzene can facilitate the dissociation of the swarm robot rapidly.

3.2.8 Effect of intensity of UV light on reversible swarming

High intensity of UV light can induce the damage of the biomolecular system which probihits the successful swarming of microrobots. To optimize the reversible swarming of the microrobots for the further advancements, it is necessary to understand the effect of intensity of UV light on the swarming.

Dissociation of swarm robots into single microrobots was observed after 60 min of ATP addition by epifluorescence microscopy changing the intensity of UV light. Neutral Density (ND) filter was employed to the UV light system to control the intensity of UV light.

Without ND filters, 100% of UV light was transmitted through the sample. ND filters are designed to reduce transmission evenly across a portion of a specific spectrum. The intensity of UV light was measured by THORLAB power meter (PM100D) using thermal power sensor S302C which was given in the **Table7**.

Five different intensity of UV light (I = 0.59 mW/cm^2, 0.50 mW/cm^2, 0.20 mW/cm^2, 0.19 mW/cm^2 and 0.06 mW/cm^2) were used to observe the dissociation of swarm robot into single MTs. Observation were performed after 60 min of ATP addition by epifluorescence microscopy which are shown in **Figure 3.22**.

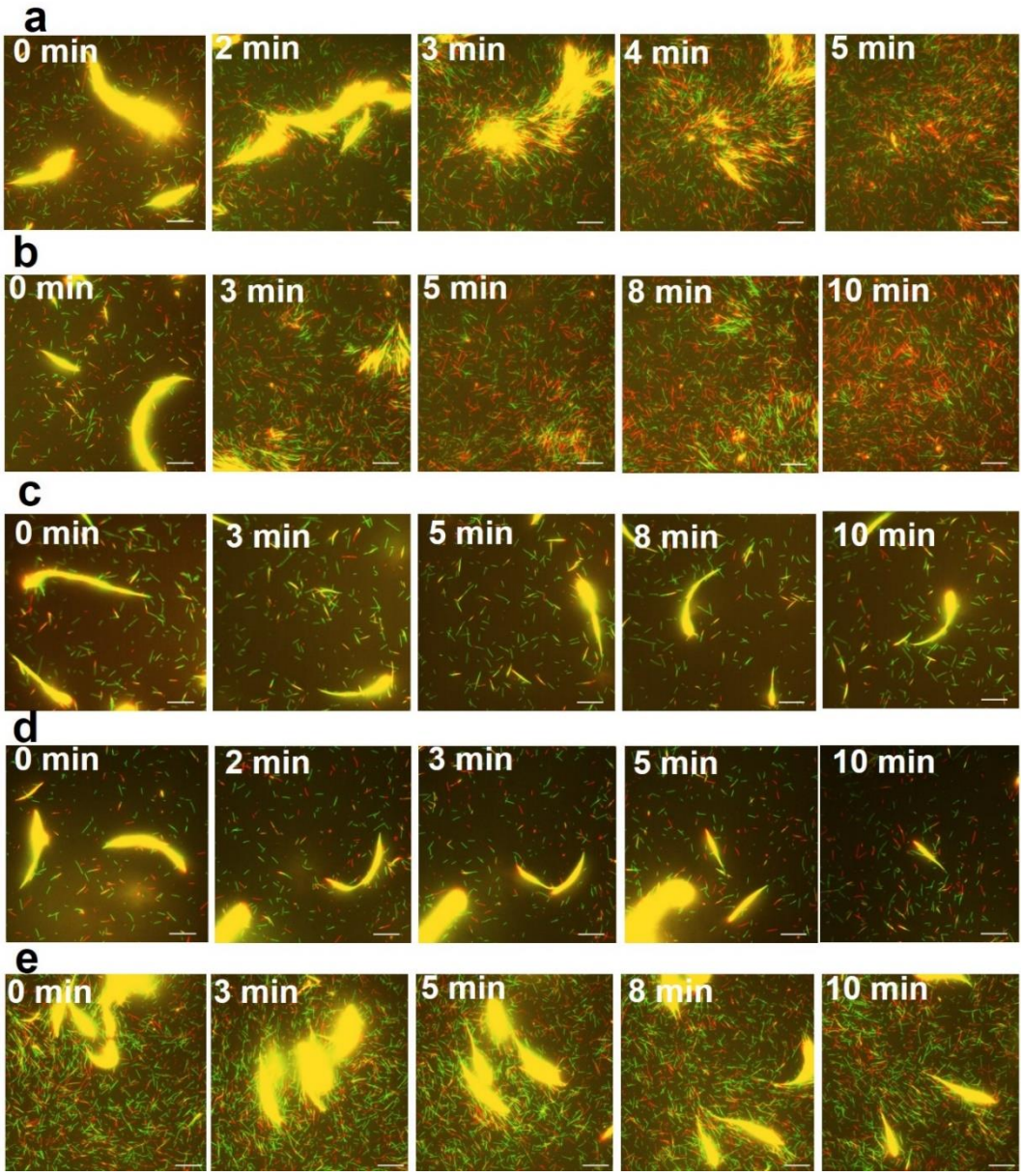

Figure 3.22 Time lapse Fluorescence microscopic images of dissociation of swarm robots into single MTs after 60 min of ATP addition under different intensity of UV light **(a)** I= 0.59 mW/cm^2, **(b)** 0.50 mW/cm^2, **(c)** 0.20 mW/cm^2, **(d)** 0.19 mW/cm^2, **(e)** 0.06 mW/cm^2. Scale bar: 20 µm.

From the **Figure 3.22**, it can be observed that when the intensity of UV light, I = 0.59 mW/cm^2 (UV transmission is 100%), all the bundles on the surface was dissociated very rapidly within 4 min of UV irradiation.

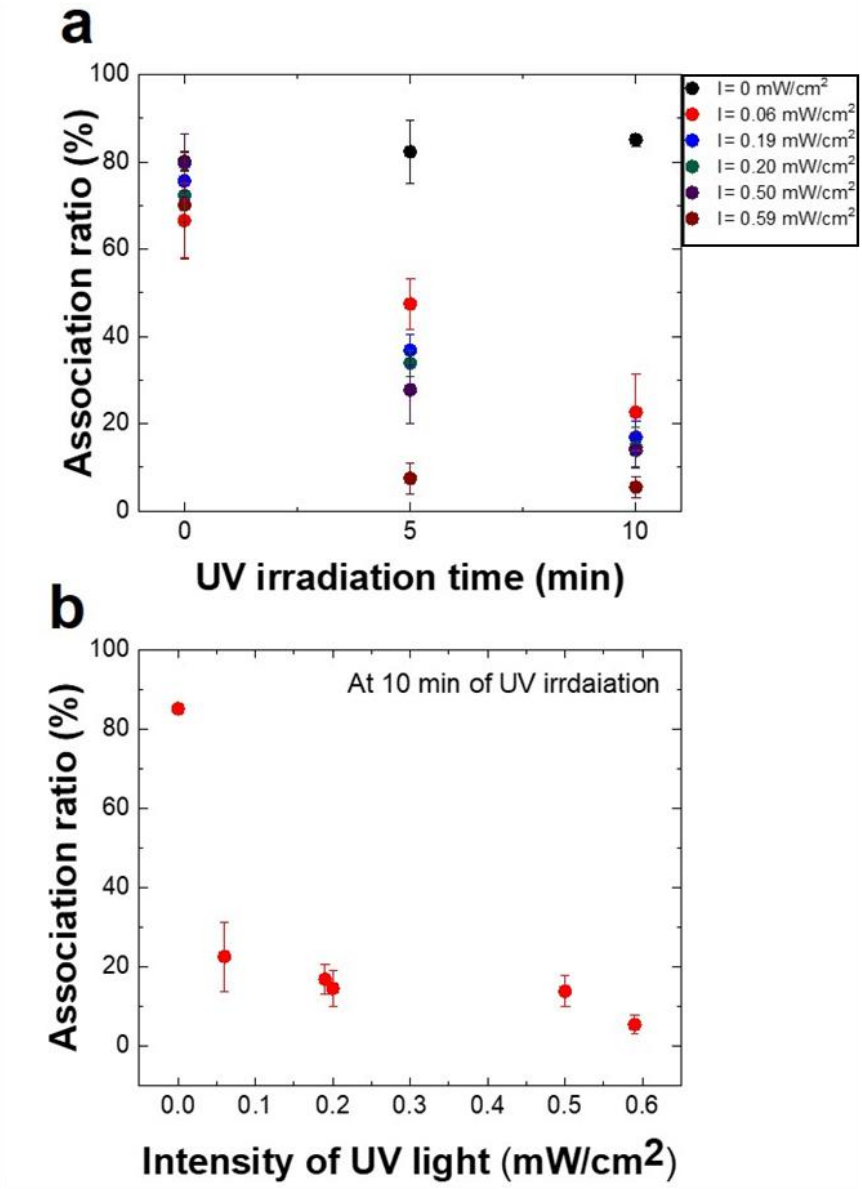

Figure 3.23 (a) Change in association ratio of swarm robots with time upon UV irradiation. The intensity of the UV light was mentioned in the square box at the right. (b) Change in association ratio of swarm robot at 10 min of UV irradiation with the intensity of light. Error bar: standard deviation.

But when 79.0% transmitted UV light (I = 0.50 mW/cm^2) was utilized on the swarming of MTs, it takes more time to dissociate the bundle of MTs into single MTs (~5 mins). Again,

during 50.0% of UV light transmission (I = 0.20 mW/cm^2), a large swarm robot did not show dissociation, but some small swarm robots dissociated. On the other hand, for 25% UV light transmission (I = 0.19 mW/cm^2), the dissociation of some small bundles was observed but with I = 0.06 mW/cm^2, the bundles were not dissociated till 30 min of UV irradiation. The result suggested that reversible swarming was mediated by the intensity of UV light which is again confirmed by the variation of the association ratio of the microrobots over the intensity of UV light.

The variation of the association ratio of the swarming robots with the intensity of the UV light was shown in **Figure 3.23** after 10 min of UV irradiation. So, the dissociation of swarm robots into single microrobots was increased with the intensity of UV light as the transmission of UV light became high.

3.2.9 Spatiotemporal control of swarming

Due to the prospect of reversible spatial and temporal control of swarm microrobots, investigations were carried out to regulate the swarming in a local region by photoirradiation. Different sized or shaped photomasks or patterns are employed in the UV light source which was connected to the fluorescence microscope directly. The wavelength of the UV light was 365 nm and the intensity of used UV light was measured as 0.59 mW/cm^2.

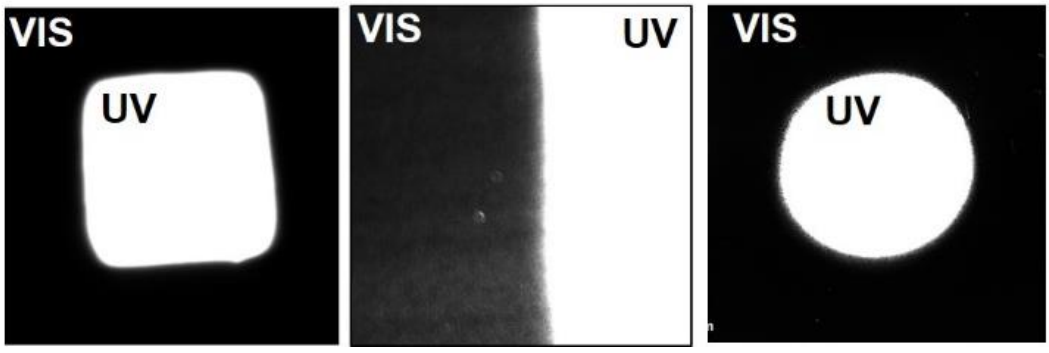

Figure 3.24 Fluorescence microscopic images of three different shaped pattern (left: square, middle: rectangular and right: circle) where the white area shows the UV irradiation area, whereas the black area shows the visible irradiation region

Three different photomasks were used to control the swarming of molecular robot spatiotemporally. The pattern structures were designed to maintain a fixed size (length/diameter/width of 4 mm) using Brother Canvas Workspace software and cut by

Brother ScanNCut printer which is shown by the fluorescence microscopic images in **Figure 3.24**.

Individual MTs were placed on a kinesin coated substrate with a density of ~50000 per mm^2 area (density was measured in 0.05 mm^2 area) containing almost equal no of complementary *p*-DNA modified swarm units. Association of the MTs was initiated after the addition of ATP buffer in the system under visible light. After 60 min of ATP addition, UV light was applied through a specific pattern in a local area using a different sized or shaped photomask. In the UV irradiation area, swarm robots started to disassemble into single MTs whereas, in the visible region the swarm robots continued to glide on the surface and formed a larger bundle with time.

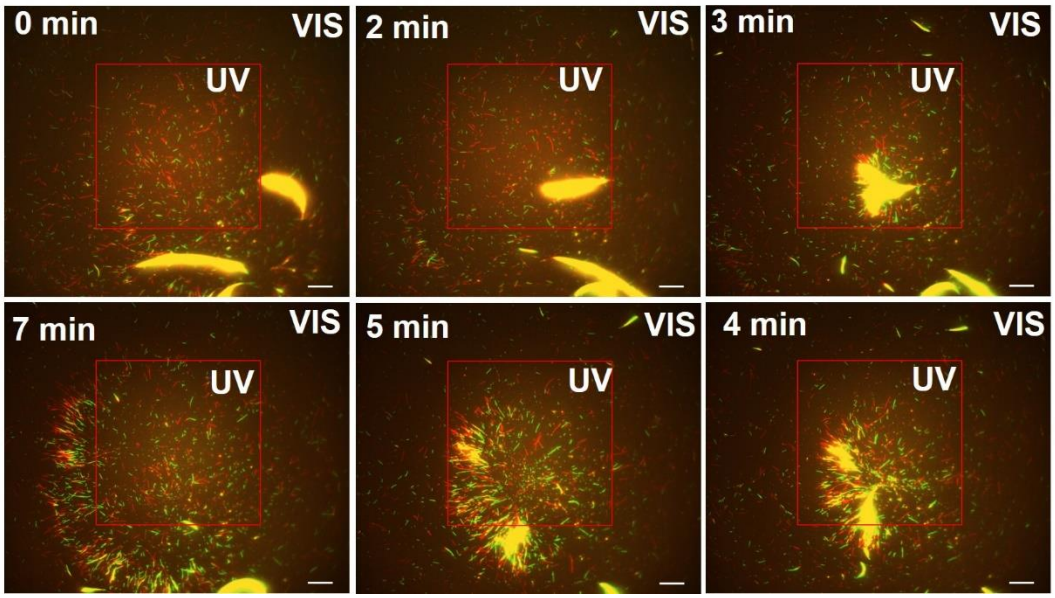

Figure 3.25 Time lapse fluorescence microscopic images of spatiotemporal regulation of reversible swarming of molecular robot into *p*DNA1 and *p*DNA2 modified GMPCPP MTs UV light was irradiated in a local area using square pattern which was shown by the red lined box. The area of the square region was 120 µm × 120 µm. Scale bar: 20 µm.

From the fluorescence microscopic images in **Figure 3.25**, when the bundle of swarm microrobots were passing through the square-shaped UV irradiation area, the swarm robot started to dissociate into single MTs due to the dissociation of the DNA duplex under UV irradiation. But outside of the irradiated local region, swarm microrobots were continued

gliding with almost the same motion in the visible area. Besides, the swarm microrobots gliding on the remaining region did not show any dissociation into single MTs.

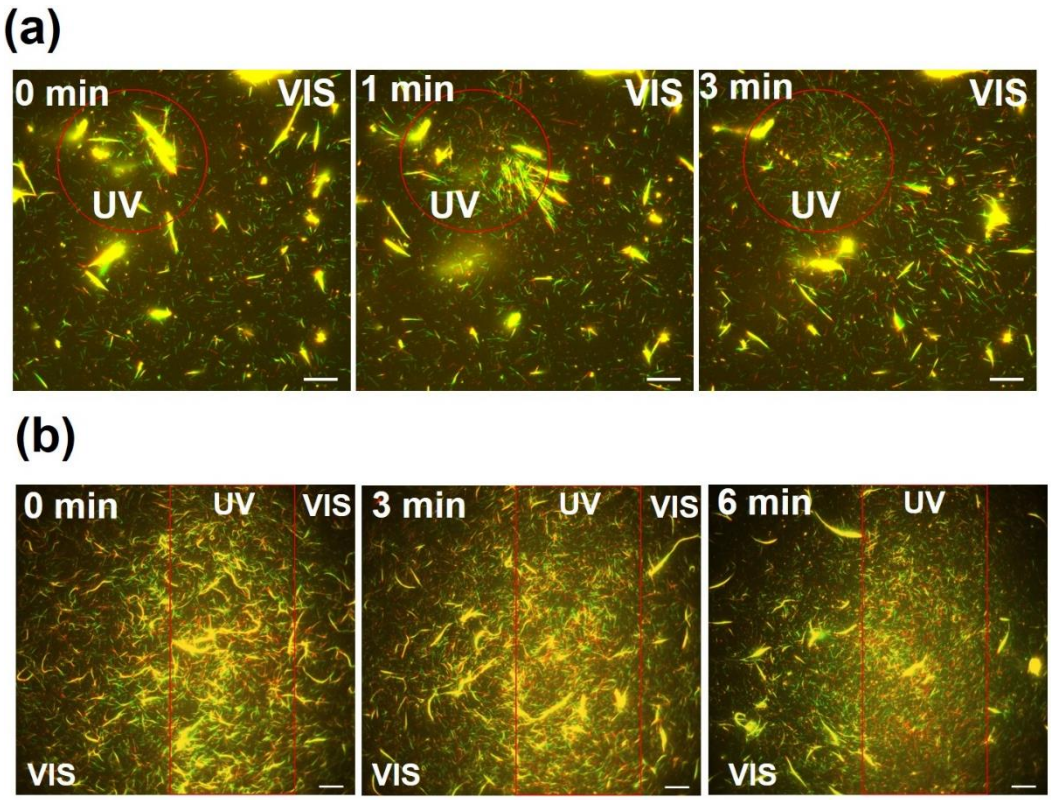

Figure 3.26 Time lapse fluorescence microscopic images of spatiotemporal control of reversible swarming of microrobot into single microrobots under UV irradiation using **(a)** a circular pattern **(b)** and a rectangular pattern. UV irradiation area was shown by the red-colored box. Scale bar: 20 µm.

The circular and rectangular-shaped pattern also used to regulate the reversible swarming of the microrobots in the spatiotemporal manner which is shown in **Figure 3.26**. Similar results were observed for the circular and rectangular-shaped pattern. The results confirmed that the reversible regulation of the swarming of the microrobots by UV irradiation through photomasks.

3.2.10 Light guided trajectories of the molecular swarm robot

In chapter 2 detailed study was performed on the light-regulated trajectories of *p*DNA conjugated microrobots driven by kinesin motors. It is also required to investigate the persistency of motion of the swarm robot under photoirradiation for further applications i.e.

the molecular shuttle based nanodevices. Prior to investigate the persistency of the motion under light, the path persistence length was measured for the *p*DNA conjugated swarm robot and the control DNA conjugated swarm microrobots. The path persistence length (L_p) was determined following the same approach described in the previous chapter.

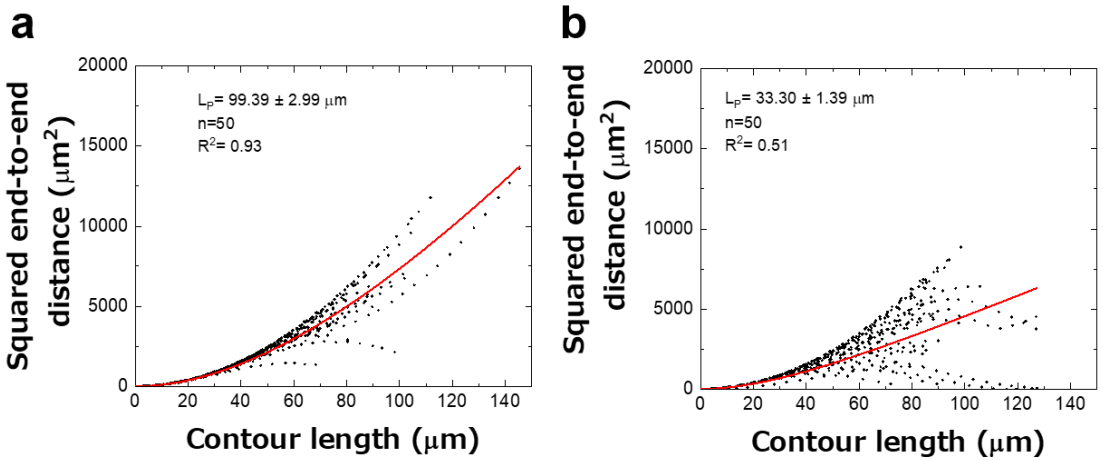

Figure 3.27 The estimated path persistence length of **(a)** swarm robot under visible light and **(b)** under UV light fitted with the $\boldsymbol{R^2 = 2L_P{}^2\left[(\frac{L}{L_P} - 1) + exp(\frac{-L}{L_P})\right]}$ where, *R* is the end-to-end distance, *L* is the contour length of the trajectories of MT, and L_p represents the path persistence length of MTs.

Comparing L_p of complementary *p*DNA modified swarm microrobots with the DNA (DNA sequences were given in **Table 8**) modified swarm microrobots, from **Figure 3.27** it was found that azobenzene incorporated DNA modified swarm robot showed lower path persistence length than the control DNA modified swarm robot. The incorporation of azobenzene in the DNA, can alter the interction of the kinesin and MT of the swarm robot under VIS light. But it was necessary to investigate the effect of UV light on the motion of the swarm microrobots. As UV irradiation breaks the hybridization of the DNA duplex which allows the disscoiation of the swarm robot, it is difficult to control the motion of the swarm robots under UV irradiation. To avoid the dissociation of swarm robot and regulate the motion of the swarm robot, control *p*DNA was mixed to the *p*DNA solution maintaining an optimized ratio. MTs were modified with a 9:1 ratio of *p*DNA and non *p*DNA during preparation and then observed by epifluorescence microscopy just after 1 h of ATP addition.

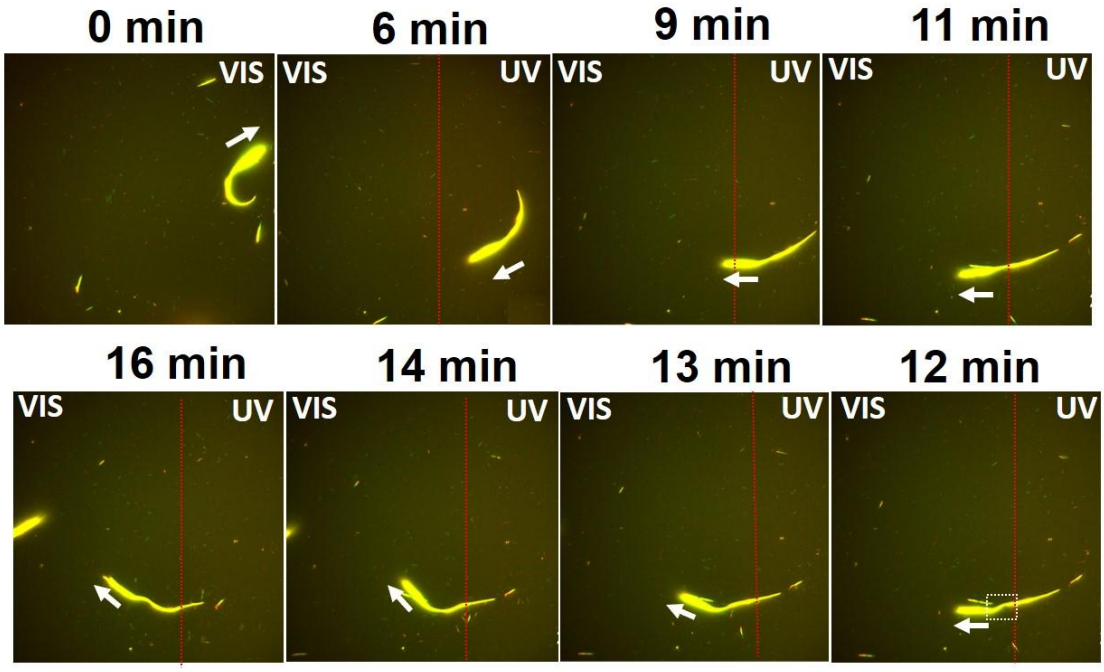

Figure 3.28 Fluorescence microscopic images of regulation of the trajectories of the swarm robot under UV-visible irradiation. Red colored line divides the UV-visible irradiation area.White box shows the change of the bundle entering to the VIS area to the UV area.

Visible and UV light was irradiated on the same surface to observe the change of the trajectories of the swarm robot. The intensity of the UV light was 0.06 mW/cm^2. From **Figure 3.28**, it can be said that a swarm robot which was gliding with a rotational motion under visible light, suddenly changed its path due to UV irradiation. In the UV region, the bundle became rigid with translational motion. During passing the UV region, the bundle showed some flexibility and again changed its path in the visible region.

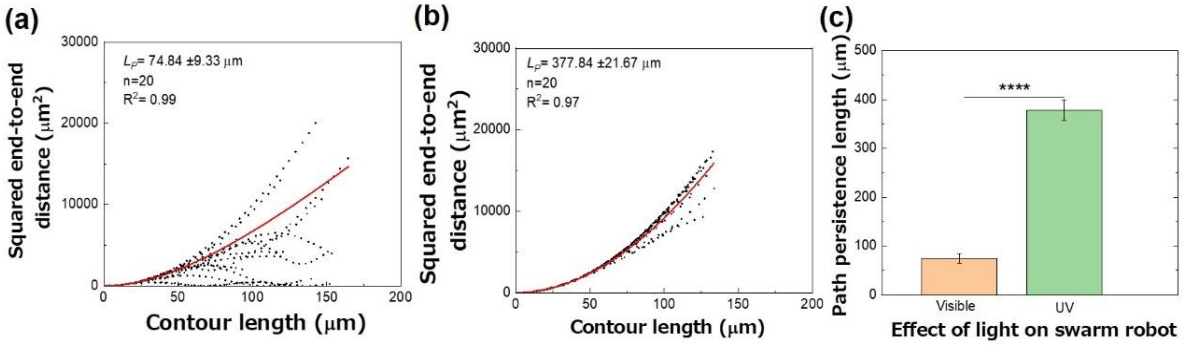

Figure 3.29 Path persistence length of swarm robot **(a)** under visible light and (b) under UV light **(c)** the comparison of the path persistence length of molecular swarm robot under light irradiation; the data were fitted with the $\boldsymbol{R^2 = 2L_P{}^2\left[(\frac{L}{L_P} - 1) + exp(\frac{-L}{L_P})\right]}$.

From **Figure 3.29**, it can be observed that swarm robots under visible irradiation showed lower L_p (74.84±9.33 µm) than under UV irradiation (377.84 ± 21.67 µm). The results indicate the higher persistency of motion of molecular swarm robot under UV irradiation compared to that of in visible light. The change in path persistence length of the swarm robot under UV light can be occurred due to the hydrophilicity of the *cis* form of azobenzene in *p*DNA.[30,31] Polarity change can alter the rigidity of the swarm robot which requires further investigation in the future.

3.3 CONCLUSIONS

In conclusion, the swarming of microrobots was successfully demonstrated in a reversible manner in response to the photo-irradiation. They exhibit swarming through the hybridization of the conjugated complementary DNA duplex under visible light. The extent of swarming through active self-assembly was controlled by tuning different physicochemical properties of DNA under photoirradiation. It was found to increase the association ratio of the microrobots with the length of *p*DNA over time whereas the increasing number of azobenzene in *p*DNA decreased the association ratio of the swarm robots. The intensity of UV light has a significant impact on the reversible swarming of the microrobots. Moreover, the spatiotemporal control of the swarming of microrobots was achieved successfully applying UV light through the local region. Additionally, the persistency of the motion of the gliding swarm microrobot was found to alter in response to the UV irradiation. Such well-controllable swarming of biomolecular motor based microrobots will open a new era to design swarming with engineered functionalities in molecular computation and molecular robotics.[32–34]

3.4 MATERIALS & METHODS

3.4.1 Purification of tubulin and kinesin

Tubulin was purified from porcine brain using high-concentration of PIPES buffer (1 M PIPES, 20 mM EGTA, and 10 mM $MgCl_2$) and stored in BRB80 buffer (80 mM PIPES, 1 mM EGTA, 2 mM $MgCl_2$, pH maintained to 6.8 using KOH pellet) Recombinant kinesin-1 consisting of the first 573 amino-acid residues of human kinesin-1 was prepared as described in the literature.[35] Azide labeled tubulin was prepared using N_3-PEG_4-NHS following the established protocol of labeling tubulin with a fluorescent dye.[25] The tubulin concentration was determined by measuring the absorbance at 280 nm using a UV spectrophotometer (Nanodrop 2000c).

3.4.2 Design and preparation of DNA sequences

All the *p*-DNA strands were selected or designed from *Tm* simulation using OligoAnalyzer 3.1 software with a *Tm* simulation using OligoAnalyzer 3.1 (https://sg.idtdna.com/calc/analyzer) software with a Tm between 0 and 50 °C for experimental testing. All the *p*DNA strands were purchased from Hokkaido System Science Co. Ltd. The *p*-DNA was modified at the 5′ end with dibenzocyclooctyne (DBCO). Quality control of all the synthesized DNA was performed by polyacrylamide gel electrophoresis (PAGE). Characterization of the *p*-DNA strands were carried out by LC-ESI-MS spectroscopy.

3.4.3 Preparation of microrobots as swarm unit

Microtubules (MTs) were polymerized from a mixture of azide labeled tubulin and Atto 550 labeled tubulin in which the concentration of tubulin was 70 µM. The molar ratio between azide labeled tubulin and ATTO 550 labeled tubulin was adjusted to 4:1. Then the tubulin mixture in polymerization buffer was incubated at 37 °C for 30 min to form MTs. 1 µL of 4×BRB80 buffer (80 mM PIPES, 1 mM EGTA, 1 mM $MgCl_2$, 1 mM GMPCPP, pH~6.8) and 0.5 µL of 1 mM taxol (in DMSO) were added to the MT solution just after polymerization to stabilize the MTs. Copper free click reaction was carried out by adding 3.5 µL DBCO conjugated *p*DNA (500 µM) to 5 µL MT solution (56 µM) and incubating at 37 °C for 6 h.[36] Cushion buffer (100 µL of BRB80 buffer supplemented with 60% glycerol) was used to separate the MTs by centrifugation at 201,000 × g (S55A2-0156 rotor,

Hitachi) for 1 h at 37 °C. After removing the supernatant, the pellet of *p*DNA conjugated MTs was washed with BRB80P (100 µL of BRB80 supplemented with 1 mM taxol) and resuspended in 15 µL of BRB80P buffer.

3.4.4 Measurement of labeling Ratio of DNA to tubulins

The *p*-DNA conjugated MTs were depolymerized to *p*-DNA conjugated tubulins by keeping the MTs on ice overnight. The absorbance spectrum of the *p*-DNA conjugated tubulin dimers was measured using a spectrophotometer (NanoDrop™ 2000c, Thermo Fisher Scientific Inc.).Then the spectrum was deconvoluted using the normal distribution function with Microsoft Excel 2016 (Windows Edition, Microsoft Corporation) with peaks at 260 nm and 280 nm. The concentrations of DNA and tubulin dimers were calculated from the Beer-Lambert law using molar extinction coefficient of tubulin dimers and DNA. Then the labeling ratio of *p*DNA to tubulin was determined from the ratio of the concentration of *p*DNA to tubulin.

3.4.5 Demonstration of swarming of microrobots

A microfluidic channel was constructed using two glass cover slides of 40×50 mm^2 and 18×18 mm^2 (MATSUNAMI Inc.) adhered together by parafilm as a spacer with a channel pattern cut off. The glass slides were plasma treated for 5 min by a plasma etcher (SEDE-GE; meiwafosis) to make it hydrophilic. The channel pattern was designed using Brother Canvas Workspace software on the parafilm and cut by Brother ScanNCut printer. The flow cell was prepared setting the designed parafilm on the large cover glass and then the small slide on the top and then heating at 70 ºC. The flow cell was filled with 5 µL casein buffer (BRB80 buffer supplemented with 0.5 mg mL^{-1} casein). After incubating for 3 min, 0.8 µM kinesin solution was introduced into the flow cell and incubated for 5 min. After washing the flow cell with 5 µL of wash buffer (BRB80 buffer supplemented with 1 mM DTT, 10 µM taxol), 5 µL of red MTs (*p*DNA1 modified ATTO550-labeled MTs) solution was introduced and incubated for 2 min, followed by washing with 10 µL of wash buffer. Subsequently, 5 µL of green MTs (*p*DNA2 modified ATTO488-labeled MTs) solution was introduced and incubated for 2 min, followed by washing with 10 µL of motility buffer. The motility of MTs was initiated by applying 5 µL ATP buffer (wash buffer supplemented with 5 mM ATP, 4.5 mg mL^{-1} D-glucose, 50 UmL^{-1} glucose oxidase, 50 UmL^{-1} catalase, and 0.2% methylcellulose (w/v)). The time of ATP addition was set as 0 h. Soon after the

addition of ATP buffer, the flow cell was placed in an inert chamber system (ICS)[29] and the MTs were monitored using an epifluorescence microscope at room temperature (25 °C).

3.4.6 Microscopy image capture

The samples were illuminated with a 100 W mercury lamp and visualized by an epifluorescence microscope (Eclipse Ti, Nikon) using an oil-coupled Nikon Plan Apo 60× objective (N.A.=1.4). UV cut-off filter blocks (TRITC: EX 540/25, DM565, BA605/55; GFP-B: EX470-40, DM500, BA535-50; Nikon) were used in the optical path of the microscope. Images were captured using a cooled-CMOS camera (NEO sCMOS, Andor) connected to a PC. Two ND filters (ND4, 25% transmittance for TRITC and ND1, 100% transmittance for GFPB) were inserted into the illumination light path of the fluorescence microscope to reduce photobleaching of the samples.

3.4.7 UV light setup

The experimental setup consists of a Nikon super high-pressure Hg lamp as a light source that passes through a UV1A filter (EX 365-10, DM400, BA390; Nikon). The beam is expanded and steered into the microscopic objective lens. The intensity of light is measured as 0.46 mW by Thorlabs power meter (PM100). The intensity of UV light can be reduced by placing a neutral density filter (ND) in its path of UV light. Photomasks or patterns are employed in the path of UV light irradiation for the spatiotemporal control of

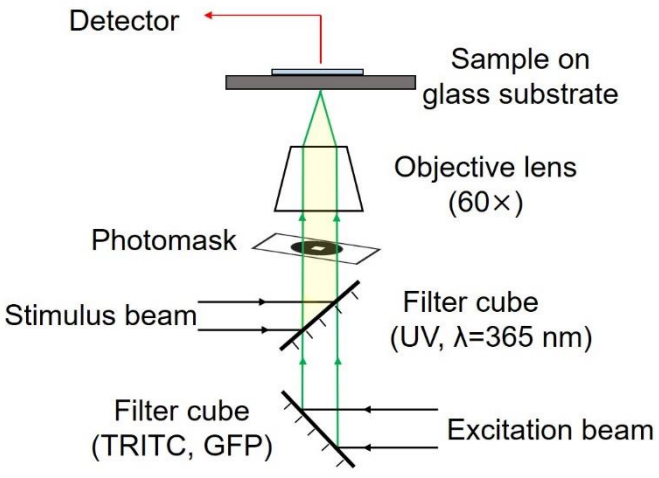

Figure 3.30 Experimental UV light setup for the spatiotemporal control of the swarming of microrobot. Different shaped or sized photomask was introduced in the path of UV irradiation during photo-control.

the reversible swarming of microrobots. The pattern structures were designed to maintain a fixed size (length/diameter/width of 4 mm) using Brother Canvas Workspace software and cut by Brother ScanNCut printer.

3.4.8 Image analysis

The fluorescence microscopy images were analyzed by NIS- Elements BR software (Nikon) and Fiji 1.52J software (National Institutes of Health, USA). Velocity of the gliding MTs was measured using the ImageJ plugin 'MTrackJ' (https://imagej.net/MTrackJ). Statistical analysis and graphs were performed with the software OriginPro Version 2019, OriginLab, USA.

3.4.9 Estimation of the association ratio of swarm units

Association ratio at a given time (t) was determined by counting the number of single MTs manually and dividing the number at a time t by the number present initially (t=0). The time dependent association ratio *R(t)* of red and green MTs was determined as follows,

$$R(t) = \frac{N_0 - N_t}{N_0}$$

Where, N_0= Initial number of single MTs and N_t = Number of single MTs after time t.

3.5 SUPPLEMENTAL INFORMATION

Table 1: The sequences of the *p*DNA used for the measurement of *Tm*.

Name of DNA	**5'-3'**	**5' end**	**3' end**
*p*DNA1	$T_{12}(TTG)_6Z_5$	DBCO	-
*p*DNA2	$(CAA)_8Z_7$	DBCO	-

Table 2: The sequences of *p*DNA with different lengths used to regulate the swarming.

Name of the *p*DNA	**Number of TTG base (n)**	**5'-3'**	**5' end**	**3' end**
*p*DNA1: **$T_{12}(TTG)_nZ_{(n-1)}$**	2	TTTTTTTTTTTTTTG**Z**TTG (**$T_{12}(TTG)_2Z_1$**)	DBCO	-
	3	TTTTTTTTTTTTTTG**Z**TTG**Z**TTG (**$T_{12}(TTG)_3Z_2$**)	DBCO	
	4	TTTTTTTTTTTTTTG**Z**TTG**Z**TTG**Z**TTG (**$T_{12}(TTG)_4Z_3$**)	DBCO	-
	5	TTTTTTTTTTTTTTG**Z**TTG**Z**TTG**Z**TTG **Z**TTG (**$T_{12}(TTG)_5Z_4$**)	DBCO	
	6	TTTTTTTTTTTTTTG**Z**TTG**Z**TTG**Z**TTG **Z**TTG**Z**TTG (**$T_{12}(TTG)_6Z_5$**)	DBCO	-
	7	TTTTTTTTTTTTTTG**Z**TTG**Z**TTG**Z**TTG **Z**TTG**Z**TTG**Z**TTG (**$T_{12}(TTG)_7Z_6$**)	DBCO	-
	8	TTTTTTTTTTTTTTG**Z**TTG**Z**TTG**Z**TTG **Z**TTG**Z**TTG**Z**TTG**Z**TTG (**$T_{12}(TTG)_8Z_7$**)	DBCO	
*p*DNA2: **$(CAA)_nZ_{(n-1)}$**	8	CAA**Z**CAA**Z**CAA**Z**CAA**Z**CAA**Z**CAA**Z** CAA**Z**CAA (**$((CAA)_8Z_7$**)	DBCO	

Table 3: The molar extinction coefficient of *p*DNA.

Name of the *p*DNA	**Number of TTG base (n)**	**Molar extinction coefficient ($Lmol^{-1}cm^{-1}$)**
*p*DNA1: **$T_{12}(TTG)_nZ_{(n-1)}$**	2	178,900
	3	205,500
	4	230,000
	5	245,400
	6	253,000
	7	268,200
	8	296,700
*p*DNA2: **$(CAA)_nZ_{(n-1)}$**	8	367,800

Table 4: The labeling ratio of *p*DNA1 to tubulin dimer for different infeed concentrations of *p*DNA modified to MT.

Infeed concentration of *p*DNA1 (µM)	**Final concentration of tubulin dimer (µM)**	**Final concentration of *p*DNA1 (µM)**	**Labeling ratio of *p*DNA1 to tubulin dimer (%)**
20	6	1	13.45
50	5	1	19.62
100	7	2	24.56
200	5	2	39.04
300	13	6	44.89
400	16	9	53.89

500	25	15	63.56
1000	32	27	85.78

Table 5: Optimized labeling ratio of DNA to tubulin for the construction of molecular swarm robot

Name of the *p*DNA	**Number of TTG base (n)**	**Infeed concentration of *p*DNA (µM)**	**Final concentration of tubulin dimers (µM)**	**Final concentration of *p*DNA in tubulin dimers (µM)**	**Labeling ratio of *p*DNA to tubulin dimers (%)**
*p*DNA1: $\mathbf{T_{12}(TTG)_nZ_{(n-1)}}$	2	10	5	2	45.75
	3	20	15	6	40.76
	4	100	10	4	40.82
	5	200	4	2	42.35
	6	200	5	2	39.04
	7	300	8	3	34.19
	8	300	11	4	31.04
*p*DNA2: $\mathbf{(CAA)_nZ_{(n-1)}}$	8	200	5	2	32.74

Table 6 The sequences of the DNA used to confirm that azobenzene facilitates the reversible swarming of microrobots.

Name of DNA	**Concentration of DNA (μM)**	**Concentration of tubulin dimers (μM)**	**DNA concentration in tubulin dimers (μM)**	**Labeling ratio of DNA to tubulin dimers (%)**
$T_{12}(TTG)_6$	100	3	1	39.45
$(CAA)_8$	100	3	1	43.65
$T12(TTG)_6Z_5$	200	5	1	32.74
$(CAA)_8Z_7$	200	5	2	39.04

Table 7 Percentage of light transmittance and UV intensity of different ND filters.

Optical density or neutral density or ND	**Denotation of ND**	**Fractional Transmittance (%)**	**Intensity of UV light (mW/cm^2)**
0 (no ND is used)	ND1	100	0.59
0.1		79	0.50
0.3	ND2	50	0.20
0.6	ND4	25	0.19
0.9	ND8	12.5	0.06

Table 8 The sequences of the DNA used to regulate the flexibility of molecular swarm robot.

Name of DNA	**5'-3'**	**5' end**	**3' end**
Non *p*DNA1	$T_{12}(TTG)_4$	DBCO	-
Non *p*DNA2	$(CAA)_8$	DBCO	-
*p*DNA1	$T12(TTG)_4Z_3$	DBCO	-
*p*DNA2	$(CAA)_8Z_7$	DBCO	-

3.6 REFERENCES

1. Bahar, S. Flocking , swarming , and communicating: The Essential Tension. The Frontiers Collection. *Springer*127–152 (2018). doi:10.1007/978-94-024-1054-9

2. Huber, L., Suzuki, R., Krüger, T., Frey, E. & Bausch, A. R. *Emergence of coexisting ordered states in active matter systems, Science* **361**, 6399, 255-258, (2018).

3. Wang, S. & Wolynes, P. G. On the spontaneous collective motion of active matter. *Proc. Natl. Acad. Sci. U. S. A.* **108**, 15184–15189 (2011).

4. Beshers, S. N.; Fewell, J. H. Models of Division of Labor in Social Insects, *Ann. Rev. Entom.* 413-440, 83–104 (2008).

5. Niven, J. E. How honeybees break a decision-making deadlock. *Science*, **335**, 6064, 43–44 (2012).

6. Xie, H. *et al.* Reconfigurable magnetic microrobot swarm: multimode transformation, locomotion, and manipulation. *Sci. Robot.* **4**, 28, eaav8006 (2019).

7. Solovev, A. A., Sanchez, S. & Schmidt, O. G. Collective behaviour of self-propelled catalytic micromotors. *Nanoscale* **5**, 1284–1293 (2013).

8. Xu, T. *et al.* Reversible swarming and separation of self-propelled chemically powered nanomotors under acoustic fields. *J. Am. Chem. Soc.* **137**, 2163–2166 (2015).

9. Wang, W., Duan, W., Ahmed, S., Sen, A. & Mallouk, T. E. From one to many: dynamic assembly and collective behavior of self-propelled colloidal motors. *Acc. Chem. Res.* **48**, 1938–1946 (2015).

10. Wang, W., Duan, W., Sen, A. & Mallouk, T. E. Catalytically powered dynamic assembly of rod-shaped nanomotors and passive tracer particles. *Proc. Natl. Acad. Sci. U. S. A.* **110**, 17744–17749 (2013).

11. Keya, J. J. *et al.* DNA-assisted swarm control in a biomolecular motor system. *Nat. Commun.* **9**, 453 (2018).

12. Keya, J. J. *et al.* Control of swarming of molecular robots. *Sci. Rep.* **8**, 1–10 (2018).

13. Kabir, A. R., Inoue, D. & Kakugo, A. Molecular swarm robots: recent progress and future challenges. *Sci. Technol. Adv. Mater.* **21**, 1, 323-332 (2020).

14. Asanuma, H., Liang, X., Yoshida, T. & Komiyama, M. Photocontrol of DNA Duplex Formation by Using Azobenzene-Bearing Oligonucleotides. *ChemBioChem* **2**, 39–44 (2001).

15. Asanuma, H., Ito, T., Yoshida, T., Liang, X. & Komiyama, M. Photoregulation of the formation and dissociation of a DNA duplex by using the *cis-trans* isomerization of azobenzene. *Angew. Chemie - Int. Ed.* **38**, 2393–2395 (1999).

16. Liang, X., Nishioka, H., Takenaka, N. & Asanuma, H. A DNA nanomachine powered by light irradiation. *ChemBioChem* **9**, 702–705 (2008).

17. Corradi, P., Menciassi, a. & Dario, P. Space applications of micro-robotics : a preliminary investigation of technological challenges and scenarios. *Proc. 5th Round Table Micro/Nano Technol. Space, Noordwijk, Netherlands* 11 (2005).

18. Schaller, V. *et al.* Frozen steady states in active systems. *Proc. Natl. Acad. Sci. U. S. A.* **108**, 48, 19183-19188 (2011).

19. Şahin, E. Swarm robotics: From sources of inspiration to domains of application. In: Şahin E., Spears W.M. (eds) Swarm Robotics. SR 2004. Lecture Notes in Computer Science, vol 3342. Springer, Berlin, Heidelberg. **3342**, 10–20 (2005).

20. Weber, C. A. *et al.* Random bursts determine dynamics of active filaments. *Proc. Natl. Acad. Sci. U. S. A.* **112**, 10703–10707 (2015).

21. Green, L. N. *et al.* Autonomous dynamic control of DNA nanostructure self-assembly. *Nat. Chem.* **11**, 510–520 (2019).

22. Hagiya, M., Aubert-Kato, N., Wang, S. & Kobayashi, S. Molecular computers for molecular robots as hybrid systems. *Theor. Comput. Sci.* **632**, 4–20 (2016).

23. Muscat, R. A., Bath, J. & Turberfield, A. J. A programmable molecular robot. *Nano Lett.* **11**, 982–987 (2011).

24. Früh, S. M., Steuerwald, D., Simon, U. & Vogel, V. Covalent cargo loading to molecular shuttles via copper-free 'click chemistry'. *Biomacromolecules* **13**, 3908–3911 (2012).

25. Peloquin, J., Komarova, Y. & Borisy, G. Conjugation of fluorophores to tubulin. *Nat. Methods* **2**, 299–303 (2005).

26. Liang, X., Takenaka, N., Nishioka, H. & Asanuma, H. Molecular design for reversing the photoswitching mode of turning on and off DNA hybridization. *Chem. - An Asian J.* **3**, 553–560 (2008).

27. Hartley, G. S. The cis-form of azobenzene. *Nature* **140**, 281 (1937).

28. Gu, R. *et al.* Photocontrolled micellar aggregation of amphiphilic DNA-azobenzene conjugates. *Colloids Surfaces B Biointerfaces* **135**, 126–132 (2015).

29. Kabir, A. M. R., Inoue, D., Kakugo, A., Kamei, A. & Gong, J. P. Prolongation of the active lifetime of a biomolecular motor for in vitro motility assay by using an inert atmosphere. *Langmuir* **27**, 13659–13668 (2011).

30. Kuzuya, A., Tanaka, K. & Komiyama, M. Photoswitching of site-selective RNA scission by sequential incorporation of azobenzene and acridine residues in a DNA oligomer. *J. Nucleic Acids* **2011**, 1-10 (2011).

31. Akter, M. *et al.* Photo-regulated trajectories of gliding microtubules conjugated with DNA. *Chem. Commun.* (2020). doi:10.1039/D0CC03124K

32. Hess, H. Engineering Applications of Biomolecular Motors. *Annu. Rev. Biomed. Eng.* 13:1, 429-450 (2011). doi:10.1146/annurev-bioeng-071910-124644

33. Van Den Heuvel, M. G. L. & Dekker, C. Motor proteins at work for nanotechnology. *Science,*. **317**, 333–336 (2007).

34. Hagiya, M., Konagaya, A., Kobayashi, S., Saito, H. & Murata, S. Molecular robots with sensors and intelligence. *Acc. Chem. Res.* **47**, 1681–1690 (2014).

35. Case, R. B., Pierce, D. W., Hom-Booher, N., Hart, C. L. & Vale, R. D. The directional preference of kinesin motors is specified by an element outside of the motor catalytic domain. *Cell* **90**, 959–966 (1997).

36. Früh, S. M., Steuerwald, D., Simon, U. & Vogel, V. Covalent cargo loading to molecular shuttles via copper-free ‘click chemistry’. *Biomacromolecules* **13**, 3908–3911 (2012).

CHAPTER 4

Active cargo transport by the swarm microrobot

ABSTRACT

Swarm robotics has emerged as a promising and significant paradigm in the robotics where multiple robots collectively solve problems by forming advantageous structures and behaviors similar to the ones observed in natural systems, such as swarms of bees, birds, or fish. to utilize in the sophisticated complex task which is difficult for a single robot. Several reports on the construction of mechanical, chemical and natural powered swarm robots were found which can design and construct complex patterns. However, the step to further applications for the engineered and nanotechnological advancement has not yet been achieved. The size of the mechanical swarm robots and the slow motion of the chemical powered robots limit the activity in the nanotechnology whereas integrating natural molecular devices as the components can increase the performance even more sophisticated task. In the previous chapter I investigated the development of the biomolecular motor-based swarm microrobot using DNA as a programmer. Photoregulated swarm microrobot was utilized as an active cargo transporter that can pick-up, transport and unload cargo efficiently than a single robot. They were found to transport cargo for a long distance without any drop-off or detaching the cargo under visible light. Additionally, They accumulate all the cargoes in selected regions by concentrating the unloaded cargoes which were confirmed from the increasing density of cargo in that region. This work is the first experimental evidence of the emergent functions of the swarming of microrobots, which will open a significant paradigm in the application of microrobots and robots.

4.1 INTRODUCTION

In nature, swarming of living organisms e.g. fish schools, ant colonies, and bird flocks is fascinating for constructing large scale complex patterns with emergent functions.[1–5] It enables the living organisms to obtain several advantages including parallelism, robustness and flexibility which are impossible to obtain by a single entity.[6] Inspired by nature, several reports were observed on the development of artificial swarm robots where multiple robots could collectively work by forming advantageous structures, resulted in greater workability and efficiency compared to a single robot. *Jasmine robots,*[7,8] *Sambot,*[9] *Kilobots,*[10,11] *SwarmBot,*[12] *chobots,*[13–16] *molecular robot*[17] are the latest advancements of the swarm robots. In the macroscopic conventional swarm robots, it has been a major challenge to control the motion and interaction of large numbers of units of the swarm at a time and the mamximum number of the units is 1000.[10] Besides, the large size and low efficiency of the swarm units limit their functions for more sophisticated applications i.e. nanotechnology and biotechnology.[18,19] On the other hand, the slow motion and poor efficiency of the chemically powered swarm robots are the main drawbacks which could be overcome by integrating motor proteins for performing even more sophisticated tasks.[20,21]

This has been addressed by the recent construction of a biomolecular motor based molecular swarm robot where complementary DNAs were employed to program the swarming of the microrobots.[17,22] In the previous chapter I discussed on the construction and optimization of the photoregulated swarm microrobots in details. But the ultimate goal is to let it work more sophistically and efficiently[23] which has not been achieved yet. Motivating from the conventional industrial robots which can pick up, transport and unload components in the designated location[24], my strategy was to utilize swarm microrobots as an efficient and well-controlled cargo transporter.

So, in this chapter, I utilized swarm microrobots for further applications as an active cargo transporter which can pick up, transport and unload cargo in a programmed manner. Although there are several reports on the biomolecular motor-based cargo transport system,[25–32] this work demonstrates the first-ever experimental evidence of the application of biomolecular motor-based swarm microrobots as a cargo transport system. Optimizing the conditions for the

swarming as described in the previous chapter, the photoregulated swarm microrobots were constructed and cargo was prepared conjugating the complementary DNA. Then the cargo loading, transportation and unloading were investigated in response to photoirradiation. The unloading of cargo was regulated in a well-organized and spatiotemporal manner under UV irradiation. The work efficiency of the swarm microrobots was measured considering the transported distance with time and compared to the single microrobot. This highly efficient and well-controlled active cargo transport system will produce new endeavors to generate artificial cargo carrier devices in the field of microrobotics as well as robotics.[33,34]

4.2 RESULTS & DISCUSSION

4.2.1 Preparation of molecular swarm robot as a molecular cargo carrier system

To utilize the swarm microrobot as an active cargo transport system, it was required to optimize the swarming and reversible swarming of microrobots in response to the UV-visible (VIS) irradiation. After the optimization of the conditions for the preparation of swarm microrobots (described in chapter 3), the best association ratio of molecular swarm robot under VIS-UV light as well as *Tm* simulation, complementary $T_{12}(TTG)_6Z_5$ and $(CAA)_8Z_7$ were selected to modify MTs for further applications.

The variation of the association ratio of swarm microrobots with increasing TTG base sequence in the *p*DNA (n) as shown in **Figure 4.1**

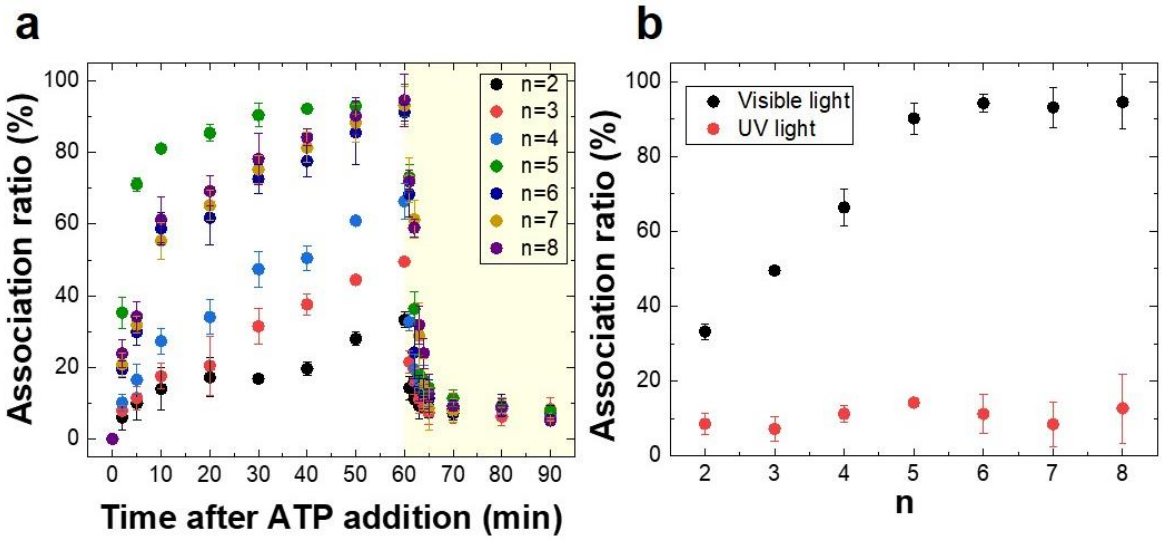

Figure 4.1 (a) Variation of association ratio of molecular swarm robot over time in response to VIS-UV light where red MTs modified with increasing length of $T_{12}(TTG)_nZ_{(n-1)}$; n = 2–8. The name of the base sequences was mentioned in the box positioned on the right of the plot. The yellow box denoted the duration of UV irradiation. Error bar: standard deviation. **(b)** Change of association ratio of molecular swarm robot over the number of TTG base sequences in $T_{12}(TTG)_nZ_{(n-1)}$ under the VIS-UV light.

The microrobot was prepared following the same procedure as described in previous chapters and the DNA sequences used for the preparation are mentioned in **Figure 4.2b and Table1**.

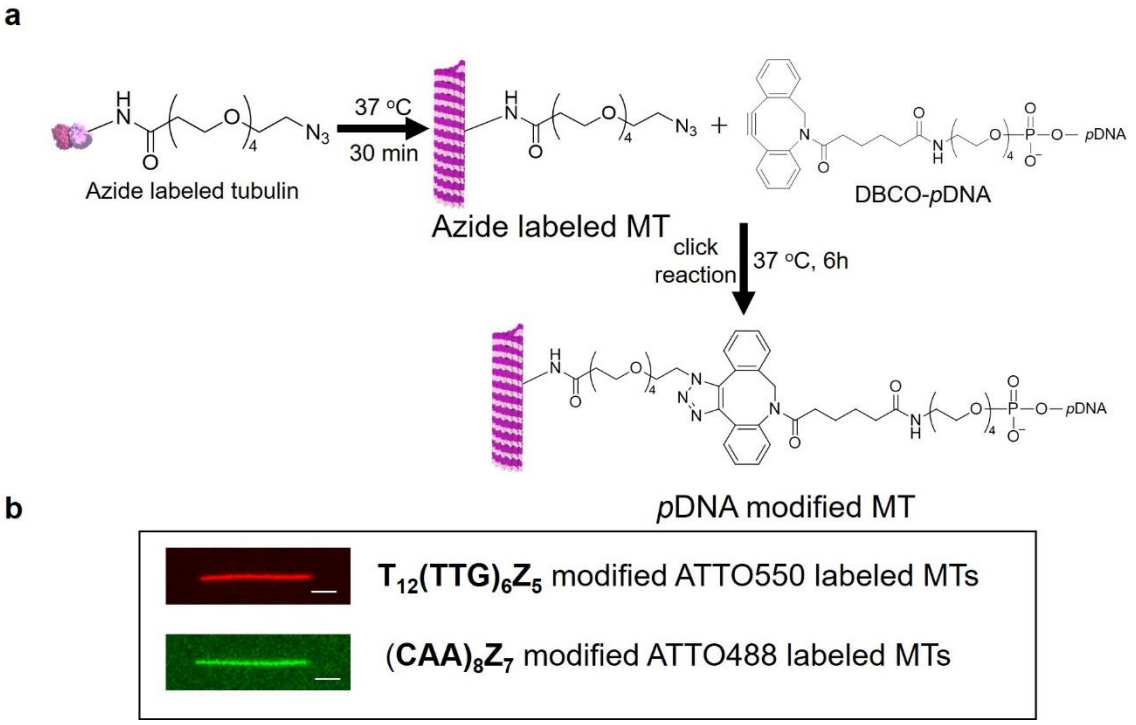

Figure 4.2.2 (a) Schematic illustration of the preparation of microrobot as a unit of molecular swarm robot conjugated with *p*DNA by click reaction **(b)** Fluorescence microscopic images of *p*DNA-conjugated MTs with sequences $T_{12}(TTG)_6Z_5$ and $(CAA)_8Z_7$ respectively, scale bar: 1 μm.

4.2.2 Cargo preparation

Polystyrene beads were employed as cargoes for the investigation of cargo transport by swarm microrobots. The diameter of that bead was 1.13 μm. The density of the bead was 1.05 g/cm^3 and the volume was 1.03×10^{-13} m^3. Amino labeled polystyrene beads were modified with azide ester by azide-alkyne cycloaddition reaction to allow the labeling with DBCO-*p*DNA. ATTO647 dye was used to allow the visualization under an epifluorescence microscope. Then $(CAA)_8Z_7$ was employed to modify the polystyrene beads for further application of swarm microrobots as cargoes.

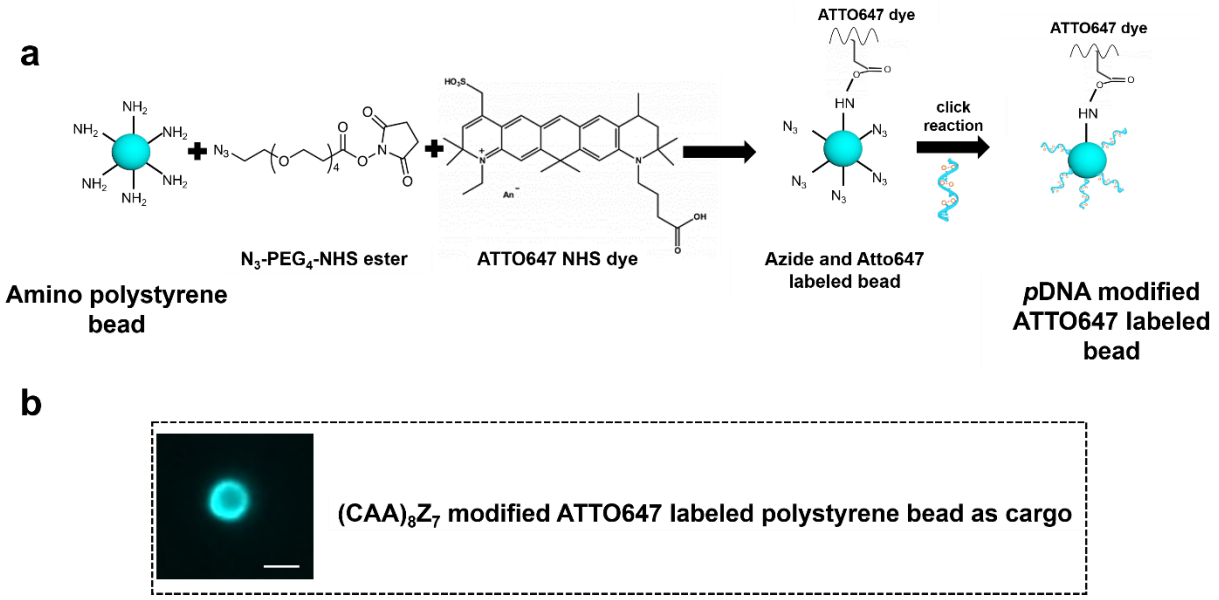

Figure 4.3 (a) Schematic diagram of the preparation of *p*DNA modified ATTO647 labeled cargo. **(b)** Fluorescence microscopic image of $(CAA)_8Z_7$ modified ATTO647 labeled polystyrene bead as cargo after dilution with 1×BRB80. Scale bar: 2 µm.

The modification of the polystyrene bead with fluorescent dye and *p*DNA by click reaction was described in **Figure 4.3a**. The microscopy image in **Figure 4.3b** confirmed the successful modification of a spherical-shaped polystyrene bead with ATTO647 fluorescent dye.

4.2.3 Photoregulated cargo loading

I demonstrated the swarm microrobot as a cargo transport system that loaded the cargo using DNA hybridization under VIS irradiation, as schematically illustrated in **Figure 4.4**. The cargo can be loaded to the swarm microrobot in a zipping geometry resulting in a 24 base pair overlap.[35,36] As the cargo and only the red MT in the swarming are modified with the complementary *p*DNA, the *cis*-to-*trans* isomerization of azobenzene under VIS light facilitates the hybridization of complementary *p*DNA modified red MT and the cargoes. When a swarm microrobot having *p*DNA1 modified red MTs and *p*DNA2 modified green MTs used to pass through a polystyrene beads, the complementary *p*DNA2 labeled cargo became attached to the red MT and selectively loaded onto the gliding swarm microrobot under VIS irradiation.

The cargo pickup by swarm microrobot was observed using epifluorescence microscopy, in which the cargoes were applied to the flow cell after 30 min of ATP addition.

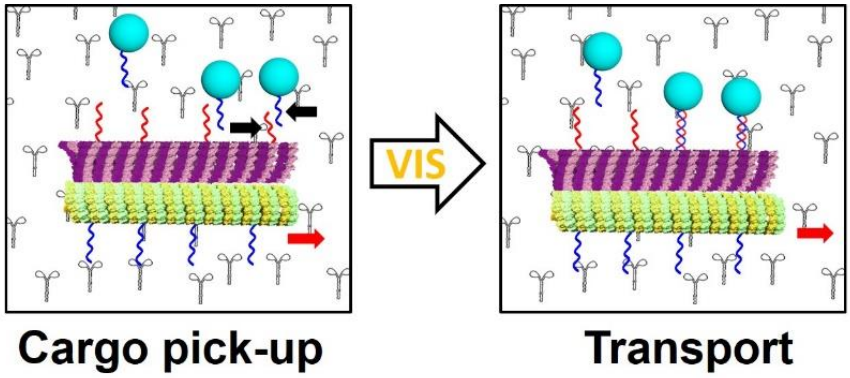

Figure 4.4 Schematic diagram of the proposed mechanism of molecular swarm robot as a molecular cargo transport system under VIS light. When a swarm robot passes through the loading site, a cargo modified with the complementary *p*DNA selectively loads onto the gliding robot through DNA hybridization.

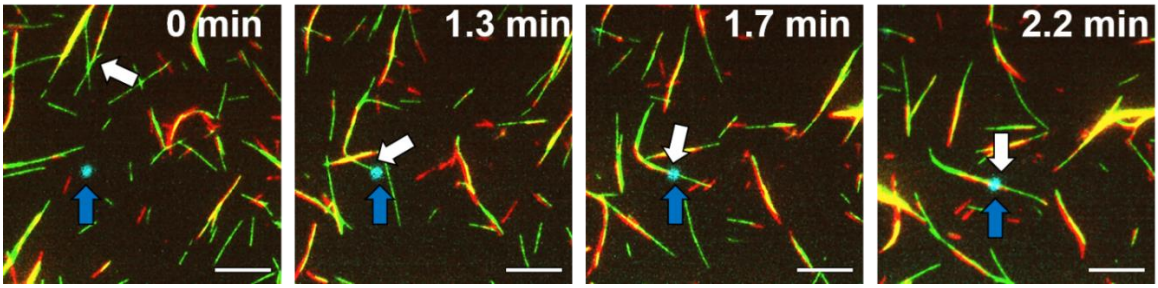

Figure 4.5 Time lapse fluorescence microscopic images of *p*DNA2 modified cargo loading and then transported by a swarm robot through the complementary *p*DNA1 modified red MTs. The blue arrow denotes the position of the cargo whereas the white one shows the position of the swarm robot. Scale bar: 10 µm.

From **Figure 4.5**, it can be demonstrated that when a small swarm robot containing five red and green MTs was passing through a cargo, the green MT could not load the cargo whether it attached to the red MT of that swarm robot. This result confirms the selective cargo loading by the molecular swarm robot due to complementary DNA hybridization.

4.2.4 Photoregulated cargo transport

After the successful cargo loading, the swarm microrobots started to transport the loaded cargo by gliding on the kinesin coated surface under VIS light which is shown schematically in **Figure 4.6a**.

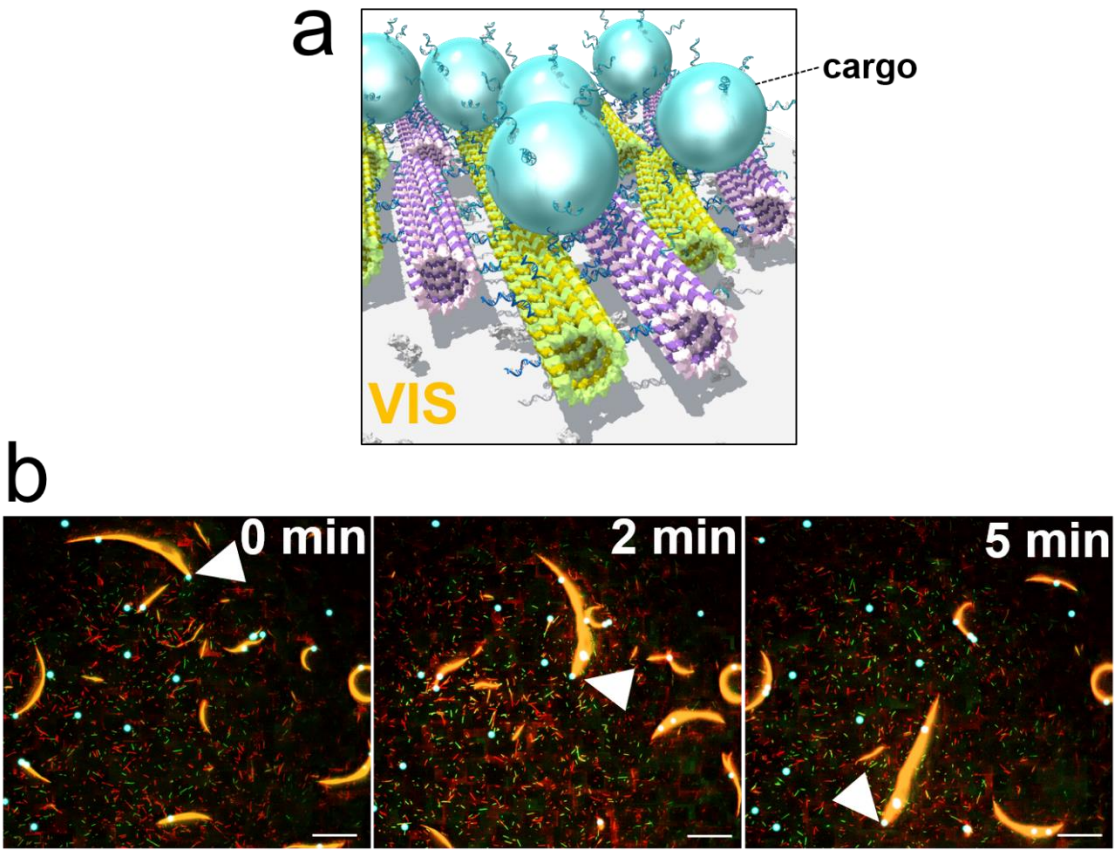

Figure 4.6 (a) Schematic diagram of the cargo transport by the molecular swarm robot under VIS light. **(b)** The time lapse fluorescence microscopy images of the transport of the loaded cargo by the swarm robot under VIS light. The white triangle showed the position of the loaded cargo by the swarm robot. Here, due to the merge of cyan and yellow color, the cyan-colored cargo became white due to merge with the yellow swarm robot. Scale bar: 20 µm.

Figure 4.6b shows the successful cargo transport by the molecular swarm robot where a ~80 µm long swarm microrobot carrying multiple cargoes. In the color-coded trajectories of cargoes in **Figure 4.7a**, the red line is showing the displacement of the loaded cargo which confirms the long traveled distance by the swarm robot. 88% of the total cargoes on the surface were loaded

and then transported by the swarm microrobot whereas biomolecular motor based molecular shuttle could load less than 30% of the total cargo.[35,37]

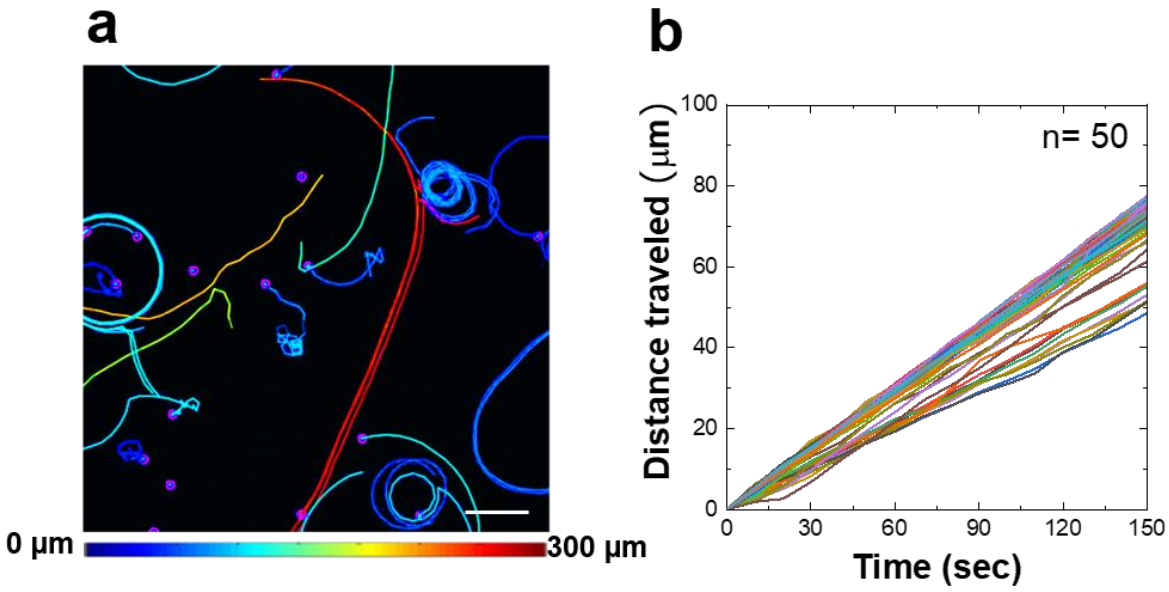

Figure 4.7 (a) Temporal color-coded trajectories of the transported cargoes by the swarm microrobot. Scale bar: 20 µm. **(b)** The distance traveled by the transported cargoes under VIS irradiation. The number of measured events was 50.

From **Figure 4.7b**, it can be observed that under VIS light almost all the loaded beads were transported smoothly with almost no pausing or detaching from the surface. The average gliding speed of the cargo loaded swarm robot was 763 ±12 nms^{-1}.

4.2.5 Photoregulated cargo unloading

When the swarm microrobot traveled under the UV region, it started to unload the loaded cargo by breaking the hydrogen bonding of the complementary DNA duplex. UV light induces the isomerization by converting the planar and non-polar *trans* azobenzene to the polar and non-planar cis form, which favors the destabilization of the DNA duplex by changing *Tm*.

This indicates that only UV irradiation facilitates the unloading of cargo from the swarm microrobot. From the schematic illustration of **Figure 4.8a**, it can be shown that the transported

cargo was unloaded by the swarm microrobot through the reversible swarming of the microrobots in response to the UV irradiation. As, complementary DNA hybridized in a zipping geometry, under UV light the DNA duplex could be separated into individual by the rupture of the bonds sequentially one by one.[29]

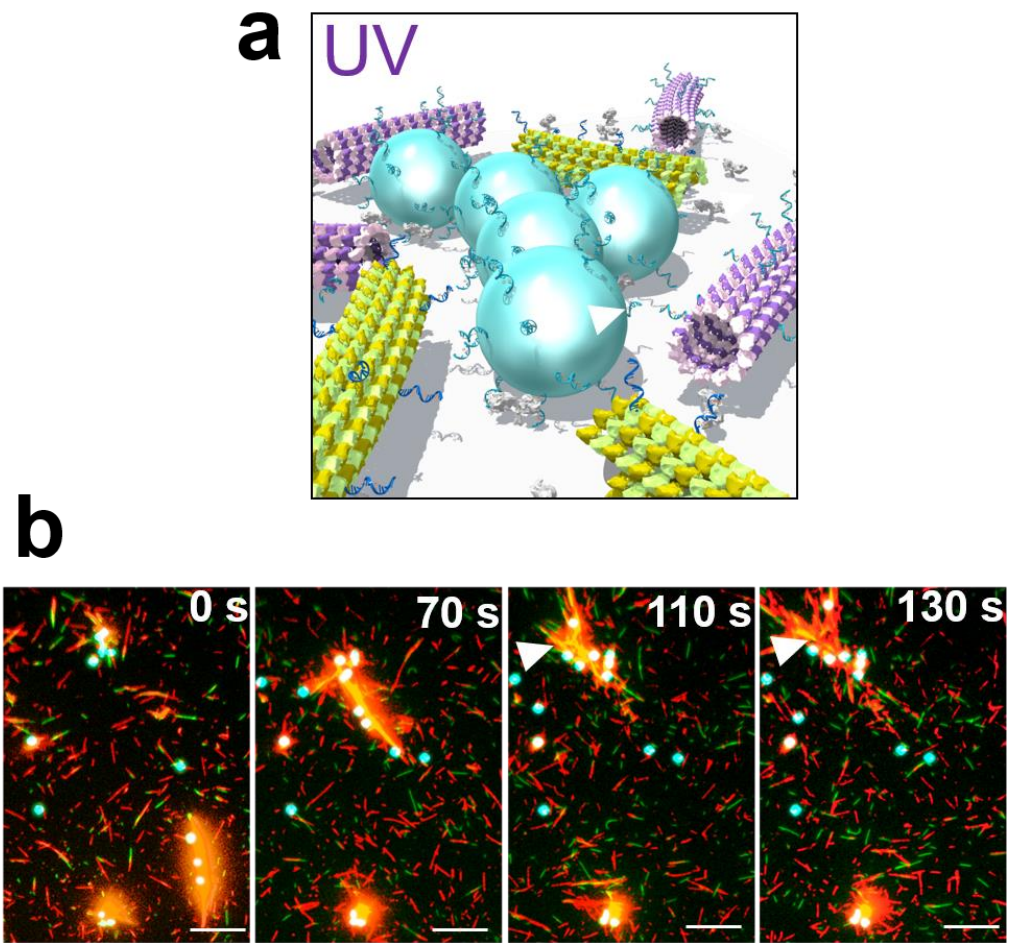

Figure 4.8 (a) Schematic illustration of cargo unloading by the molecular swarm robot through destabilization of complementary DNA duplex. **(b)** Time lapse fluorescence microscopic images of unloading of cargo by the molecular swarm robot under UV irradiation. Scale bar: 10 µm.

Figure 4.9b shows unloading of the cargo by the swarm microrobot in response to UV irradiation. The unloading of cargo was increased with time of UV irradiation and almost 99% of the transported cargoes were unloaded.

In the experiment, the intensity of the UV light was 0.59 mW/cm^2 and the flow cell was kept in an inert chamber to avoid photobleaching of the materials.

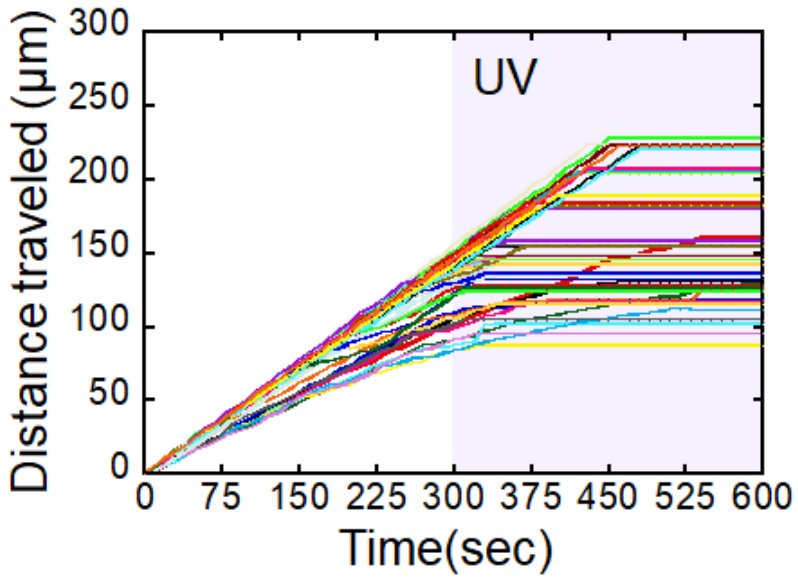

Figure 4.9 Change in traveled distance of the transported cargoes with time under VIS-UV irradiation. The violet box from 300 sec is showing the duration of the UV irradiation.

The traveled distance of the cargo loaded to the swarm microrobot was measured which is shown in **Figure 4.9.** The average gliding velocity of one or multiple cargoes loaded swarm robot was 575±67 nms^{-1}. Almost all the loaded beads were transported smoothly under VIS light whereas, with the UV initiation, the cargoes started to detach or showed pausing. In the consequence, the displacement rate of the loaded beads was decreased and started to unload from the dissociated bundles. After unloading the cargoes the single microrobot passed with the velocity of 527±81 nms^{-1}which was considered almost similar to the swarm microrobot (575±67 nms^{-1}).

4.2.6 Spatiotemporal regulation of cargo unloading

Controlling the cargo loading and unloading in specific regions and time, has been one of the major challenges to establish the active cargo transport system for further applications in nanodevices. The spatiotemporal regulation of the cargo unloading was explored to achieve the

targeted delivery and unloading of the cargo in local regions. With this approach, applications can be realized where motor-driven processes are needed to enable transport and active sorting of analytes and nanosystems, or the reconfiguration or self-repair of materials and devices.

Incorporation of azobenzene photoswitch enabled the spatiotemporal regulation in response to photoirradiation as described in chapter 3. When the cargo loaded swarm microrobot came into the UV irradiation area from the VIS light region, the swarm microrobot unloaded the cargo in that UV region which is schematically shown in **Figure 4.10**.

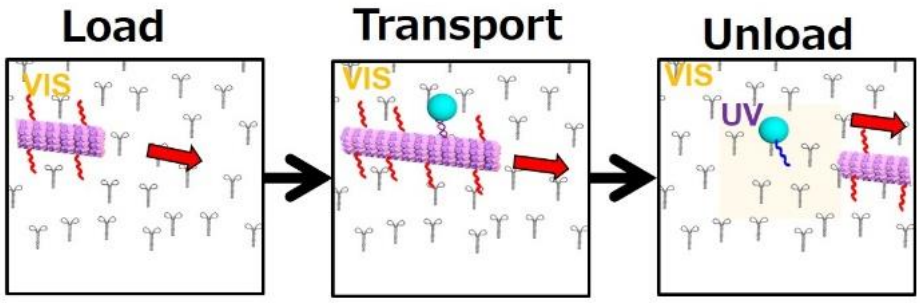

Figure 4.10 Schematic diagram of the spatiotemporal cargo unloading by the molecular swarm robot where UV was irradiated into the yellow-colored specific region of unloading.

Different shaped or sized photomasks or patterns were used to control the unloading region. The area of the square is 128 µm ×128 µm (showing with a red-colored box). The cargoes were applied to the flow cell after 10 min of ATP addition and UV light was illuminated through the square pattern on the surface.

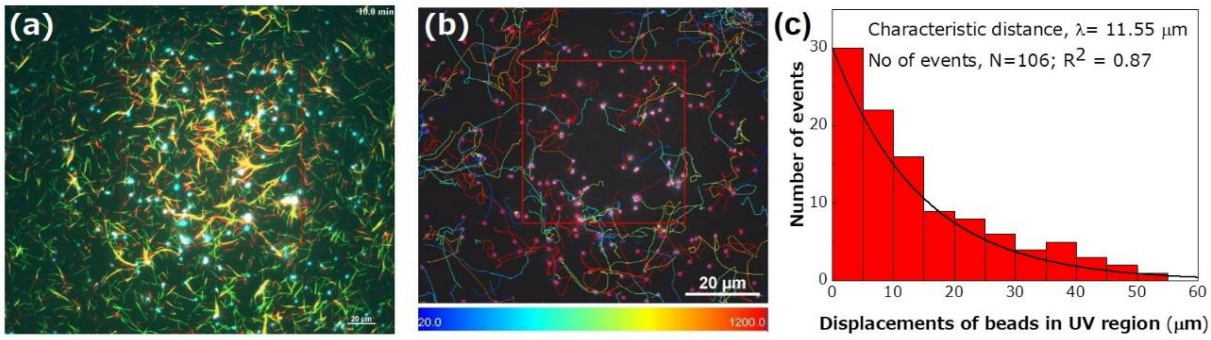

Figure 4.11 Spatiotemporal regulation of cargo unloading by molecular swarm robot **(a)** Fluorescence microscopic image of cargo unloading under UV irradiation using a square shaped pattern (the region was shown with a red square box) by molecular swarm robot Scale bar: 20

μm **(b)** Twenty-minute trajectories of the displacements of cargoes; Color map depicts time in seconds **(c)** Displacement distribution of cargoes to detach from MTs in UV region. Here, N and R^2 in the graph indicate the number of measurements and the square of the regression error. Each bin maintains the width of 5 μm. The fitting was done using the exponential decay equation $y = y_0 + A_1*\exp(-(x-x_0)/t_1)$.

From **Figure 4.11a**, it can be shown that almost all the transported cargoes were unloaded into the square pattern under UV light irradiation. The swarm microrobots entered into the UV region with a velocity of 443±65 nms^{-1} but after unloading single microrobots crossed that area with a velocity of 393±45 nms^{-1}. So, the velocity of the microrobots was found to decrease slightly in the UV region. Long time UV irradiation might affect the velocity of the microrobots. In the unloading area, 39 unloading events took place and the efficiency of unloading is ~67% concerning total beads and ~91% concerning the transported beads.

In the color-coded trajectories shown in **Figure 4.11b**, it can be confirmed that swarm microrobot transported cargo over a long distance under the VIS region but in the UV region, they passed short distances.

From the distribution curve in **Figure 4.11c**, the characteristic distance is measured as 11.55 μm to unload the cargo in response to UV irradiation (the decay rate is ~0.87). This result indicates the average traveled distance of the cargo before unloaded under UV irradiation which is 11.55 μm. Though the distance varies with the length and width of the swarm microrobot, the swarm robot might travel a minimum of 11.55 μm before unloading.

4.2.7 Cargo transport efficiency

Controlling the transportation for a long-distance has emerged as another challenge in the biomolecular motor based molecular shuttle which reduces its efficiency in the engineered nanodevices. Several extensive studies were reported on the molecular shuttle based nanodevices but low efficiency of cargo loading or transportation was observed due to the small collision probability, as a sparse cargo density was chosen to allow for optical visualization of events. Engineering such integrated systems require the attachment of the cargo firmly with the transporter. Also, the surface of the system concurrently has to allow for cargo transfer when it comes to a collision with transporter passing by.[26] In this manner, the thermodynamically stable

swarm microrobot might be the best approach to make an appropriate collision with the cargo and hold that cargo firmly than other MT-based molecular shuttle systems. [31,38,39]

To understand the behavior of loading-drop off events by molecular swarm robot and the traveled distance, one 78.87 µm long swarm robot was tracked for ~50 min after loading a cargo.

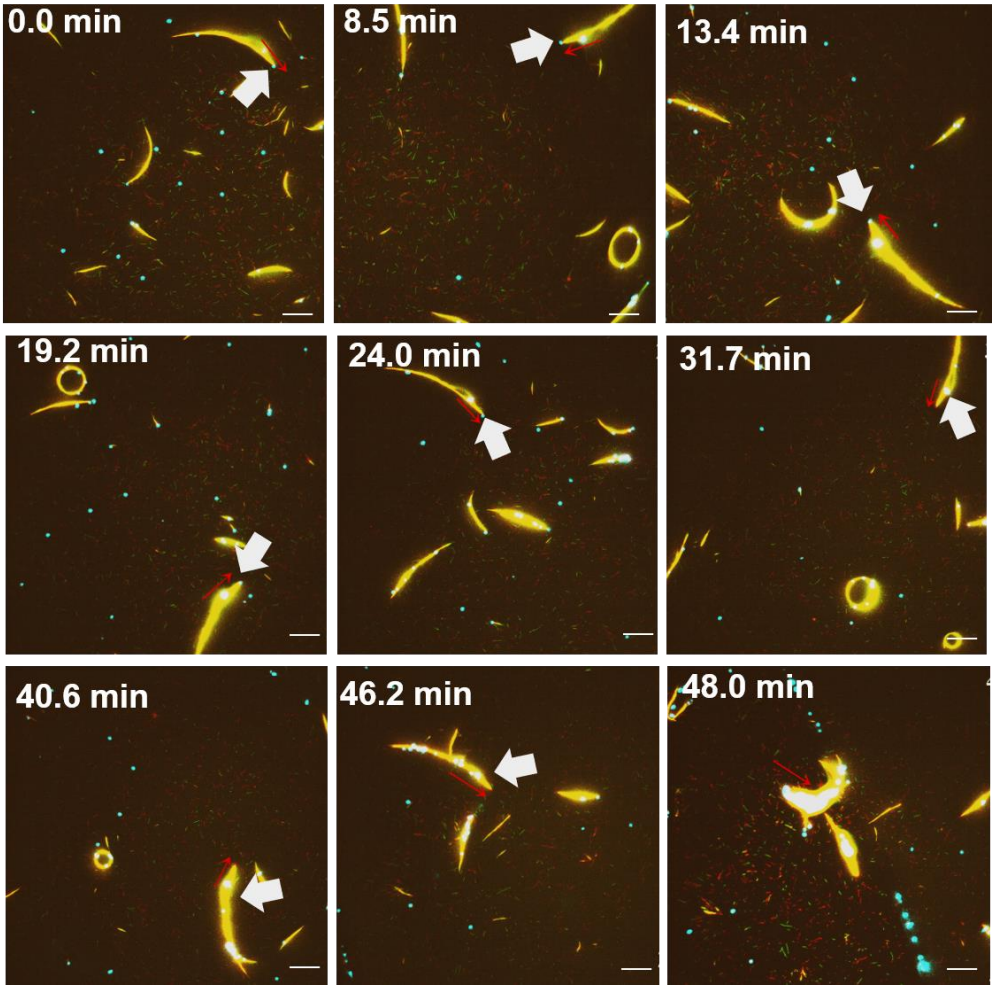

Figure 4.12 Time lapse fluorescence microscopic images of cargo transport by swarm robot. The direction of the targeted swarm robot is shown with the red arrow and the loaded cargo is shown by the white arrow. Scale bar: 20 µm.

The swarm microrobot loaded cargo on its leading-edge which was considered as 0 min after loading and then it moved for 48 min after loading. The swarm robot traveled a total of 1095.64 µm before drying the flow cell. The cargo on the leading edge was snatched by a small swarm

robot after traveling 690.18 µm of distance from the loading position after 28 min. The cargoes carrying on the middle part of the swarm robot seemed more stable than the leading position. From **Figure 4.12**, it can be observed that the swarm robot did not drop off or detach any loaded cargo until others snatched the cargo during traveling which confirmed the high sticking probability of molecular swarm robot to grasp micro-sized cargo very strongly.

To compare the efficiency of loading and transport of cargo with the single microrobot, investigations were also carried out by them (**Figure 4.13)**. Here, the density of single microrobots (red swarm unit) was kept same as the density of the red MTs in the experiments of swarm robot.

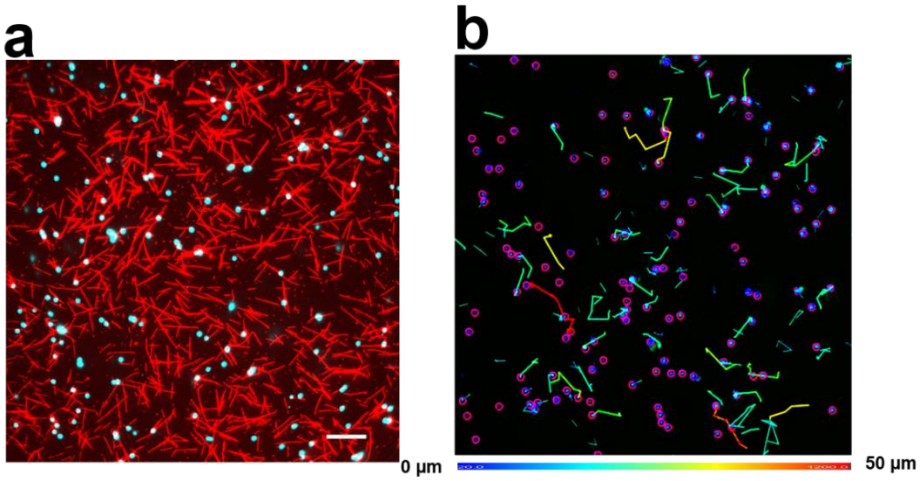

Figure 4.13 (a) Fluorescence microscopy image of the cargo transport by single microrobot under VIS irradiation. Scale bar: 20 µm. **(b)** Color coded trajectories of the displacements of cargoes by the single microrobots; Color map depicts displacement of cargoes.

The single microrobots were found to have lower loading events compared to the swarm microrobots. This may be happened due to the small collision with the cargo which hinders the effective grasp of cargo by the single microrobot. The trajectories in **Figure 4.13b** confirms that single microrobot could not travel a long distance with the loaded micro-sized cargo.

The single microrobot detached or dropped off the cargo after passing short distance under VIS light. This confirmed that the single microrobot cannot hold micro-sized cargo firmly for a long time.

The traveled distance was measured for the single microrobots under visible light which showed that could not transport the cargo for the long distance which agreed the trajectories of the single microrobots. **(Figure 4.14)**

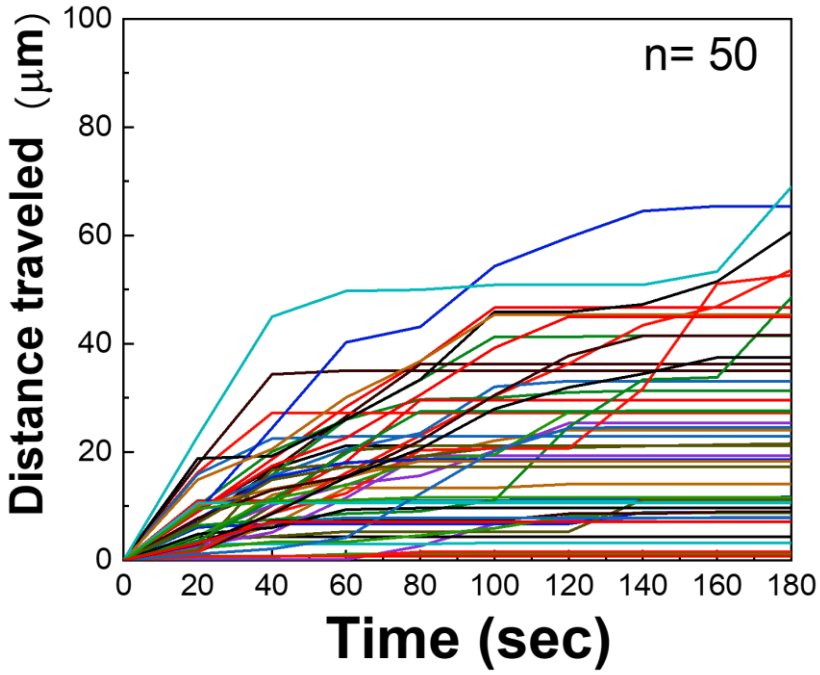

Figure 4.14 Distance traveled by the loaded cargoes by single microrobot over time under visible irradiation.

To compare the transportability of the swarm microrobot with the single microrobot, the transport efficiency was measured from the traveled distance of loaded cargo in response to VIS-UV light. From **Figure 4.15**, the average transport efficiency for the molecular swarm

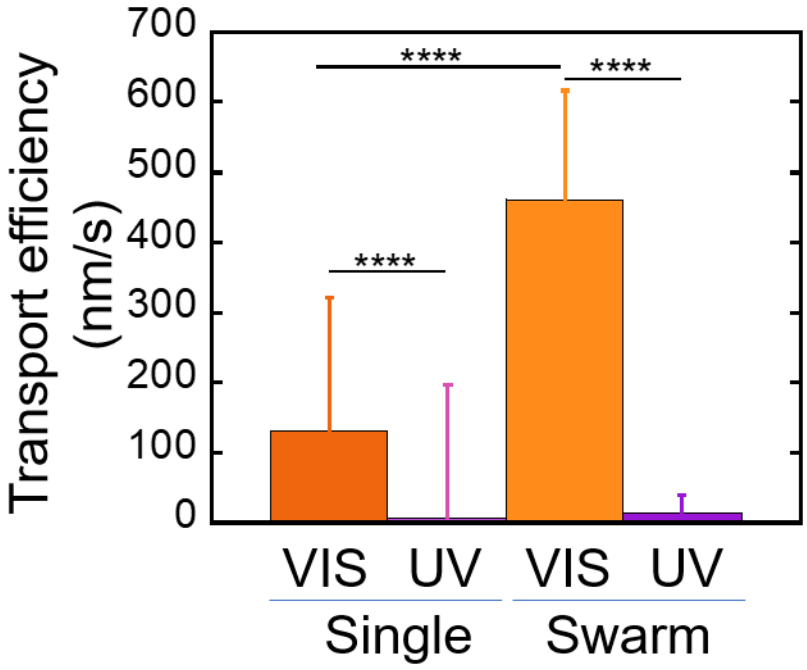

Figure 4.15 The comparison of transport efficiency of the swarm and single microrobots under UV-VIS light. Here transport efficiency was measured considering the transported distance after loading of cargo over time. Statistical analysis using Student's t-test confirmed significant difference between the two data sets at P<0.0001 indicated by ****.

robot was 7 times higher than the single microrobot under VIS light, which signifies the emergence behavior of the swarm microrobot in active cargo transport.

Swarming exhibited the complex behavior and able to demonstrate the work feasibility several times higher than individual microrobot. The mutual interactions among lots of microrobots in swarm robots provide the emergent behaviors that was not found in the single microrobots.

During UV light irradiation, the transport rate decreased for both swarm and single microrobots. For single microrobots, the average transport efficiency was almost zero under UV irradiation which resulted in no transport under UV irradiation.

4.2.8 Effect of the size of the cargoes on load and transport

Polystyrene beads having a diameter of 1.13 µm were used as cargo in all the experiments. It was necessary to investigate the effect of the size of cargo on the loading efficiency by swarm

microrobot. Three different diameters of amino polystyrene beads were employed as the cargo after modification. The diameter of the cargoes was 3.40 µm, 7.24 µm, and 8.66 µm. The fluorescence microscopic images of different diameters of ATTO647 modified cargo were shown in **Figure 4.16**.

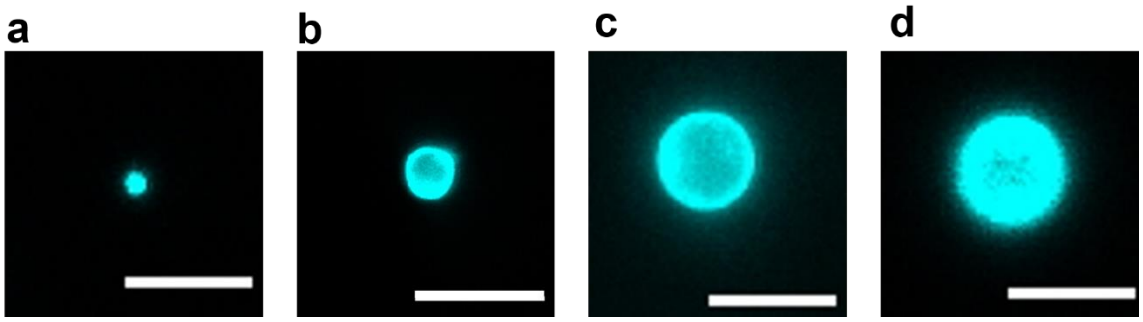

Figure 4.16 Fluorescence microscopic images of **(a)**1.13 µm, **(b)** 3.40 µm, **(c)** 7.24 µm and **(d)** 8.66 µm diameter of *p*DNA2 modified ATTO647 labeled polystyrene microbeads as cargo. Scale bar: 10 µm.

Cargo was loaded after 30 min of ATP addition to the flow cell and then observed by epifluorescence microscopy (**Figure 4.17)**. The density of the cargo and the length of the swarm microrobot were not the same in all the cases.

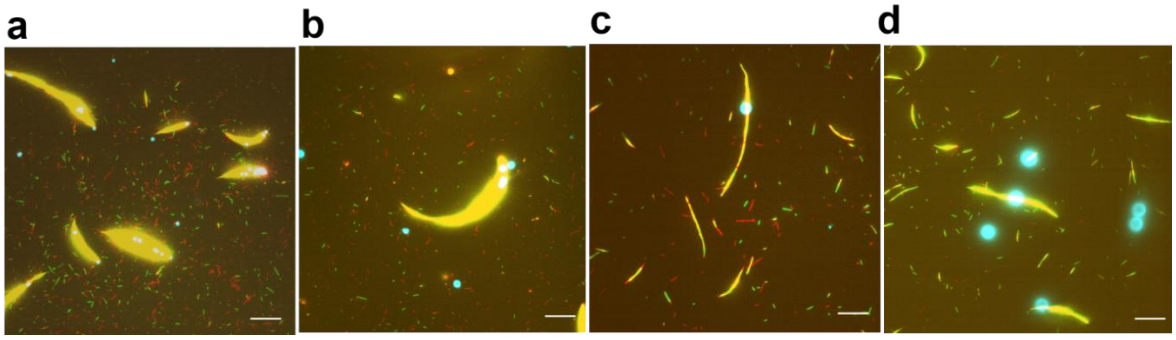

Figure 4.17 Fluorescence microscopic images of different diameter **(a)**1.13 µm, **(b)** 3.40 µm, **(c)** 7.24 µm and **(d)** 8.66 µm of cargo loaded molecular swarm robot. Scale bar: 20 µm.

From **Figure 4.17**, swarm microrobots were observed to load and transport different sized cargo very efficiently. It can be shown that the number of free unloaded beads on the surface is lower. Swarm microrobots load different diameters of micro-sized cargoes and transport. Even 10 µm of swarm robot load 8.66 µm of cargo and transport a long distance.

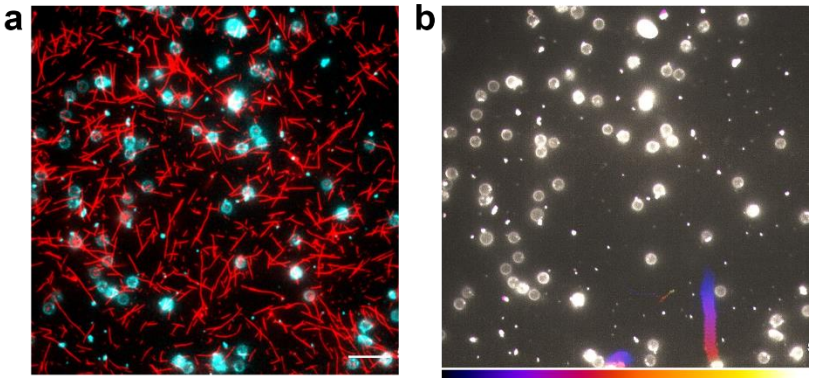

Figure 4.18 (a) Fluorescence microscopic image of the transport of 3.40 µm diameter of cargo by single microrobot and **(b)** color-coded image of the displacement of 3.40 µm diameter of cargo.

Another investigation was explored to observe large-sized cargo loading ability by the single microrobots shown in **Figure 4.18**. Single microrobot loaded one 3.40 µm dimeter cargo but after 3 min it dropped off that cargo. It showed that molecular swarm robots have a stronger affinity of binding than the single microrobots.

4.2.9 Cargo accumulation in a selected region

The cargo concentrate ability by swarm microrobot in a specific location would bring significant innovation in the field of molecular robotics. Swarm microrobots could increase the efficiency as well as mobility of the cargo sorting by concentrating in a specific area. To explore cargo accumulation, the density of the cargoes was monitored in the selected area for a long time. Cargo loaded swarm microrobot came into that area, unload the cargo and pass until all the cargo sorted efficiently as shown schematically in **Figure 4.19**.

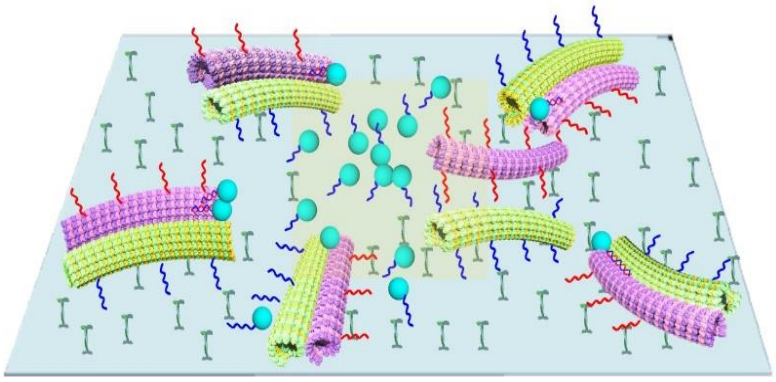

Figure 4.19 Schematic diagram of the cargo accumulation by molecular swarm robot in the region of interest (ROI).

After 10 min of ATP addition, cargoes were loaded to the flow cell and after 30 min of ATP addition, UV light was irradiated into the specific area. The change of the density of cargoes was monitored in a square-shaped UV area and observed by epifluorescence microscope.

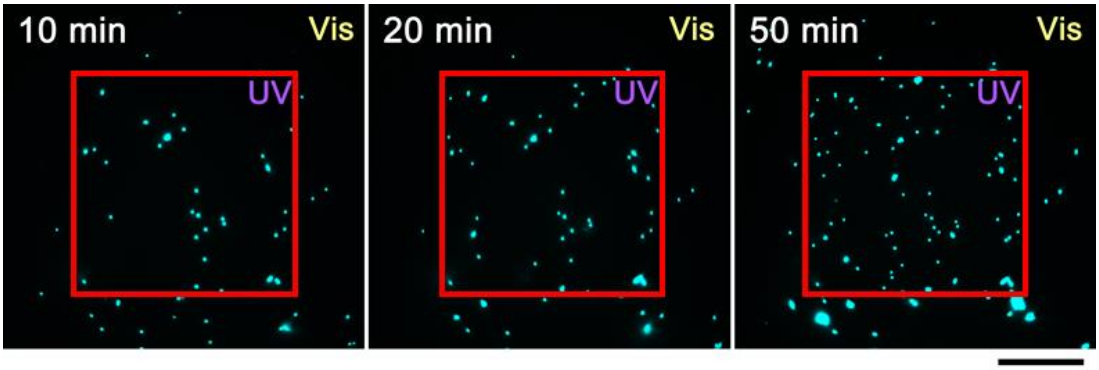

Figure 4.20 Time lapse fluorescence microscopic images of cargo sorting by the molecular swarm robot. The red squared box showed the ROI or the unloading area where cargoes are accumulating after UV irradiation.

From **Figure 4.20**, it can be shown that after 10 min of UV irradiation, the beads were started to concentrate in the square region. After 50 min of UV irradiation, the number of cargoes increased several times. Swarm microrobots pick-up multiple cargoes at a time and deliver to the specified destination until all the cargoes are sorted in that area. This result signifies the cargo sorting tendency by swarming in a specific region. The density of the cargoes was counted with NIS analysis software by dividing the square region into four different parts.

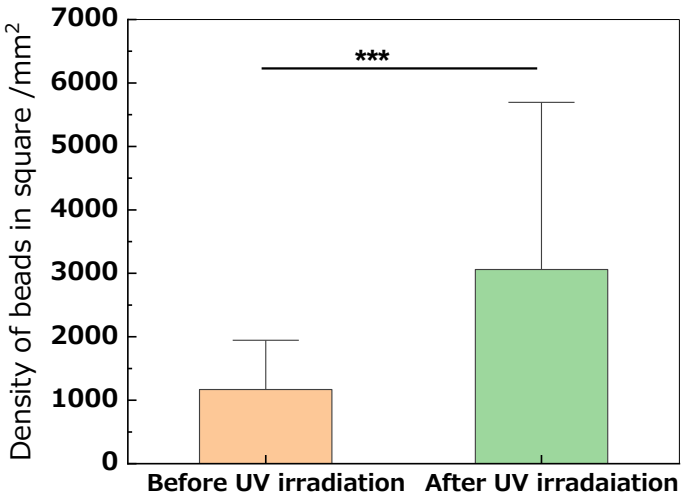

Figure 4.21 A box chart showing the variation of the number of cargoes per 64×64 mm^2 area of the square pattern after 60 min of UV irradiation. Statistical analysis using Student's t-test confirmed significant difference between the two data sets at P<0.001 indicated by ***.

The density of beads significantly increased after UV irradiation for 60 min in the specific region which can be observed from the box chart in **Figure 4.21.** These results confirmed the cargo sorting ability of it by concentrating the cargoes in the selected regions.

4.3 CONCLUSIONS

In conclusion, the photoregulated swarm microrobots worked as an efficient cargo transport system that pick-up, transport and unload cargo. They transported multiple cargoes at a time for a long-distance without any cargo drop-off or detachment under VIS light. They could attach and bind micro-sized cargo firmly which was not achieved by the single microrobot. The work efficiency of the swarming of microrobots was seven times higher than the single microrobot. This result confirmed the emergent functions of the swarming as the efficient active cargo transporter. They unloaded cargo in selected regions in response to UV irradiation. Additionally, they could be useful for sorting cargoes by pick-up single or multiple cargoes at a time and deliver to the specified destination until all the cargoes concentrate in that area. With systematic approaches, molecular swarm robots could exhibit more complex tasks in sophisticated microscopic environments. This work is the first experimental evidence of the emergent functions of the swarming which will open a paradigm in the application of the microrobots in the nanotechnological engineering system.[21,34,40,41]

4.4 MATERIALS & METHODS

4.4.1 Purification of tubulin and kinesin

Tubulin was purified from the porcine brain using high-concentration of PIPES buffer (1 M PIPES, 20 mM EGTA, and 10 mM $MgCl_2$) and stored in BRB80 buffer (80 mM PIPES, 1 mM EGTA, 2 mM $MgCl_2$, pH maintained to 6.8 using KOH pellet)[42] Recombinant kinesin-1 consisting of the first 573 amino-acid residues of human kinesin-1 was prepared as described in the literature[43]. Azide labeled tubulin was prepared using N_3-PEG_4-NHS following the established protocol of labeling tubulin with a fluorescent dye[44]. The tubulin concentration was determined by measuring the absorbance at 280 nm using a UV spectrophotometer (Nanodrop 2000c).

4.4.2 Design and preparation of DNA sequences

The *p*DNA strands were selected optimizing the swarming of the microrobots varying different physicochemical properties. *p*DNA strands were purchased from Hokkaido System Science Co. Ltd. The *p*DNA was modified at the 5′ end with dibenzocyclooctyne (DBCO). Quality control of all the synthesized DNA was performed by polyacrylamide gel electrophoresis (PAGE). Characterization of the *p*DNA strands was carried out by LC-ESI-MS spectroscopy.

4.4.3 Preparation of microtubules (MTs)

MTs were polymerized from a mixture of azide labeled tubulin and Atto 550 labeled tubulin in which the concentration of tubulin was 70 µM. Molar ratio between azide labeled tubulin and ATTO 550 labeled tubulin was adjusted to 4:1. Then the tubulin mixture in polymerization buffer was incubated at 37 °C for 30 min to form MTs. 1 µL of 4×BRB80 buffer (80 mM PIPES, 1 mM EGTA, 1 mM $MgCl_2$, 1 mM GMPCPP, pH~6.8) and 0.5 µL of 1 mM taxol (in DMSO) were added to the MT solution just after polymerization to stabilize the MTs. Copper free click reaction was carried out by adding 3.5 µL DBCO conjugated *p*DNA (500 µM) to 5 µL MT solution (56 µM) and incubating at 37 °C for 6 h.[4] Cushion buffer (100 µL of BRB80 buffer supplemented with 60% glycerol) was used to separate the MTs by centrifugation at 201,000 × g (S55A2-0156 rotor, Hitachi) for 1 h at 37 °C. After removing the supernatant, the pellet of *p*DNA-conjugated MTs was washed with 100 µL BRB80P (BRB80 supplemented with 1 mM taxol) and resuspended in 15 µL of BRB80P buffer.

4.4.4 Demonstration of swarming of MTs

A microfluidic channel was constructed using two glass cover slides of 40×50 mm^2 and 18×18 mm^2 (MATSUNAMI Inc.) adhered together by parafilm as a spacer with a channel pattern cut off. The glass slides were plasma treated for 5 min by a plasma etcher (SEDE-GE; Meiwafosis) to make it hydrophilic. The channel pattern was designed using Brother Canvas Workspace software on the parafilm and cut by Brother ScanNCut printer. The flow cell was prepared setting the designed parafilm on the large cover glass and then the small slide on the top and then heating at 70 ^oC. The flow cell was filled with 5 μL casein buffer (BRB80 buffer supplemented with 0.5 mg mL^{-1} casein). After incubating for 3 min, 0.8 μM kinesin solution was introduced into the flow cell and incubated for 5 min. After washing the flow cell with 5 μL of wash buffer (BRB80 buffer supplemented with 1 mM DTT, 10 μM taxol), 5 μL of red MTs (*p*DNA1 modified ATTO550-labeled MTs) solution was introduced and incubated for 2 min, followed by washing with 10 μL of wash buffer. Subsequently, 5 μL of green MTs (*p*DNA2 modified ATTO488-labeled MTs) solution was introduced and incubated for 2 min, followed by washing with 10 μL of motility buffer. The motility of MTs was initiated by applying 5 μL ATP buffer (wash buffer supplemented with 5 mM ATP, 4.5 mg mL^{-1} D-glucose, 50 UmL^{-1} glucose oxidase, 50 UmL^{-1} catalase, and 0.2% methylcellulose (w/v)). The time of ATP addition was set as 0 h. Soon after the addition of ATP buffer, the flow cell was placed in an inert chamber system (ICS)[45] and the MTs were monitored using an epifluorescence microscope at room temperature (25 °C). The samples were illuminated with a 100 W mercury lamp and visualized by an epifluorescence microscope (Eclipse Ti, Nikon) using an oil-coupled Nikon Plan Apo 60× objective (N.A.=1.4). UV cut-off filter blocks (TRITC: EX 540/25, DM565, BA605/55; GFP-B: EX470-40, DM500, BA535-50; Nikon) were used in the optical path of the microscope. Images were captured using a cooled-CMOS camera (NEO sCMOS, Andor) connected to a PC. ND filters were inserted into the illumination light path of the fluorescence microscope to reduce photobleaching of the samples.

4.4.5 Modification of beads as cargoes

18 μL of 20 mM N_3-PEG_4-NHS ester (dry DMSO; 332 g/mol) and 2 μL of 20 μM ATTO647 dye were added to 20 μL of amino polystyrene beads (5% w/v; *Spherotech Inc.*) followed by the removal of supernatant from the bead suspension. The bead suspension was incubated at

room temperature for 1 h. Then the suspension was again incubated for 30 min at room temperature after addition of 20 μL of 20 mM glycine solution and next, centrifuged three times after washing by 20 μL of BRB80. After removing the supernatant, 7 μL of 200 μM of CAA8Azo7 DNA was added to the bead and incubated at room temperature for 24 h. Then, the bead was again washed by 20 μL of BRB80 and centrifuged. At last, the bead was diluted 10 times by BRB80 solution.

4.4.6 Demonstration of cargo transport by swarming of microrobots

The procedure is almost the same as the previous section of the demonstration of the swarming of microrobots. After the addition of ATP, the flow cell was kept inside the inert gas chamber for 5 min and then, 5 μL of ATTO647 labeled $(CAA)_8Azo_7$ modified cargo (in BRB80) was injected into the gliding assay chamber in which association of MTs already formed. After waiting for 2 min, 5 μL of wash buffer was added to wash the excessive unloaded beads and at last 5 μL of ATP buffer was again added to the flow cell. Then, observations were done immediately by epifluorescence microscopy. The unloading of beads was observed under UV light irradiation.

4.4.7 UV light setup

The experimental setup consists of a Nikon super high-pressure Hg lamp as a light source that passes through a UV1A filter (EX 365-10, DM400, BA390; Nikon). The beam is expanded and steered into the microscopic objective lens. The intensity of light is measured as 0.46 mW by Thorlabs power meter (PM100). The intensity of UV light can be reduced by placing a neutral density filter (ND) in its path. Photomask or pattern are employed in the path of UV light irradiation for the spatiotemporal control of the reversible swarming of molecular robot or the cargo unloading from the robot. The pattern structures were designed to maintain a fixed size (length/diameter/width of 4 mm) using Brother Canvas Workspace software and cut by Brother ScanNCut printer.

4.5 SUPPLEMENTAL INFORMATION

Table 1: The sequences of the *p*DNA used for modification of the MTs for cargo transporter swarm microrobot. Here, Z represents the azobenzene moiety in DNA.

Name of DNA	**Infeed concentration (µM)**	**5'-3'**	**5' end**	**3' end**
*p*DNA1	200	$T_{12}(TTG)_6Z_5$	DBCO	-
*p*DNA2	200	$(CAA)_8Z_7$	DBCO	-

4.6 REFERENCES

1. Pearce, D. J. G., Miller, A. M., Rowlands, G. & Turner, M. S. Role of projection in the control of bird flocks. *Proc. Natl. Acad. Sci. U. S. A.* **111**, 10422–10426 (2014).

2. Bahar, S. Flocking , swarming , and communicating: The Essential Tension. The Frontiers Collection. *Springer*127–152 (2018). doi:10.1007/978-94-024-1054-9.

3. Couzin, I. D., Krause, J., James, R., Ruxton, G. D. & Franks, N. R. Collective memory and spatial sorting in animal groups. *J. Theor. Biol.* **218**, 1–11 (2002).

4. Reynolds, C. W. Flocks, herds, and schools: A distributed behavioral model. *Proc. 14th Annu. Conf. Comput. Graph. Interact. Tech. 1987* **21**, 25–34 (1987).

5. Aoki, I. A Simulation study on the schooling mechanism in fish. *Nippon Suisan Gakkaishi* **48**, 1081–1088 (1982).

6. Bibic, S. M., Cipu, E. C. & Buiu, C. A bioinspired mathematical model for a robotic swarm to discriminate between self and nonself robots. *2015 19th International Conference on System Theory, Control and Computing (ICSTCC)* 279–284 (2015). doi:10.1109/ICSTCC.2015.7321306

7. Kernbach, S. & Kernbach, O. Collective energy homeostasis in a large-scale microrobotic swarm. *Rob. Auton. Syst.* **59**, 1090–1101 (2011).

8. Kernbach, S. *et al.* Adaptive collective decision-making in limited robot swarms without communication. *Int. J. Rob. Res.* **32**, 35–55 (2013).

9. Wei, H., Cai, Y., Li, H., Li, D. & Wang, T. Sambot: A self-assembly modular robot for swarm robot. *Proc. - IEEE Int. Conf. Robot. Autom.* 66–71 (2010). doi:10.1109/ROBOT.2010.5509214

10. Rubenstein, M., Ahler, C. & Nagpal, R. Kilobot: A low cost scalable robot system for collective behaviors. *Proc. - IEEE Int. Conf. Robot. Autom.* 3293–3298 (2012). doi:10.1109/ICRA.2012.6224638

11. Rubenstein, M., Cornejo, A. & Nagpal, R. Programmable self-assembly in a thousand-robot swarm. *Science.* **345**, 6198, 795– 799 (2014).

12. Mondada, F. *et al.* Swarm-Bot: A new distributed robotic concept. *Auton. Robots* **17**, 193–221 (2004).

13. Sarvašová, N., Ulbrich, P., Tokárová, V., Zadražil, A. & Štěpánek, F. Artificial swarming: Towards radiofrequency control of reversible micro-particle aggregation and deposition. *Powder Technol.* **278**, 17–25 (2015).

14. Grančič, P. & Štěpánek, F. Active targeting in a random porous medium by chemical swarm robots with secondary chemical signaling. *Phys. Rev. E - Stat. Nonlinear, Soft Matter Phys.* **84**, 1–7 (2011).

15. Grančič, P. & Štěpánek, F. Swarming behavior of gradient-responsive Brownian particles in a porous medium. *Phys. Rev. E - Stat. Nonlinear, Soft Matter Phys.* **86**, 1–6 (2012).

16. Grančič, P. & Štěpánek, F. Swarming behavior of gradient-responsive colloids with chemical signaling. *J. Phys. Chem. B* **117**, 8031–8038 (2013).

17. Keya, J. J. *et al.* DNA-assisted swarm control in a biomolecular motor system. *Nat. Commun.* **9**, 453 (2018).

18. Critchlow, A. K. Introduction to robotics. New York:Macmillan Publishing Co (1985).

19. Wiesel-Kapah, I., Kaminka, G. A., Hachmon, G., Agmon, N. & Bachelet, I. Rule-based programming of molecular robot swarms for biomedical applications. *IJCAI Int. Jt. Conf. Artif. Intell.* 3505–3512 (2016).

20. Thubagere, A. J. *et al.* A cargo-sorting DNA robot. *Science*, **357**, 6356 (2017).

21. Ricotti, L. & Menciassi, A. Nanotechnology in biorobotics: opportunities and challenges. *J. Nanoparticle Res.* **17**, 1–10 (2015).

22. Keya, J. J. *et al.* Control of swarming of molecular robots. *Sci. Rep.* **8**, 1–10 (2018).

23. Şahin, E. Swarm robotics: From sources of inspiration to domains of application. *Lect. Notes Comput. Sci.* **3342**, 10–20 (2005).

24. Liu, H., Stoll, N., Junginger, S. & Thurow, K. A fast method for mobile robot transportation in life science automation. *Conf. Rec. - IEEE Instrum. Meas. Technol. Conf.*

238–242 (2013). doi:10.1109/I2MTC.2013.6555416

25. Nitta, T. & Hess, H. Dispersion in active transport by kinesin-powered molecular shuttles. *Nano Lett.* **5**, 1337–1342 (2005).

26. Agarwal, A., Katira, P. & Hess, H. Millisecond curing time of a molecular adhesive causes velocity-dependent cargo-loading of molecular shuttles. *Nano Lett.* **9**, 1170–1175 (2009).

27. Hess, H., Clemmens, J., Qin, D., Howard, J. & Vogel, V. Light-Controlled Molecular Shuttles Made from Motor Proteins Carrying Cargo on Engineered Surfaces. *Nano Lett.* **1**, 235–239 (2001).

28. Fruh, S. M., Steuerwald, D., Simon, U. & Vogel, V. Covalent Cargo Loading to Molecular Shuttles via Copper-free " Click Chemistry ". *Biomacromolecules* **13**, 12, 3908-3911 (2012). doi:10.1021/bm301437c.

29. Schmidt, C. & Vogel, V. Molecular shuttles powered by motor proteins: Loading and unloading stations for nanocargo integrated into one device. *Lab Chip* **10**, 2195–2198 (2010).

30. Brunner, C., Wahnes, C. & Vogel, V. Cargo pick-up from engineered loading stations by kinesin driven molecular shuttles. *Lab Chip* **7**, 1263–1271 (2007).

31. Ramachandran, S., Ernst, K. H., Bachand, G. D., Vogel, V. & Hess, H. Selective loading of kinesin-powered molecular shuttles with protein cargo and its application to biosensing. *Small* **2**, 330–334 (2006).

32. Böhm, K. J., Stracke, R., Mühlig, P. & Unger, E. Motor protein-driven unidirectional transport of micrometer-sized cargoes across isopolar microtubule arrays. *Nanotechnology* **12**, 238–244 (2001).

33. Adir, O. *et al.* Integrating Artificial Intelligence and Nanotechnology for Precision Cancer Medicine. *Adv. Mater.* **32**, 1–15 (2020).

34. Smith, L. M. Nanotechnology: Molecular robots on the move. *Nature* **465**, 167–168 (2010).

35. Schmidt, C. & Vogel, V. Molecular shuttles powered by motor proteins: Loading and unloading stations for nanocargo integrated into one device. *Lab Chip* **10**, 2195–2198 (2010).

36. Kufer, S. K., Puchner, E. M., Gumpp, H., Liedl, T. & Gaub, H. E. Single-molecule cut-and-paste surface assembly. *Science* **319**, 5863, 594–596 (2008).

37. Hiyama, S. *et al.* Autonomous loading, transport, and unloading of specified cargoes by using DNA hybridization and biological motor-based motility. *Small* **4**, 410–415 (2008).

38. Hess, H. & Vogel, V. Molecular shuttles based on motor proteins: Active transport in synthetic environments. *Rev. Mol. Biotechnol.* **82**, 67–85 (2001).

39. Früh, S. M., Steuerwald, D., Simon, U. & Vogel, V. Covalent cargo loading to molecular shuttles via copper-free 'click chemistry'. *Biomacromolecules* **13**, 3908–3911 (2012).

40. Kabir, A. M. R., Inoue, D. & Kakugo, A. Molecular swarm robots: recent progress and future challenges. *Sci. Technol. Adv. Mater.* **21**, 323-332, 1 (2020). doi 10.1080/14686996.2020.1761761

41. Ceylan, H., Giltinan, J., Kozielski, K. & Sitti, M. Mobile microrobots for bioengineering applications. *Lab Chip* **17**, 1705–1724 (2017).

42. Castoldi, M. & Popov, A. V. Purification of brain tubulin through two cycles of polymerization – depolymerization in a high-molarity buffer. **32**, 83–88 (2003).

43. Case, R. B., Pierce, D. W., Hom-booher, N., Hart, C. L. & Vale, R. D. The directional preference of kinesin motors is specified by an element outside of the motor catalytic domain. **90**, 959–966 (1997).

44. Peloquin, J., Komarova, Y. & Borisy, G. Conjugation of fluorophores to tubulin. *Nat. Methods* **2**, 299–303 (2005).

45. Kabir, A. M. R., Inoue, D., Kakugo, A., Kamei, A. & Gong, J. P. Prolongation of the active lifetime of a biomolecular motor for in vitro motility assay by using an inert atmosphere. *Langmuir* **27**, 13659–13668 (2011).

CHAPTER 5

Concluding Remarks

This dissertation mainly represents the development of photoregulated microrobots using the self-propelled biomolecular motor system programmed by photoresponsive azobenzene incorporated DNA. Motion and mutual interaction of microrobots were regulated in response to the photoregulation incorporating a photoswitchable sensor into the processor of robot.

In chapter 2, persistency of the motion of microrobots are explored in response to photoirradiation. Microrobots were constructed successfully employing biomolecular motor system i.e. MT-kinesin as the actuator, DNA as the information processor and azobenzene as the photosensor. Single strand photoresponsive DNA (*p*DNA) was used as an effective tool to regulate the trajectories of microrobots driven by kinesins without sacrificing the mobility of the MTs. The persistency of the motion of MTs, characterized as the path persistence length was reversibly regulated by light without interrupting the interaction between MT and kinesins. Persistency in motion was found to increase and decrease upon UV and visible light irradiation respectively. In addition, *p*DNA was found to work as UV shield in protecting MTs from the harmful effect of UV light. This work will advance the ability to control persistency in the motion of microrobot and will accelerate the ongoing development in molecular robotics and their swarming. The outcomes in this work are expected to promote further development of phototactic molecular robots which would be able to self-align or navigate by responding to any light source.

In chapter 3, photoregulated swarming of biomolecular motor based microrobots was established through DNA hybridization of complentary *p*DNA duplex. Complementary *p*DNA modified microrobots or swarm units were prepared using click reaction prior to the swarm demonstration. The effects of related physicochemical parameters e.g. time, length, concentration of DNA etc. were systematically investigated which contribute to the size and morphology of the swarm robots. UV light was irradiated to initialize the trans to cis isomerization of the azobenzene which allowed the reversible swarming of the microrobots through dissociation into single microrobots. Moreover, the effects of wavelength, the intensity of light and the number of azobenzene molecules in DNA were also investigated on the reversible swarming of microrobots. The swarming was regulated

in specific locations using different sized and shaped photomasks through the UV light source in a spatiotemporal manner. Additionally, the persistency in the motion was controlled in response to UV light. The systematic and spatiotemporal control over molecular swarm robots could be achieved as a new paradigm in molecular robotics for a future advanced engineering system.

In chapter 4, the utilization of the photoregulated molecular swarm robots for active cargo transport are described. Molecular swarm robots were found to exhibit complex tasks efficiently by loading, transporting and unloading polystyrene bead as the cargo in response to the photoirradiation. They transport multiple cargoes at a time for a long-distance without any cargo drop-off or detachment under VIS light. The work efficiency was compared to the single microrobot which confirms the emergent functions of the swarm robot as an efficient active cargo transporter. They unloaded cargo in selected regions in response to UV irradiation. Additionally, they sort cargoes by pick-up single or multiple cargoes at a time and deliver to the specified destination until all the cargoes are concentrated in that area. It could be confirmed by the increasing density of cargoes in that selected region. With systematic approaches, molecular swarm robots could exhibit more complex tasks in sophisticated microscopic environments. This work represents the first-ever experimental evidence of the emergent functions of the swarming of microrobots which will open a paradigm in the application of the microrobots in the nanotechnological engineering system.

Finally, I would like to draw a future perspective of my entire work. Incorporation of photoresponsive azobenzene in the DNA gives us a new concept to program the motion as well as the interaction of the microrobots in a reversible and spatiotemporal manner. The spatiotemporal control of the swarming of the microrobots would make an innovation in the field of swarm robotics. The study would serve the knowledge in the viewpoint from biology, chemistry and engineering system not only to realize swarming but also to develop swarm robots with different functionalities like flexibility, parallelism, robustness that can perform a different complicated task through its group behavior. This work will contribute to the construction of phototactic microrobots that could autonomously self-align or navigate by responding to any light source and also in the establishment of photoregulated nanotrafficking system that could control the movement and transport of the microrobots in any direction. The high workability of the molecular swarm robot would be helpful to design and construct an efficient robot to work in more sophisticated nanotechnological applications. Proper utilization of the DNA origami arrays in the biomolecular motor based

molecular robot, could improve the robustness of the robot for a more complex task. Small chemicals, metal nanoparticles, and proteins can be transported as molecular cargo so that cargo sorting could be used for chemical synthesis or molecular manufacturing. For molecular manufacturing, swarm robots could be triggered to rearrange circuit components, such as nanoparticles, so that the function of the device can be adaptive to environmental signals much efficiently. With systematic approaches, microrobots could be easily programmed like macroscopic robots at the molecular level. Finally, the microrobots are expected to have great contributation in the emergence of a new dimension in chemical synthesis, molecular manufacturing and artificial intelligence based on the fusion of biotechnology, nanotechnology and informatics.

List of Publications

Papers (related to this dissertation)

Chapter 2

Photo-regulated trajectories of gliding microtubules conjugated with DNA

Mousumi Akter, Jakia Jannat Keya, Arif Md. Rashedul Kabir, Hiroyuki Asanuma, Keiji Murayama, Kazuki Sada, and Akira Kakugo, *Chemical Communications*, **2020**, *56*, 7953-7956.

Chapter 3

Photoregulated swarming of biomolecular motor based molecular robot

Mousumi Akter, Jakia Jannat Keya, Arif Md. Rashedul Kabir, Hiroyuki Asanuma, Keiji Murayama, Kazuki Sada, and Akira Kakugo, *to be submitted*.

Chapter 4

Molecular swarm robot-a highly efficient cargo transport system

Mousumi Akter, Jakia Jannat Keya, Arif Md. Rashedul Kabir, Hiroyuki Asanuma, Keiji Murayama, Kazuki Sada, and Akira Kakugo, *to be submitted*.

Other papers (not related to this dissertation)

Hydrophilic ionic liquid-assisted control of the size and morphology of ZnO nanoparticles prepared by a chemical precipitation method

Mousumi Akter, Shazia Sharmin Satter, Ajay Kumar Singh, M. Yousuf Ali Mollah, and Md. Abu Bin Hasan Susan, *RSC Advances*, **2016**, *6*, 92040-92047.

List of Conference Presentations

Conference (related to this dissertation)

1. Mousumi Akter, Jakia Jannat Keya, Arif Md. Rashedul Kabir, Kazuki Sada, Hiroyuki Asanuma, Akinori Kuzuya, Akira Kakugo, "**Spatiotemporal regulation of microtubule swarming using Photoresponsive DNA"** 生体分子機械による革新的動力システム会議, 2 November 2018, Hokkaido University, Sapporo, Japan.
2. Mousumi Akter, Jakia Jannat Keya, Arif Md. Rashedul Kabir, Kazuki Sada, Hiroyuki Asanuma, Akinori Kuzuya, Akira Kakugo, "**Spatiotemporal control of biomolecular motor based swarming using photoresponsive DNA"**, 6th International Life Science symposium (ILSS)-IGP symposium, 3 November 2018, Hokkaido University Conference Hall, Sapporo, Japan.
3. Mousumi Akter, Jakia Jannat Keya, Arif Md. Rashedul Kabir, Kazuki Sada, Hiroyuki Asanuma, Akinori Kuzuya, Akira Kakugo, "**How ATP fueled molecular robot acts as highly efficient cargo carrier"**, The 8th Conference on Exploring Next-Generation Materials Science and Nanoscience (8th CENG-MSN) and Workshop on Soft and Nano Materials Orchestrated with Wisdom from Japan 2019 (SNOWJ 2019), 11-15 January 2019, Niseko Chomin Center, Hokkaido, Japan.
4. Mousumi Akter, Jakia Jannat Keya, Kentaro Kayano, Arif Md. Rashedul Kabir, Daisuke Inoue, Kazuki Sada, Hiroyuki Asanuma, Henry Hess, Akinori Kuzuya, Akira Kakugo, "***Trans* on switched cargo transportation by molecular swarm robot**", The 10th Graduate School of Chemical Sciences and Engineering (CSE) and Ambitious Leaders' Program (ALP) International Summer School, 13-14 July 2019, Pirka Kotan, Hokkaido, Japan.
5. Mousumi Akter, Jakia Jannat Keya, Kentaro Kayano, Arif Md. Rashedul Kabir, Daisuke Inoue, Kazuki Sada, Hiroyuki Asanuma, Henry Hess, Akinori Kuzuya, Akira Kakugo, "**Regulation of *trans* on switched cargo transportation by molecular swarm robot**", 2nd Asian-French Workshop on Polymer Science 2019 (CSE International Student Symposium 2019), 18-21 July 2019, Hokkaido University, Sapporo, Japan.

6. Mousumi Akter, Jakia Jannat Keya, Arif Md. Rashedul Kabir, Kazuki Sada, Hiroyuki Asanuma, Akinori Kuzuya, Akira Kakugo, "**Photo-regulated spatiotemporal cargo transportation by molecular swarm robot**", The 57th Annual meeting of the Biophysical Society of Japan (BSJ 2019), 24-26 September 2019, Seagaia Convention Center, Miyazaki, Japan.
7. Mousumi Akter, Jakia Jannat Keya, Arif Md. Rashedul Kabir, Kazuki Sada, Hiroyuki Asanuma, Akinori Kuzuya, Akira Kakugo, "**Spatiotemporal *trans* on switched cargo transportation by molecular swarm robot**", Okinawa Colloids 2019, 3-8 November 2019, Bankoku Shinryokan, Okinawa, Japan.
8. Mousumi Akter, Jakia Jannat Keya, Arif Md. Rashedul Kabir, Kazuki Sada, Hiroyuki Asanuma, Akinori Kuzuya, Akira Kakugo, "**Spatiotemporal regulation of *trans* on switched molecular swarm robot**", The 20th RIES-HOKUDAI International Symposium, 2-3 December 2019, Hokkaido University Conference Hall, Sapporo, Japan.
9. Mousumi Akter, Jakia Jannat Keya, Arif Md. Rashedul Kabir, Kazuki Sada, Hiroyuki Asanuma, Akinori Kuzuya, Akira Kakugo, "**Molecular swarm robot- a highly efficient molecular cargo carrier system**", Hokkaido University-National Central University Joint Symposium on Materials Chemistry and Physics 2019, 12-13 December 2019, Hokkaido University, Sapporo, Japan.
10. Mousumi Akter, Jakia Jannat Keya, Arif Md. Rashedul Kabir, Kazuki Sada, Hiroyuki Asanuma, Akinori Kuzuya, Akira Kakugo, "**Photo-activated cargo transportation by molecular swarm robot**", 31st Gel Research Symposium, 16-17 January 2020, AIST Waterfront, Tokyo, Japan.
11. Mousumi Akter, Jakia Jannat Keya, Arif Md. Rashedul Kabir, Hiroyuki Asanuma, Akinori Kuzuya, Kazuki Sada, Akira Kakugo, "**Molecular swarm robot- a highly efficient molecular cargo carrier system**", 54th Society of Polymer Science (SPSJ) Winter Meeting, 27 January 2020, Hokkaido University Conference Hall, Sapporo, Japan.
12. Mousumi Akter, Jakia Jannat Keya, Arif Md. Rashedul Kabir, Hiroyuki Asanuma, Akinori Kuzuya, Kazuki Sada, Akira Kakugo, "**Molecular swarm robot- a highly efficient molecular cargo transport system**", Chemical Society of Japan (CSJ) Hokkaido Branch Meeting 2020 (TOUKIKEN), 28-29 January 2020, Hokkaido University Conference Hall, Sapporo, Japan.

Conference (not related to this dissertation)

1. Mousumi Akter, Muhammed Shah Miran, Md. Yousuf Ali Mollah and Md. Abu Bin Hasan Susan, "**Hydrophilic Ionic Liquid Assisted Synthesis of ZnO Nanoparticles and their Morphology Analysis**" 37th Annual Conference of Bangladesh Chemical Society, 11 April 2015, Cumilla University, Cumilla, Bangladesh.
2. Mousumi Akter, Muhammed Shah Miran, Md. Yousuf Ali Mollah and Md. Abu Bin Hasan Susan, "**Hydrophilic Ionic Liquid Assisted Synthesis of ZnO Nanoparticles and their Morphology Analysis**" 2nd International Bose Conference, 3-4th December 2015, Nawab Ali Chowdhury Senate Bhaban, Dhaka, Bangladesh.
3. Mousumi Akter, Muhammed Shah Miran, Md. Yousuf Ali Mollah and Md. Abu Bin Hasan Susan, "**Hydrophilic Ionic Liquid Assisted Synthesis and Characterization of ZnO Nanoparticles and their Morphology Analysis**" 16th Asian Chemical Congress, 16-19 March 2016, BUET, Dhaka, Bangladesh.
4. Mousumi Akter, Muhammed Shah Miran, Md. Yousuf Ali Mollah and Md. Abu Bin Hasan Susan, "**Hydrophilic Ionic Liquid Assisted Synthesis and Characterization of ZnO Nanoparticles and their Morphology Analysis**" 1st Symposium on Chemistry for Global Solidarity, 14 October 2016, Jagannath University, Dhaka, Bangladesh.
5. Mousumi Akter, M. Muhibur Rahman, M. Yousuf Ali Mollah and Md.Abu Bin Hasan Susan, "**Hydrophilic Ionic Liquid-Assisted Synthesis of ZnO Nanostructures by Hydrothermal Method and their Antibacterial and Optical properties**", Conference on Material Science and Nano-electrochemistry, 8-9 April 2017, Rajshahi University, Rajshahi, Bangladesh.
6. Mousumi Akter, Muhammed Shah Miran, Md. Yousuf Ali Mollah, Md. Abu Bin Hasan Susan, "**Hydrophilic Ionic Liquid Assisted Synthesis of ZnO Nanostructures by hydrothermal method and their Antibacterial Activities**", International Conference on Genomics, Nanotech & Bioengineering, 15 May 2017, North South University, Dhaka, Bangladesh.

Acknowledgments

First and foremost, praise is to the Almighty ALLAH for giving me the blessing, strength, opportunity and endurance to complete my Ph.D. dissertation in time. His continuous grace and mercy were with me throughout my life and even more during the tenure of my research. I considered myself blessed to achieve the most prestigious MEXT scholarship to continue my Ph.D. research in the Graduate School of Chemical Sciences and Engineering of Hokkaido University. I would like to acknowledge all the people who have supported and helped me throughout the long and winding roads towards Ph.D.

In the beginning, I would like to thank my supervisor, Prof. Kazuki Sada, for his invaluable support and understanding during my entire journey of Ph.D. I want to especially mention his kind guidance and directions from the start of writing to the submission of my dissertation. I am also very much grateful to Prof. Kazuyasu Sakaguchi (Laboratory of Biological Chemistry, HU), Prof. Manabu Tokeshi (Laboratory of Bioanalytical Chemistry, HU) and Prof. Koichiro Ishimori (Structural Chemistry Lab, HU) members of my Ph.D. committee for their insightful suggestions to improve my dissertation.

I would like to express my greatest appreciation to my principal investigator Dr. Akira Kakugo (Associate Professor, Material Chemistry Laboratory, HU) for his guidance and supports and above all, allowing me to work in an advanced and fascinating swarming system. I am very grateful for his wonderful motivations, thoughtful suggestions, influential comments, kind considerations and encouragement throughout the whole journey.

I would like to thank Dr. Kento Kokado (Associate Professor, Nakamura Laboratory, Research Institute for Electronic Science, HU) for his kind suggestions in the regular monthly meetings. I also like to express my gratitude to Dr. Arif Md. Rashedul Kabir (Assistant Professor, Material Chemistry Laboratory, HU) for his kind support, helpful discussions and warmth guidance to complete my dissertation on time.

I offer my sincere gratitude to Prof. Henry Hess (Laboratory for nanobiotechnology and synthetic biology, Columbia University, USA) for his insightful discussions and suggestions to improve my research work and think from different perspectives. I also want to thank Prof. Hiroyuki Asanuma (Asanuma Lab, Department of Biomolecular Engineering, Nagoya University) for his active collaboration. I would like to offer my humble gratitude to Dr. Daisuke Inoue (Assistant Professor, Cytoarchitec lab, Kyushu University) for his kind cooperation, helpful discussions throughout the work.

I express my gratitude to all the former and current members of Material Chemistry Laboratory, Hokkaido University for their kind support and help. I would like to acknowledge my wonderful mentor, Dr. Jakia Jannat Keya (JSPS Postdoctoral Fellow, Material Chemistry Laboratory, HU) for her kind support and discussions throughout my life in Japan. I am also very grateful to Dr. Syeda Rubaiya Nasrin (Postdoctoral Researcher, Material Chemistry Laboratory, HU) for the unconditional love and support from the first day of my stay in Japan. I also want to thank Dr. Shizuka Anan (present-Assistant Professor, Kyushu University) for her kind support in the lab. I would like to especially remember some of my friends in this lab who became alumni- Xinmeng Wang, Kentaro Kayano and Akimitsu Azuma. I would like to acknowledge and convey my best wishes to my dear fellows- Soukurou Sunaga, Takashi Machida, Farhana Afroze, Satsuki Ishii and Mst. Rubaya Rashid. I also like to thank-Tokiyo Katou, Yuma Tanaka, Kento Matsuda, Kouta Mishima, Tansi Yu, Tasrina Munmun, Hiroki Amaya, Akira Kabasawa, Miwa Kubota, Yugo Tsuonda, Masato Yamashita, Tokiya Ohira, Sorachi Saito, Mariko Tsutsumi, Kohei Nishiyama and Motoaki Horii for their friendly manners and kind cooperation during my work.

I would like to acknowledge my beloved origin-Department of chemistry, University of Dhaka, Bangladesh and I feel always blessed and proud of being a student of the most prestigious University of Bangladesh. I would like to show my gratitude to Prof. Md. Abu Bin Hasan Susan (Material Chemistry Research Lab, Department of chemistry, University of Dhaka) for his wide range guidance and motivations which initially inspired me to the scientific research. I would like to thank Prof. Mohammad Yousuf Ali Mollah (Acting chairman of University Grants Commission, Bangladesh), Prof. Mominul Islam, Prof. Mohammad Shah Miran and Dr. Saika Ahmed (Assistant Professor, University of Dhaka) for their kind support and inspirations.

Then, I would like to show my gratitude to the world's best parents-Abdul Malek Sharker and Mrs. Fatema Bhuiyan for their trust and support throughout my life. I also want to mention my younger brothers- Forhad Sharker Fahad and Yasin Arafath Sharker for their love and admiration. Finally, I would like to appreciate my amazing husband Md Shahjahan (Ph.D. student, Laboratory of molecular photonics, HU), without his support and inspiration it was impossible to continue and finish my Ph.D. on time with a kid. And I would like to give the biggest thank to my lovely daughter Ayesha Shahreen Ruhana, her smile gave me the joy, refreshment and strength in this depressing period and inspired me to be the greatest version of myself.

Mousumi Akter